EQC Project 10/589

Liquefaction Characteristics of Pumice Sands

RP Orense & MJ Pender
Department of Civil & Environmental Engineering
University of Auckland

AS O'Sullivan
Hiway Geotechnical Ltd

March 2012

Contents

Executive Summary

Pumice materials are frequently encountered in many engineering projects in the North Island of New Zealand. Because of their lightweight, highly crushable and compressible nature, they are problematic from engineering and construction viewpoint. Most existing engineering correlations originally developed for ordinary sands are not applicable to this material. In terms of evaluating liquefaction potential, empirical procedures currently available for sands were derived primarily from hard-grained (quartz) sands. No information is available whether these procedures are applicable to pumice deposits because there has been very little research done to examine the liquefaction characteristics of pumice.

Thus, a research programme was undertaken to understand the cyclic/dynamic properties of pumice. Several series of undrained cyclic triaxial tests were performed on two sets of pumice samples. One set was undisturbed samples taken from pumiceous deposits and the corresponding liquefaction resistances were determined. The other set was reconstituted specimens of commercially-available pumice sands where the effects of various parameters, such as relative density, confining pressure, and particle gradation, on the undrained behaviour and liquefaction resistance were investigated. A comparison of the results was made with those of hard-grained sands. Particle crushing, both at the end and at various stages of the tests, was examined.

The results of the cyclic undrained triaxial tests were supplemented by monotonic undrained tests on reconstituted pumice sand specimens. The influence of relative density, effective confining pressure and gradation characteristics on the undrained response was also investigated. Finally, geotechnical investigations, consisting of cone penetration testing and seismic dilatometer tests were performed at two sites where the undisturbed samples were obtained. The cyclic resistance ratio (CRR) obtained for the undisturbed samples were then compared with the estimated CRR from conventional methods which are based on field testing.

The cyclic tests on the undisturbed pumiceous samples have higher liquefaction resistance than specimens reconstituted to the same density. This is because the soil structure (fabric, stress history, cementation, etc.) was totally erased when the specimens were preapred. Although dense reconstituted pumice specimens have higher liquefaction resistance than loose ones, the difference was not as remarkable as that observed on hard-grained Toyoura sand, where relative density affects the response significantly. Specimens with reduced grain size (and higher fines content) showed slower development of excess pore water pressure and lower liquefaction resistance, similar to the behaviour of hard-grained sand with non-plastic fines. The higher liquefaction resistance of pumice when compared with hard-grained sands is a result of particle crushing which occurred during cyclic shearing. As cyclic shearing and particle crushing occurred, the soil structure was gradually stabilized, resulting in higher liquefaction resistance.

Within the range of confining pressure used in the tests, particle crushing in pumice occurred during cyclic shearing and not during the consolidation process. In addition, the degree of particle crushing increased with the amplitude of the applied cyclic shear stress ratio. During the initial stage of shearing, the increase in surface area (as a result of particle crushing) was small; however, as the liquefaction stage was reached, the surface area per unit volume of the specimen increased remarkably because large strains occurred with associated translation and rotation of particles causing the higher degree of crushing. For specimens that did not liquefy, particle breakage during cyclic shearing was more or less gradual, with almost linear variation with the logarithm of the number of cycles applied.

Under monotonic undrained loading, specimens reconstituted under loose and dense states practically showed similar response, indicating that relative density did not have significant effect on the behaviour of pumice. Within the range of effective confining pressures investigated, pumice specimens showed contractive response followed by dilative behaviour. The contractive response was more significant at high confining pressure. The stress-strain relations depicted a stiffer response at small strain level, followed by development of large strains and greater dilatancy when the phase transformation (from contractive to dilative) state is reached.

The pumice sands used in the tests have angles of internal friction at failure of about 42-44^{o}, and these values were not affected by relative density. It was noted that these friction angles were far greater than those for natural hard-grained sands. The friction angles at phase transformation were between 34-37^{o}, which were again much higher than those of hard-grained sands.

Even under large strain level, pumice sands did not reach steady state of deformation. This can be attributed to breakage of particles during shearing, which resulted in more resistant soil structure that did not allow deformation at constant shear stress to occur. As a result, it can be surmised that critical state soil mechanics may not be applicable to crushable soils like pumice.

Finally, comparison of laboratory-obtained cyclic resistance and those estimated from conventional liquefaction potential evaluation procedures showed that penetration-based approaches, such as cone penetration tests and seismic dilatometer tests, underestimated the liquefaction resistance of pumice soils. It is hypothesized that the shear stresses during penetration were so severe that particle breakage formed new finer grained materials, the mechanical properties of which were very different from the original pumice sand. Thus, any procedure where the liquefaction resistance is correlated with density will not work on pumiceous deposits.

On the other hand, the empirical method based on shear wave velocity seemed to produce good correlation with liquefaction resistance of pumiceous soils. Although the shear wave velocity in this research was obtained from SDMT where the penetrating rod may have induced particle breakage in the adjacent zone, the shear waves travelled through the intact particles and not on the crushed ones. It follows that non-destructive methods of measuring shear wave velocity, such as through spectral analysis of surface waves (SASW) or multi-channel analysis of surface waves (MASW), are better alternatives in estimating the in-situ liquefaction resistance of pumiceous deposits.

Acknowledgment

The authors would like to acknowledge the assistance of Dr. A Tai, Messrs Y Lu, C Chan and N Taghipouran in performing the laboratory tests presented herein. The testing and sampling at Carrs Rd site, Waikato was made possible with the help of Mr A Holland of AECOM. The help of Mr G Blakeley, also of AECOM, in sampling and testing at Mikkelsen Rd site adjacent to Waihou Substation (near Te Aroha) is also acknowledged. Access to the site was provided by Transpower. The CPT and SDMT tests were performed by Mr M Holtrigter of Ground Investigation Ltd.

The guidance and advice of Prof K Ishihara (Chuo University, Japan) and Prof M Hyodo (Yamaguchi University) regarding sampling and testing of pumice sands are gratefully acknowledged. The liquefaction tests for verification purposes were conducted using the testing apparatus of the Geotechnical Engineering laboratory of the Department of Civil and Environmental Engineering, Yamaguchi University and with the assistance of staff and postgraduate students.

This research was made possible through the Earthquake Commission (EQC) Biennial Contestable Grant No. 10/589.

1 INTRODUCTION

1.1 General Remarks

Because of New Zealand's tectonic location, the seismic-resistant design of soil structures requires a clear understanding of the properties of local soils and their behaviour under earthquake loading. The 2010-2011 Christchurch earthquakes have demonstrated the impact of soil liquefaction on residential structures, commercial buildings, bridges, roads and other engineering structures (e.g., Cubrinovski et al., 2010; Orense et al., 2011a-c; Robinson et al., 2011; Yamada et al., 2011). With the central government, local councils and community residents now fully aware of the devastating effects of earthquakes in general and of soil liquefaction in particular, attention has shifted to the seismic performance of local soils, i.e., whether soils in certain localities will undergo the same degree of liquefaction as the Christchurch soils did.

A cursory review of the current state of research on soil liquefaction showed that nearly all the work on this topic has been directed towards understanding the properties of hard-grained (quartz) sands; very little research has been done on the dynamic characteristics of volcanically-derived sands. However, it is known that New Zealand's active geologic past has resulted in widespread deposits of volcanic soils throughout the country. The 1987 Edgecumbe earthquake, for example, showed widespread liquefaction of sands of volcanic origin.

Pumice deposits are found in several areas of the North Island. They originated from a series of volcanic eruptions centred in the Taupo and Rotorua regions, called the "Taupo Volcanic Zone". The pumice material has been distributed initially by the explosive power of the eruptions and associated airborne transport; this has been followed by erosion and river transport. Presently, pumice deposits exist mainly as deep sand layers in river valleys and flood plains, but are also found as coarse gravel deposits in hilly areas. Although they do not cover wide areas, their concentration in river valleys and flood plains means they tend to coincide with areas of considerable human activity and development. Thus, they are

frequently encountered in engineering projects and their evaluation is a matter of considerable geotechnical interest.

Pumice sand particles may be readily crushed against a hard surface by finger-nail pressure presumably, in part at least, because the particles have internal voids. Because of their lightweight, highly crushable and compressible nature, they are problematic from engineering and construction viewpoint. Moreover, no information is available about whether empirical correlations and procedures derived for hard grained soils are applicable to pumice deposits because there has been very little research done to examine the liquefaction characteristics of pumice. Basic geotechnical engineering concepts indicate that since pumice is crushable, then it is contractive; and when a material is contractive, it is liquefiable. Does this kind of reasoning also work for crushable soils like pumice?

To understand better the engineering characteristics of pumice, the research team, together with their colleagues in the Geomechanics group at the University of Auckland, have performed a number of laboratory studies (e.g., Pender, 2006; Pender et al., 2006; Kikkawa, 2008; Kikkawa et al., 2009, 2011a, b). We conducted K_0 compression testing on dry pumice sand with measurement of gas permeability to track particle crushing effects on void space reduction. Also, we examined the effect of vertical stress relaxation on the stress-strain relations of dense and loose pumice specimens. Moreover, we did heavy compaction on the pumice using vibration delivered by a Kango hammer and compared the stress-strain curves for the compacted pumice and one that has not been subject to vibratory compaction. All of these experiments were geared towards understanding the monotonic (static) behaviour of pumice sand.

As an extension of the earlier works mentioned above, we developed an experimental programme to investigate the cyclic/dynamic properties of pumice. The main focus of the research was to understand the undrained cyclic characteristics of undisturbed and reconstituted pumiceous soils through cyclic triaxial testing. Several undrained monotonic triaxial tests were also conducted to supplement the cyclic test results. Moreover, geotechnical investigations, including cone penetration testing and seismic dilatometer testing, were conducted at the sites where the undisturbed pumice samples were obtained. Finally, the validity of the conventional methods of evaluating the liquefaction resistance

developed for hard-grained sands was examined to see if they are applicable to crushable soils like pumice.

1.2 Purpose and Scope

In general, the major aim of this research is to investigate the liquefaction characteristics of pumice deposits, especially those found in the upper and central North Island. The detailed objectives are:

(1) to investigate the undrained cyclic response of undisturbed pumiceous soil samples through triaxial tests;
(2) to understand the undrained cyclic behaviour of loose and dense pumice deposits, and to compare their behaviour with those observed in typical (hard-grained) sands;
(3) to examine the effect of particle crushing during cyclic loading on the pore water pressure response and cyclic strength characteristics of pumice;
(4) to investigate the liquefaction characteristics of reconstituted pumice sands through monotonic undrained triaxial tests; and
(5) to establish the best possible method(s) of evaluating the in-situ liquefaction resistance of pumice deposits by examining the applicability of existing procedures commonly adopted for hard-grained sands.

Because of time and budgetary constraints, the undisturbed samples used in this study were taken at only two sites – one in Hamilton and another in Waihou. Although efforts were made to identify the possible test sites, access and testing schedule limited the sampling and testing at these two sites. The reconstituted specimens used in the triaxial tests consisted of commercially available pumice sands.

1.3 Relevance of the Study

This research study is in line with the Earthquake Commission's strategic aim of "understanding and assessing the hazards", particularly in formulating "new techniques for analysis of ground conditions that influence the local intensity and effect of seismic hazards". Moreover, this research involved the close collaboration between university researchers,

including some undergraduate students, and engineering contractors, who assisted in identifying possible sites and who performed the field tests.

The research project is very relevant to New Zealand conditions in three ways. Firstly, New Zealand lies in a tectonic region and earthquake-induced liquefaction could cause significant damage to the built-environment. Therefore, there is a need to investigate the dynamic behaviour of local soils in order to mitigate possible damage. Secondly, current methodologies of liquefaction potential evaluation are based on data from overseas derived primarily from hard-grained sands. There is no information available whether these procedures are applicable to pumice deposits, especially those found here in New Zealand. And thirdly, no significant study has been done in New Zealand as far as investigating the dynamic properties of local soils is concerned. Many consultants and practitioners have been constantly asking us for advice on how to evaluate the liquefaction susceptibility of pumice deposits. The outputs of this research will fill the knowledge gap in this area and produce design procedures which could be used by the local profession.

1.4 Organization of the Report

This report describes:

- a literature review of the performance of volcanic soils during past earthquakes and the engineering properties of pumice, as well as liquefaction potential evaluation procedures currently employed in practice;
- the soil properties of the pumice sands used in the tests as well as the outline of the laboratory testing procedures and field testing methods undertaken;
- the results of the monotonic and cyclic undrained triaxial tests conducted to develop an understanding of how the pumice sand behaves during undrained monotonic/cyclic loading;
- The assessment of the liquefaction resistance of pumice sand vis-à-vis hard-grained sand; and
- the major conclusions derived from this study and recommendations for future work.

2 LITERATURE REVIEW

2.1 General Remarks

As first stage, the performance of volcanic soils, especially pumice sands, during past earthquakes here in New Zealand and abroad is examined. Emphasis is placed on the 1987 Edgecumbe earthquake and on Japanese and South/Central American earthquakes which caused damage to soils of volcanic origin. In addition, known geotechnical properties of pumice sands are summarised. The results of the recent works of the research team, which were mentioned in Chapter 1, are compared with past studies to present a more comprehensive picture of the engineering properties of the material. To complete the picture, a review of the current state of practice in evaluating liquefaction potential of sandy deposits is discussed.

2.2 Performance of Volcanic Soils during Past Earthquakes

2.2.1 *Japan*

Japan has large areas covered by crushable volcanic ash sediments. With its high seismicity, failure of volcanic soils during earthquakes is very common (Ishihara and Harada, 1996; Miura and Yagi, 1995). These are particularly predominant in the south of Kyushu, particularly in Kagoshima Prefecture, where they are known as Shirasu. These ash deposits are frequently exposed as soft rock escarpments which are mined for use in reclaimed land fill. It is frequently pumped from inland locations as slurry to form a loose saturated fill. The Shirasu has an essential feature of a porous solid resulting from a pyroclastic material (Suzuki and Yamamoto, 2004). The particle density of Shirasu (G_s=2.4-2.5) is generally lower when compared with that of other sandy soils. Shirasu is also very crushable due to the brittleness of the soil particles. During the 1968 Ebino earthquake, sand boiling due to liquefaction was observed on the plains and river terraces formed from Shirasu and subsidence of bridge piers was reported (Yamanouchi, 1968). In addition, structural damage due to liquefaction was

observed during the 1997 Northwestern Kagoshimaken earthquake in areas of coastal land reclamation at Akune harbour and Izumi and inland at Iriki (Okabayashi et al. 1998). During the same earthquake, the occurrence of re-liquefaction in a Shirasu ground which had once liquefied during the main shock was reported (Yamamoto et al., 1997).

During the 2003 Sanriku-Minami Earthquake which occurred in Tohoku, Japan, it was reported that the failed soil of volcanic origin, which is shown in Figure 2.1(a), behaved like mud and flowed laterally over a distance of 180 m in spite of the gentle slope of the ground (JSCE-JGS, 2003; Uzuoka et al., 2005). Because the soil at the source of failure and the flowed mass were unsaturated, it is difficult to explain how such movement over a long distance could occur without considering the possible occurrence of soil liquefaction. Such cases involving unsaturated volcanic soils undergoing flow-type of failure have also been reported during other earthquakes (e.g., Mishima & Kimura, 1970).

2.2.2 *South and Central America*

Following the February 27, 2010 Maule, Chile earthquake (M_w = 8.8), manifestations of soil liquefaction were observed along the shore of the Villarica Lake Temuco (Crenairz 2010). At some locations, sands of lighter colour were seen on top of the essentially very dark and almost black sand from volcanic origin (Villarica Volcano was about 13 km away), as illustrated in Figure 2.1(b). The sand at these spots was mixed with some light-brown coloured type of soil, forming circular holes on the ground. A ground crack was also observed on the beach, while a few hundred meters away, a large section of the long flat beach sank by about 3 m.

Most of the landslides during the 2001 El Salvador Earthquake occurred in the central volcanic ridge running east to west of the country. The geographic distribution of landslide sites in the country roughly corresponds to locations of young volcanic soils in valleys (Orense et al., 2002). Of particular interest are the large-scale landslides and shallow slope failures that occurred in the Cordillera del Bálsamo, such as the one that occurred in Las Colinas where many people died. At this site, clear stratification of the tuffs and pumice was distinctly observed and some soil layers in the slope were moist, but not saturated (Figure 2.1c). Based on observations, two conceivable phenomena arose regarding the role of water in the Las Colinas landslide. Firstly, liquefaction may have occurred in the saturated volcanic

materials (pumice) overlying the less permeable loamified soil layer, triggering the flow-like failure of the slope. Secondly, water may have been released anywhere within the failure plane during the earthquake, causing the decrease in the shear strength of the materials. If the materials were collapsible soils with some degree of cementation in unsaturated condition, water infiltration could have easily destroyed the cementation and resulted in collapse of the soil structure.

2.2.3 *New Zealand*

Closer to home, the 1987 Edgecumbe earthquake (M=6.3) induced widespread liquefaction such as sand boils and lateral spreading of embankments (Pender and Robertson 1987). The occurrence of these sand boils, as shown in Figure 2.1(d), was restricted to the immediate epicentral area of the Rangitaiki Plains, which lie at the northeast end of the Taupo Volcanic Zone (TVZ). The alluvial soils comprising the plains are transected by the a river system (Tarawera, Rangitaiki and Whakatane rivers) which has changed significantly throughout the Holocene due mainly to the deposition of large amounts of volcanically derived pumice alluvium and ash which buried pre-existing river channels on a number of occasions. Although widespread, soil liquefaction was generally confined to those areas containing saturated flood plain sediments and buried river channels. It involved loose sand and silt size soils from horizons as much as 12 m below the ground surface (Franks, 1988).

Other ground damage resulting from liquefaction of underlying soils included lateral spreading of the ground surface, in particular man-made embankments. This type of damage affected a number of flood control and road embankments close to the main rivers of the plain and often produced secondary damage in the form of stopbank or embankment slumping-type failures. This was most evident along the Tarawera River and, to a limited extent, along the Rangitaiki and Whakatane rivers.

(a)

(b)

(c)

(d)

Figure 2.1: Failure of volcanic soils during past earthquakes: (a) failure of gentle fill slope in Tsukidate town (Japan) during the 2003 Sanriku-Minami Earthquake (photo courtesy of Kokusai Kogyo, Ltd.); (b) sand boils observed in Villarica Lake Temuco after the 2010 Maule (Chile) earthquake (photo by Crnaiz, 2010); (c) the Las Colinas landslide during the 2001 El Salvador Earthquake; and (d) sand boils near Powell Road during the 1987 Edgecumbe earthquake (photo by GNS Science).

2.3 Engineering Properties of Pumice

Pumice is characterised by soft vesicular grains of low crushing strength, giving the material high void ratio and high compressibility. To understand better the engineering characteristics of pumice, the research team, together with their colleagues in the Geomechanics group at the University of Auckland, have performed a number of laboratory studies.

Wesley (2001) investigated the specific gravity of pumice sand of various particle sizes by two methods, i.e., NZ standard method with and without vacuum air extraction. He observed that the specific gravity of pumice sand decreased with increasing particle size, indicating that the proportion of internal voids into which water penetrates increased with increasing particle size. In addition, he noted that because the specific gravity of the soil particles measured by both methods was not the same as that of quartz (which is about 2.65) even when the particle size was 0.04 mm, some internal voids may not be interconnected to the outside surface. Therefore, it is necessary to distinguish between internal voids of particles and voids consisting of spaces between particles. Then, when a particle is crushed, the voids would increase because the internal voids would be exposed outside and manifest themselves as voids between particles.

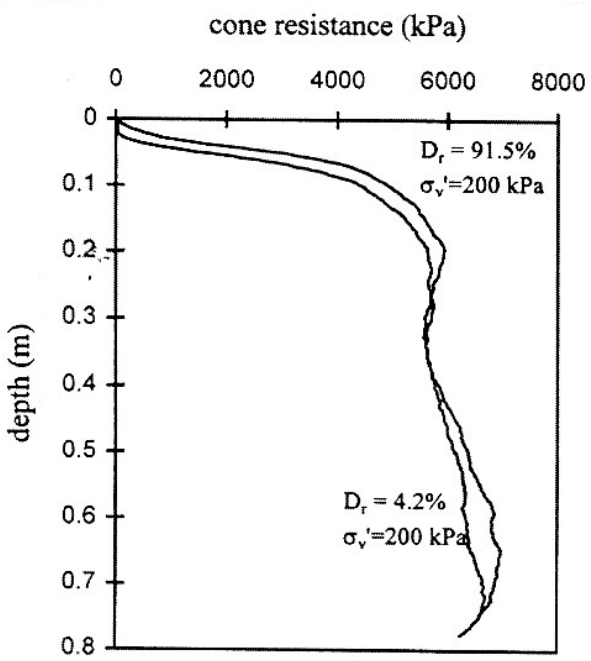

Figure 2.2: CPT resistance obtained from calibration chamber testing of loose and dense pumice sand (Wesley et al., 1999).

Moreover, previous research showed that the q_c values obtained from cone penetration tests (CPT) on pumice sand were only marginally influenced by the density of the material, as shown in Figure 2.2. It was also noted that pumice sand showed very gentle increase with confining stress as compared to normal (i.e. hard grained) sands (Wesley et al. 1999). Thus, conventional relationships between q_c value, relative density, and confining stress are not

valid for these soils. Therefore, alternative relationships specifically for pumice sands need to be developed.

In order to investigate the characteristics of pumice, we scanned pumice particles using an X-ray CT scanning machine (Kikkawa et al. 2009). Figure 2.3 shows a horizontal cross-sectional binary image of a pumice particle of length about 4.3 mm. It can be observed that there are not only surface voids but also internal voids. The surface voids are interconnected with the outside surface but the internal voids are not connected with the outside surface. The presence of these surface and internal voids makes the pumice particles easily deformable. From CT images, we calculated the solid density of pumice particles as 2.2 g/cm^3, which was almost the same as the density corresponding to a particle size ~75 μm as measured using the standard method (2.34 g/cm^3). The apparent density of pumice sands was calculated as 0.89 g/cm^3, which was lower than the density of water; that is why almost all pumice particles float on water. Based on digital analysis of CT images, pumice particles are very fragile not only because they are porous but also because they are angular in shape; it is the combination of these two factors that makes the particles highly crushable (Kikkawa et al. 2011b).

Figure 2.3. Cross-sectional binary image of one pumice particle.

We also conducted K_0 compression testing on dry pumice sand with measurement of gas permeability to track particle crushing effects on void space reduction (Kikkawa 2008). Also, we examined the effect of vertical stress relaxation on the stress-strain relations of dense and loose pumice specimens. The test results showed that stress relaxation increased with increasing displacement rate and the differences between the stress relaxation in loose and dense pumice sands increased with increasing displacement rate.

Finally, we performed hydrostatic compression, consolidated drained (CD) and undrained (CU) tests on loose and compacted pumice sand (Kikkawa et al, 2011a). Heavy compaction was implemented using vibration delivered by a Kango hammer. We compared the stress-strain curves for the compacted pumice and one that has not been subject to vibratory compaction. It was found that although there was substantial volume change in the pumice sand during hydrostatic compression, negligible particle crushing occurred in these tests. On the other hand, substantial particle crushing was induced during CD and CU testing. From the tests, it was clear that particle crushing was caused by the application of shear stress rather than by normal stress.

All of these experiments were geared towards understanding the monotonic (static) behaviour of pumice sand. Indeed, all the tests results shown so far indicate that pumice is a special type of soil, possibly the most fragile of the suite of crushable sands found at various locations around the world. How it responds to cyclic loading, such as that induced by earthquakes, is of interest not only to practicising engineers but to researchers as well who are working on the micro and macro-mechanics of granular media.

2.4 Evaluation of Liquefaction Potential of Sands

It is widely recognized that the basic mechanism of liquefaction in a deposit of loose saturated sand during earthquakes is the progressive build-up of excess pore water pressure due to application of cyclic shear stresses induced by the upward propagation of shear waves from the underlying rock formation. When the state of sand packing is loose enough and the magnitude of cyclic shear stress is great enough, the pore pressure builds-up to a point where it becomes equal to the initial confining stress. At this state, no effective stress or inter-granular stress is acting on the sand, and the individual particles are in suspended state. Thus the soil loses its strength and behaves as liquid, and the liquefied soil mass can undergo large deformation.

2.4.1 *Liquefaction Susceptibility*

The susceptibility of soil deposits to liquefaction is determined by a combination of various factors to which they may be subjected, such as soil properties, geological conditions and ground motion characteristics. These factors are summarized in Table 2.1. Note that soil properties and geological conditions determine the resistance of the deposit to liquefaction, while earthquake characteristics control the seismic loading conditions.

Table 2.1: Factors affecting liquefaction susceptibility

Soil Properties	Unit weight, grain size characteristics, relative density, fines content, soil structure, shear modulus, damping ratio, degree of saturation
Geological conditions	Geologic history (aging, cementation), effective confining pressure, initial static shear stress, overconsolidation ratio, boundary conditions (drainage, seepage, deformation), lateral earth pressure coefficient
Earthquake Characteristics	Intensity of ground shaking (horizontal acceleration, magnitude) duration of shaking (or number of cycles), direction of shearing, strain level

Among the factors listed above, the three most important ones are the following:

- The ground is loose sandy deposit
- The ground water table is high and the ground is saturated
- The earthquake intensity is sufficiently large and the duration of shaking is sufficiently long

2.4.2 *Factor of Safety against Liquefaction*

Various methods have been proposed for predicting the liquefaction potential of soils. The most commonly adopted methods in practice generally consists of the following steps:

(1) estimation of liquefaction resistance of soils in a deposit (or seismic capacity), *CRR*.

(2) estimation of the maximum or equivalent cyclic shear stress likely to be induced in the

soil deposit during an earthquake (or seismic demand), *CSR*.

(3) estimation of liquefaction potential of the deposit, based on (1) and (2). The liquefaction potential is usually expressed in terms of Factor of Safety Against Liquefaction, F_L, and is given by:

$$F_L = \frac{CRR}{CSR} \tag{2.1}$$

If $F_L < 1.0$, the shear stress induced by the earthquake exceeds the liquefaction resistance of the soil and therefore, liquefaction will occur. Otherwise, when $F_L \geq 1.0$, liquefaction will not occur. A detailed discussion of various methods currently used in geotechnical engineering practice is presented by Youd et al. (2001).

2.4.3 *Evaluation of CSR*

Seed and Idriss (1971) proposed a simplified procedure to estimate the cyclic shear stress induced by the earthquake. In this procedure, the cyclic shear stress ratio, *CSR*, developed at a particular depth beneath a level ground surface is estimated by

$$CSR = \frac{\tau_{ave}}{\sigma_v'} = 0.65 \frac{a_{\max}}{g} \frac{\sigma_v}{\sigma_v'} r_d \tag{2.2}$$

where τ_{ave} is the average cyclic shear stress during a particular time history, σ_v' and σ_v are the effective and total vertical overburden stresses, respectively, at the depth in question, a_{max} is the peak horizontal ground acceleration generated by the earthquake and g is the acceleration due to gravity. Several expressions have been proposed for the stress reduction factor, r_d, which is expressed as a function of depth; one expression is

$$r_d = \begin{cases} 1.0 & z \leq 4\text{m} \\ 1 - 0.015(z-4) \geq 0.6 & z > 4\text{m} \end{cases} \tag{2.3}$$

On the other hand, a plausible method for evaluating the liquefaction resistance is to retrieve and test good-quality undisturbed soil specimens in the laboratory, as done routinely in Japan. One method is to freeze the soil using liquid nitrogen and then frozen soil cores are obtained

(Yoshimi et al., 1978; Hatanaka et al., 1985). Because the cost in getting good-quality samples is quite prohibitive for typical projects and to avoid the difficulties associated with sampling and laboratory testing, field tests, such as the standard penetration test (SPT), the cone penetration test (CPT) and shear-wave velocity measurements (V_s) have become the state-of-practice for routine liquefaction investigations.

2.4.4 *Evaluation of CRR using SPT-based Procedure*

The Standard Penetration Test (SPT) is employed to determine the SPT *N* value, which gives an indication of the soil stiffness and can be empirically related to many engineering properties. The test is conducted inside a borehole. A split spoon sampler is attached to the bottom of a core barrel and lowered into position at the bottom of the borehole. The sampler is driven into the ground by a drop hammer weighing 68 kg falling through a height of 76 cm. The number of hammer blows is counted. The number required to drive the sampler three successive 150 mm increments is recorded. The first increment (0-150 mm) is not included in the *N* value as it is assumed that the top of the test area has been disturbed by the drilling process. The SPT *N* is the number of blows required to achieve penetration from 150-450 mm. The hammer weight, drop height, spoon diameter, rope diameter etc. are standard dimensions. After the test, the sample remaining inside the split spoon is preserved in an airtight container for inspection and description.

Criteria for evaluation of liquefaction resistance based on the SPT are largely embodied in the *CSR* versus $(N_1)_{60}$ plot reproduced in Figure 2.4. $(N_1)_{60}$ is the SPT blow count normalized to an overburden pressure of approximately 100 kPa (1 ton/ft^2) and a hammer energy ratio or hammer efficiency of 60%. The normalization is usually done using the following equation:

$$(N_1)_{60} = C_n \frac{ER_m}{60} N_m \tag{2.4}$$

where C_n is a correction coefficient for overburden pressure $C_N = \sqrt{98/\sigma_v'(\text{kPa})}$, ER_m is the actual energy efficiency delivered to the drill rod, and N_m is the measured *N*-value. Hence, knowing $(N_1)_{60}$, the cyclic stress ratio required to induce liquefaction for a *M*7.5 earthquake can be obtained from the figure. For earthquakes of other magnitudes, the appropriate cyclic

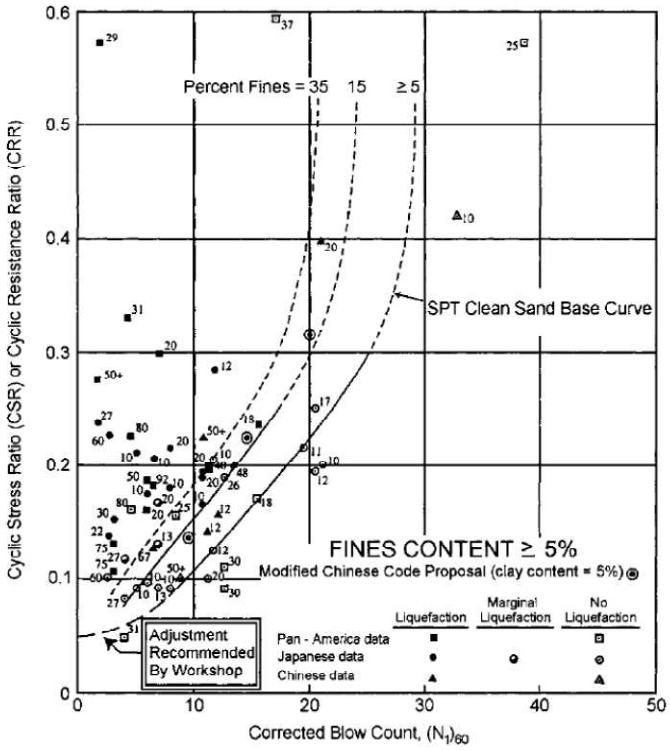

Figure 2.4: Relationship between stress ratios causing liquefaction and $(N_1)_{60}$ value for M=7.5 earthquakes (after Youd et al. 2001).

stress is obtained by multiplying it with a magnitude scaling factor, *MSF*. The *CRR* curves on this figure were conservatively positioned to separate regions with data indicative of liquefaction from regions with data indicative of non-liquefaction. Curves were developed for granular soils with the fines contents of 5% or less, 15%, and 35% as shown on the plot. The *CRR* curve for fines contents <5% is the basic penetration criterion for the simplified procedure and is referred to as the ‘‘SPT clean-sand base curve.’’ The flowchart of this procedure is summarised in Figure 2.5.

Note from Figure 2.4 the apparent increase in *CRR* with increased fines content. Whether this increase is caused by an increase in liquefaction resistance or a decrease in penetration resistance is not clear. The effect of fines content on *CRR* is considered by adjusting $(N_1)_{60}$ to an equivalent clean sand value $(N_1)_{60cs}$

$$(N_1)_{60cs} = \alpha + \beta(N_1)_{60} \tag{2.5}$$

where α and β are coefficients determined from the following relationships:

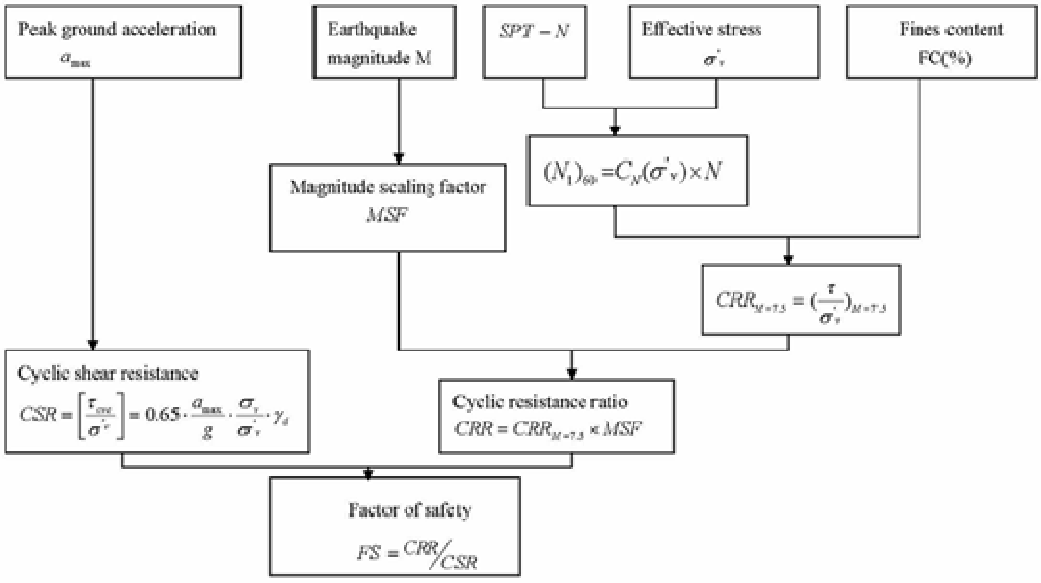

Figure 2.5: Evaluation of soil liquefaction based on Seed-Idriss approach

$$\beta = \begin{cases} 1.0 & \text{for } F_c \le 5\% \\ \left[0.99 + \left(F_c^{1.5}/1000\right)\right] & \text{for } 5\% < F_c < 35\% \\ 1.2 & \text{for } F_c \ge 35\% \end{cases} \quad (2.6a)$$

$$\alpha = \begin{cases} 0 & \text{for } F_c \le 5\% \\ \exp\left[1.76 - \left(190/F_c^{2}\right)\right] & \text{for } 5\% < F_c < 35\% \\ 5 & \text{for } F_c \ge 35\% \end{cases} \quad (2.6b)$$

2.4.5 *Evaluation of CRR using CPT-based Procedure*

Cone Penetration Test (CPT) is conducted to obtain the cone resistance, the side friction and, if there is a piezocone, the pore pressure in the deposit. A primary advantage of the CPT is that a nearly continuous profile of penetration resistance is developed for stratigraphic interpretation. The continuous profile also allows a more detailed definition of soil layers. In the test, a 60^o cone with face area 10 cm^2 and 150 cm^2 'friction sleeve' is hydraulically pushed into the ground at a constant speed (ranging from 1.5 to 2.5 cm/s). The force required to maintain this penetration rate, and the shear force acting on the friction sleeve is recorded.

Liquefaction potential can also be evaluated using the results of cone penetration tests. In fact, procedures which use CPT resistance are very similar to those using SPT resistance. Based on in-situ investigation, a boundary can be defined separating liquefiable from non-liquefiable conditions, as shown in Figure 2.6. In the graph, qc1 is the cone tip resistance, q_c, normalized by the overburden pressure, σ_{v0}':

$$q_{c1} = \frac{q_c}{P_a}\left(\frac{P_a}{\sigma_{v0}'}\right)^n \tag{2.7}$$

where Pa = 1 atm of pressure in the same unit as σ_{v0}' and n = exponent that varies with the soil type. Thus, once the cone penetration resistance q_c for a deposit is known, the liquefaction resistance can be estimated from the chart and, consequently, the liquefaction potential can be evaluated. A primary advantage of the CPT is that a nearly continuous profile of penetration resistance can be developed for stratigraphic interpretation. As a result, a continuous profile of factor of safety against liquefaction can be obtained.

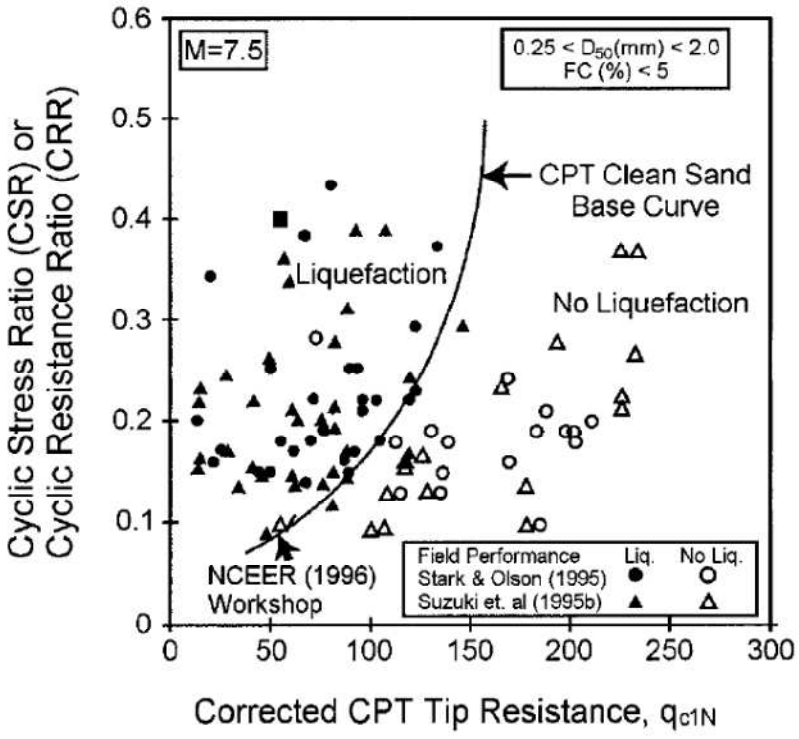

Figure 2.6: Curve recommended for calculation of *CRR* from CPT data (Robertson and Wride, 1998).

2.4.6 *Evaluation of CRR using V_s-based Procedure*

Shear wave velocity tests measure the small-strain shear modulus (stiffness) of the soil, and thus they represent an engineering property measurement rather than an index test. There are several different methods for measuring V_s in situ, such as cross hole, downhole, seismic CPT, seismic dilatometer and spectral analysis of surface waves (SASW). A general advantage of V_s tests is that they can be used for sites underlain by soils that are difficult to penetrate (e.g., gravel, cobble, etc); on the other hand, they provide very limited spatial resolution for characterizing site stratigraphy and heterogeneity and sampling is not possible.

The shear wave velocity of the deposit can also be used to evaluate its liquefaction potential. Essentially, the procedure is similar to other penetration-based approaches, and the boundary curves separating liquefaction and non-liquefaction obtained by various researchers are shown in Figure 2.7. In the plot, the shear wave velocity is normalized using the following equation:

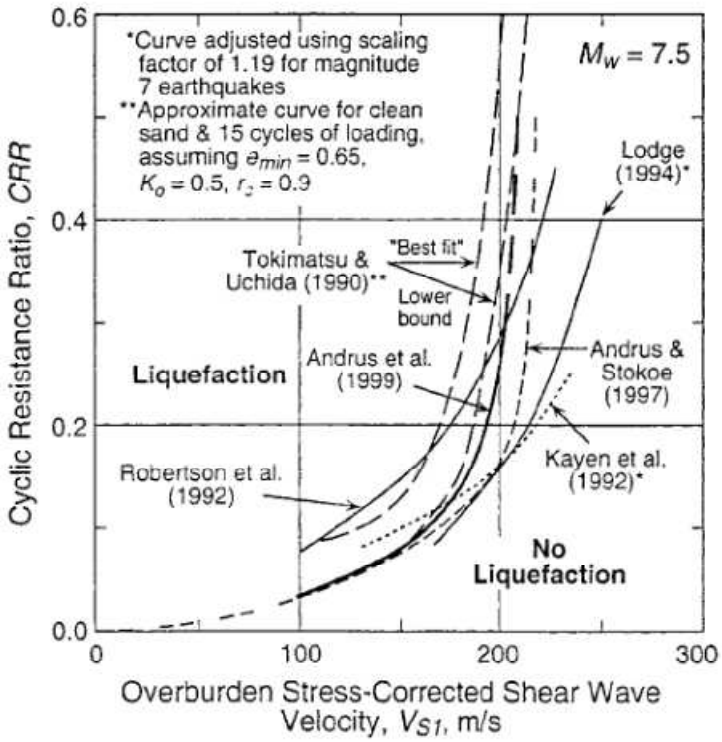

Figure 2.7: Curves showing the relation between *CRR* and normalized V_s (Youd et al., 2001).

$$V_{s1} = V_s \left(\frac{P_a}{\sigma'_{v0}} \right)^{0.25} \tag{2.8}$$

where V_{s1} is the overburden stress-corrected shear wave velocity, P_a is the atmospheric pressure (100 kPa) and σ'_{v0} is the initial vertical stress in the same units as P_a. The above equation assumes a constant coefficient of earth pressure of K_0=0.5.

2.4.7 *Evaluation of CRR using Procedure based on SDMT*

The seismic dilatometer SDMT offers an alternative or integration to current methods for evaluating the liquefaction resistance of sands based on CPT or SPT, within the framework of the simplified penetration tests vs case histories based approach. SDMT is the combination of the traditional "mechanical" flat dilatometer introduced by Marchetti (1980) with a seismic module placed above the DMT blade. The SDMT module is a probe outfitted with two receivers for measuring the shear wave velocity V_S of the soil profile. In essence, SDMT provides, among other measurements, two parameters that previous experience has indicated as bearing a significant relationship with the liquefaction resistance of sands: the shear wave velocity, V_S, whose relationship with liquefaction resistance has been illustrated above, and the horizontal stress index K_D, whose use for liquefaction studies was summarized by Monaco et al. (2005) and Marchetti et al. (2008). The curve correlating *CRR* and K_D is shown in Figure 2.8. The advantage of SDMT is that two independent evaluations of liquefaction resistance at each test depth can be obtained from K_D and from V_S (redundant correlations); on the other hand, unlike the CPT- and SPT-based correlations which are supported by large databases, SDMT correlations are based on a smaller database.

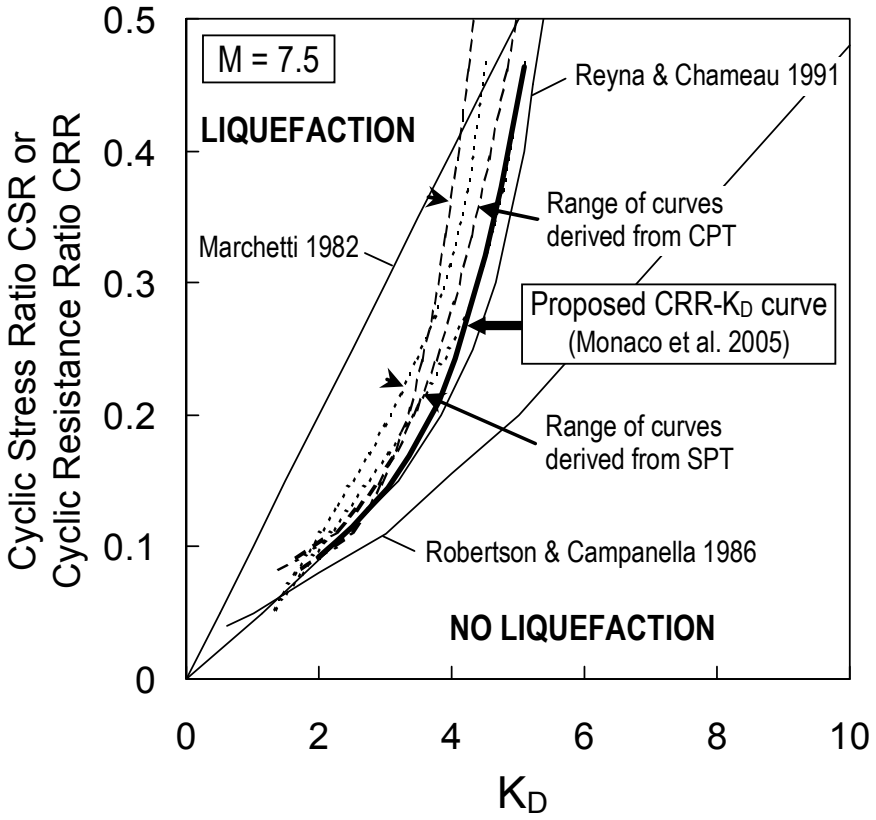

Figure 2.8: *CRR-K_D* curves for evaluating liquefaction resistance from DMT (Monaco et al., 2005).

3 SOILS USED AND TEST PROCEDURES

3.1 General Remarks

Two sets of samples were used in the laboratory tests: “undisturbed” soils samples obtained at two sites in North Island, and “reconstituted” samples using commercially available pumice sand. The properties of these materials are described in this chapter, together with a general description of the sites where the undisturbed samples were obtained.

The undrained triaxial tests (monotonic and cyclic) were conducted in the Geomechanics Laboratory of the University of Auckland. Two different triaxial machines were used for the monotonic and cyclic undrained tests. In addition, field tests consisting of cone penetration tests (CPT) and seismic dilatometer tests (SDMT) were performed at the sites where the undisturbed samples were obtained. This chapter also outlines the testing concept and the testing procedures used to prepare and perform the undrained triaxial tests as well as the SDMT tests.

3.2 Sampling and Field Testing Sites

Undisturbed samples were obtained at two sites: (1) at Carrs Road in Hamilton; and (2) Mikkelsen Road in Waihou.

3.2.1 *Carrs Rd Site*

The test site is located at the Carrs Road Interchange, which was being modified as part of the Hamilton Ring Road Upgrade Extension (HRRUE) project of the Hamilton City Council. The project will extend the Wairere Drive 4-lane configuration from Crosby Road to Cambridge Road. AECOM were commissioned to undertake the design of this section of the project while Hiway GeoTechnical Ltd (HGT) was invited to provide possible ground

improvement options. The researchers coordinated with AECOM and HGT to obtain undisturbed soils samples and to perform CPT and SDMT at the site.

The geological profile at Carrs Road site consists of interbedded and intertonged layers of sandy silts and silty sands of the Hinuera Formation to a depth of over 30 m. At the Carrs Road Interchange, the proposed main alignment intersects an ash hill. The geological profile here consists typically around 6 m of ash or residually weathered ignimbrite, underlain by around 6-8 m of moderately to highly sensitive, completely weathered (CW) ignimbrite. The sensitivity of the CW ignimbrite was observed during the site investigation when sections of the borehole core were recovered in a fully liquefied state and the CPT cone resistance was extremely low (q_c < 0.1MPa; F_r < 1%). A further complication is that at the Carrs Road interchange, the proposed main alignment will be in 6 m of cut and will therefore rest on the CW ignimbrite layer. The drillhole log and CPT sounding data for this site are shown in Appendix A.

3.2.2 *Mikkelsen Rd Site*

The test site is located on the southern part of the Transpower Substation in Mikkelsen Road, Waihou, about 40 km east-northeast of the Carrs Rd site. Initially, AECOM performed detailed investigation at the site as part of the upgrade project being undertaken by Transpower. Undisturbed samples were provided by AECOM, while we commissioned additional CPT and SDMT to be performed at the site.

Similar to the one in Carrs Road, the geological profile at Mikkelsen Road consists of interbedded and intertonged layers of sandy silts and silty sands of the Hinuera Formation (described as current bedded fluviatile pumice, rhyolote and ignimbrite sands and gravels interbedded with organic silts) to a depth of over 20 m. The drillhole log and CPT sounding data for this site are shown in Appendix B.

3.3 Soils Tested

The soils tested in this study were all pumiceous soils – two were sourced from the central portion of North Island detailed in Section 3.2 while the third was the commercially available pumice sand.

The undisturbed Carrs Rd samples were obtained at depths between 8.0-8.5 m using 60 mm diamater push tubes in December 2009; the samples were completely to heavily weathered ignimbrite and consisted of light brown-yellow/white silt. The closest SPT *N*-value was 18 (at depth=15 m). On the other hand, the undisturbed Mikkelsen Rd samples were sourced at three depths: 3.0-3.3 m, 6.0-6.6 m and 12.0-12.4 m. Sampling was done in November 2010 using 60 mm push tubes. The soils obtained were generally light grey white fine to coarse sand, predominantly pumice. The SPT *N*-values were 11 and 13 at depth=4.5 m and 6.6 m, respectively. Because of its loose nature (some cores were lost), the push tubes were placed in a freezer for 1-2 days before they were extracted. Although the two sets of samples thus taken may have been "disturbed" one way or the other, the degree of disturbance may be considered insignificant, as the samples maintained their soil structure and fabric; thus they are referred to as 'undisturbed" in this report.

Most of the tests presented in this report were performed on commercially-available pumice sand. This is not a natural deposit but was derived by processing sand from the Waikato River. The particles were centrifugally separated from the other river sand particles so that the samples consist essentially of pumice grains. This material has been used extensively in the Geomechanics Laboratory of the University of Auckland as discussed in the previous chapter. Pumice sands with three different grading curves were used: Pumice-A sand (0.075 – 2.0 mm), Pumice-B sand (0.15 – 0.60 mm) and Pumice-C sand (F_c=50%); the last was used to investigate the effect of crushed particles on the cyclic response of the soil.

The properties of the tested soils, obtained using methods based on NZ Standards (1986), are shown in Table 3.1 while the corresponding grain size distribution curves are shown in Figure 3.1. It is observed from the grain size distribution curves that the Carrs Rd samples have very high fines content (F_c, defined here as the percentage by weight of particles smaller than 0.075 mm). For the pumice sand, the specific gravity of the material generally increases as the mean particle size D_{50} decreases, similar to the observation made by Wesley (2001). A

comparison of the void ratio characteristics of pumice sand is shown in Figure 3.2, where it is observed that pumice more or less fits the trend for most natural (hard-grained) sands. Note however that methods to determine the maximum and minimum void ratios were based on NZ Standards, whereas those shown in the figure for hard-grained sands were determined using Japanese standards.

Table 3.1: Properties of the soils used.

Material	Specific Gravity	Maximum void ratio	Minimum void ratio
Carrs Rd	2.65[1)]	N/A[2)]	N/A[2)]
Mikkelsen Rd	2.49	1.165	0.717
Pumice-A sand	1.95	2.584	1.760
Pumice-B sand	2.10	2.640	1.420
Pumice-C sand	2.38	2.091	1.125

1) Taken from AECOM Technical Report

2) Not applicable since sample has very high fines content

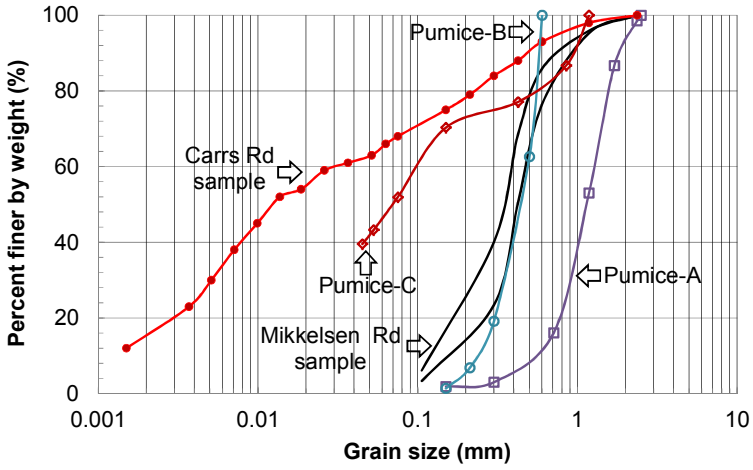

Figure 3.1: Grain size distribution curves of soils used in the tests.

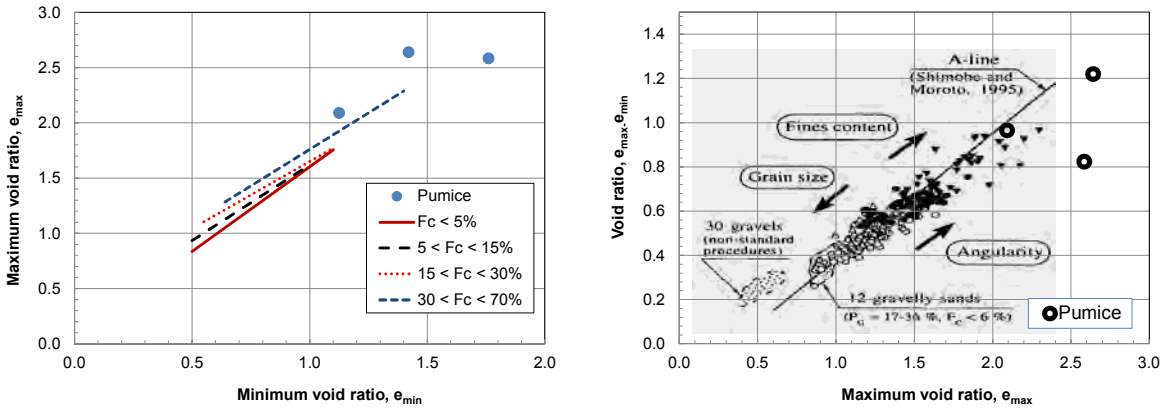

(a) (b)

Figure 3.2: Comparison of void ratios of pumice with natural sands: (a) e_{max} vs. e_{min} relation; and (b) e_{max} vs e_{max}–e_{min} relation (modified from Cubrinovski and Ishihara, 2002).

3.4 Laboratory Test Procedures

Laboratory tests are usually performed on relatively small specimens that are assumed to be representative of the soil in-situ. The specimens are usually tested as "elements" under uniform initial stresses and uniform changes in stress/strain conditions. Laboratory testing has been a very important tool in investigating the seismic behaviour of soils.

Undrained monotonic and cyclic triaxial tests were conducted on reconstituted pumice sand specimens, while only cyclic tests were conducted on the undisturbed samples from Carrs Rd and Mikkelsen Rd sites. Details of the triaxial test apparatus, sample preparation, and testing procedures are described below.

3.4.1 *Triaxial Testing*

The triaxial test apparatus has been widely used for testing cohesionless soils in the laboratory under both monotonic and cyclic loading conditions. Although the basic design is the same as the conventional triaxial apparatus used for testing cohesive soils, cyclic triaxial testing requires that the apparatus be capable of applying extensional loads to the specimen so that triaxial extension can be produced cyclically within the specimen. During the triaxial

test, the sample is consolidated under a confining pressure and subjected to a sequence of constant-amplitude cyclic axial stress (under undrained conditions). This loading procedure creates stress conditions on a plane of 45° through the sample which is the same as those produced on the horizontal plane in the ground during earthquakes. The stress conditions under each stage of loading are illustrated in Figure 3.3. When the axial stress, referred to as deviator stress, σ_d, is applied undrained, the shear stress induced on the 45° plane is $\sigma_d/2$. The normal stress $\sigma_d/2$ is also induced on this plane but this purely compressive component does not cause any change in the effective confining stress σ_c', and therefore can be disregarded.

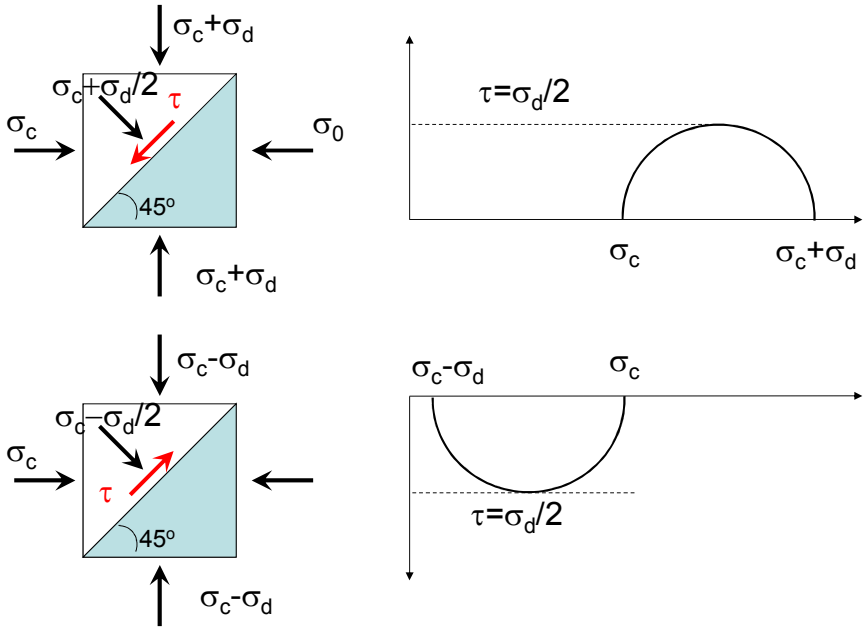

Figure 3.3: Stress state in cyclic triaxial test

3.4.2 *Triaxial Test Apparatus*

All tests were carried out in a temperature-controlled laboratory room. The undrained monotonic tests were performed using the gear-type apparatus shown in Figure 3.4(a) where the samples used have 38 mm diameter. On the other hand, the loading for the cyclic triaxial tests was provided by an MTS machine, as illustrated in Figure 3.4(b).

(a)

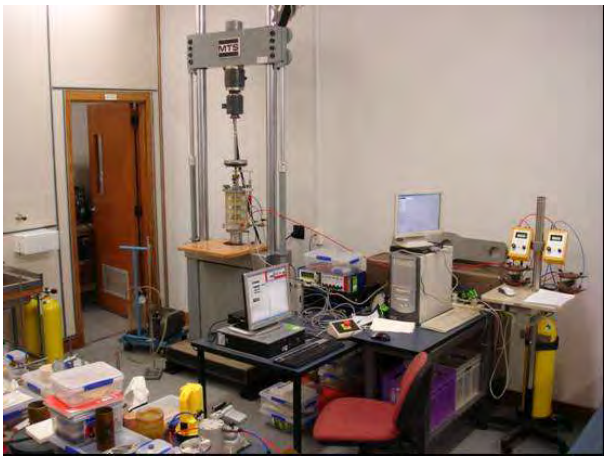

(b)

Figure 3.4: Triaxial machines used in the tests: (a) for monotonic CU tests; and (b) cyclic undrained tests.

3.4.3 *Sample Preparation*

Undisturbed specimen

After obtaining the soil samples from the site using 60 mm push tubes, they were carefully transported to the laboratory. In case the soil sample was deemed stable, they were extracted from the tube using hydraulic jack (see Figures 3.5a-b). In some cases, the soil sample was deemed loose and extracting them straight away will destroy the structure and fabric; this was noted in the soil samples taken from shallow depths (3 m and 6 m) at Mikkelsen Rd site. In these cases, the tubes, with the soil sample inside, were placed in a freezer for 1-2 days. Then, the frozen specimen was extruded from the sampling tube (see Figure 3.5c). Trimming was carried out at the two ends of the specimens for the preparation of square ends. The height of the specimen used was 120 mm for the Carrs Rd samples, and 100 mm for Mikkelsen Rd samples (due to sample unavailability). Filter papers were placed at the ends to prevent clogging of the porous discs. The specimen was placed inside a rubber membrane and for frozen specimens, they were allowed to thaw prior to testing. Saturation of the specimen was ensured by allowing water to enter the specimen by increasing the back pressure. B-value check was carried out to confirm that fully saturated condition had been achieved. Specimens were then isotropically consolidated at the target effective confining pressure, σ_c'.

Reconstituted specimen

For the reconstituted specimens, it was not easy to completely saturate the pumice sand because of the presence of voids from the surface to the particle interior. For this purpose, saturated specimens were made using de-aired pumice sands, i.e., sands were first boiled in water to remove the entrapped air. To prepare the test specimens, the sand was water-pluviated into a two-part split mould which was then gently tapped until the target relative density was achieved. Next, the specimens were saturated with appropriate back pressure and then isotropically consolidated at the target effective confining pressure, σ_c'. B-values > 0.95 were obtained for all specimens. The test specimens for the monotonic tests were 38 mm in diameter and 80-85 mm high (see Figure 3.5d), while for the cyclic tests, they were 75 mm in diameter and 150 mm high (see Figure 3.5e).

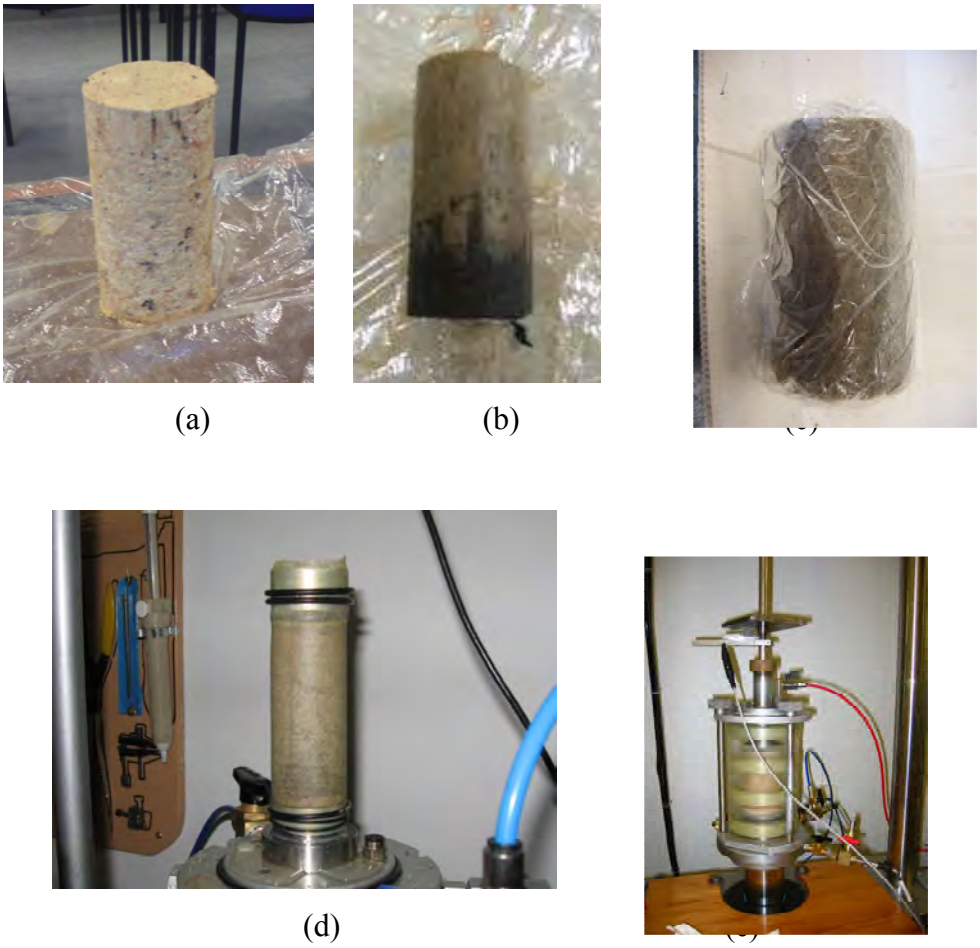

Figure 3.5: Soil samples used in the test: (a) undisturbed sample from Carrs Rd site; (b) undisturbed sample from 12 m depth of Mikkelsen Rd site; (c) frozen undisturbed sample from 6 m depth of Mikkelsen Rd site; (d) reconstituted dense pumice sand specimen used in monotonic tests; and (e) reconstituted pumice specimen in the cyclic triaxial cell.

3.4.4 *Shearing*

Monotonic tests

Undrained montonic loading was applied to the specimens using axial compression. The loading rate for the tests was 0.015 mm/min. To begin shearing, the back pressure valve was closed (undrained test). The target strain was 30% to observe the specimen under the steady state of deformation. Some specimens did not reach this strain level due to a number of factors, such as irregular specimen deformations and erratic load cell readings, rendering the data unreliable.

Cyclic tests

The cyclic loading in the tests were applied by a hydraulic-powered loading frame from Material Testing Systems (MTS). Since stress-reversal (the MTS machine needed to apply both compressive and tensile loads on the specimen) was required in the tests, special arrangements were made to the testing setup to allow for a seamless transition when the axial force changed from compression to tension on the specimen and vice versa:

(a) The cell base was screwed to the MTS actuator to prevent separation when a high tensile force was applied.
(b) A ball and socket top cap, with a rotating nut on top, was used instead of the conventional top cap. Because the thread size in the nut matched that of the screw thread on the bottom end of the loading ram (referred to as loading ram A), this allowed the ram to be tightened onto the top cap after the triaxial cell had been put in place.
(c) The external load cell was screwed to the top of loading ram A once the triaxial cell had been assembled. Loading ram A was housed inside linear ball bushing to minimise ram friction.
(d) A flat plate was put on top of the load cell to facilitate the placement of weights which were used to counteract cell pressure uplift.
(e) A second loading ram (referred to as loading ram B), which was screwed on top of the load cell, could be connected to the cross-head of the MTS machine via the union nut hanging on the cross-head.

A sinusoidal cyclic axial load was applied in the tests at a frequency of 0.1Hz under undrained condition. Initially, the plan was to proceed loading until the specimen began to show signs of liquefaction, which was indicated by a sudden runaway axial deformation developed in the specimen accompanied by the equalisation of cell and pore pressures. Very

few of the specimens however demonstrated this type of failure. Instead, termination of the testing was determined by top cap separation. In some tests, the application of cyclic deviator stress was terminated when the prescribed number of load applications was reached. In addition to the axial load, the cell pressure, pore pressure, volume change and axial displacement were all monitored electronically and these data were recorded via a data acquisition system onto a computer for later analysis.

3.4.5 *Potential Sources of Error*

There are potentially a number of sources of error when testing sandy soils in a triaxial apparatus. These are addressed with respect to the tests carried out during this study.

1. Membrane Penetration: the reconstituted pumice sand has mean diameter of D_{50}=1.2 mm. Considering that the smallest diameter of the specimen (Pumice sand A) used was 38 mm, the diameter to grain size ratio is large enough such that the potential error in void ratio arising from membrane penetration effects was considered to be insignificant.
2. Bedding Error: Although a procedure to mitigate bedding errors between the specimen surface and top-cap is recommended, it is generally employed only when measuring the small-strain deformation of a specimen. Since this was not of interest in this study, no further adjustments were made.
3. Specimen barrelling: Lubricants were placed on the pedestal and on the top cap to promote uniform radial deformation and reduce specimen barrelling. Unfortunately, this was not entirely successful, as specimen barrelling did occur, especially at larger axial strains (see Section 4.6). In this case, the results were carefully studied.

3.5. Experimental Programme

The experimental programme for the monotonic consolidated undrained (CU) tests on reconstituted pumice sands is summarised in Table 3.2 while the programme for the cyclic undrained tests is listed in Table 3.3. Note that this researched focused on cyclic testing, and the monotonic tests were used only to supplement the test findings.

Table 3.2 Experimental programme for monotonic CU tests on reconstituted pumice sand

Test No.	Soil	Initial void ratio, e	Initial relative density, D_r (%)	Eff. Pressure, σ_c' (kPa)
A-50	Pumice-B	2.354	23.9	50
A-100-a	Pumice-B	2.251	31.9	100
A-100-b	Pumice-B	2.190	36.9	100
A-200	Pumice-B	2.230	33.6	200
A-250	Pumice-B	2.200	36.1	250
A-400	Pumice-B	2.305	27.5	400
A-800	Pumice-B	2.308	27.2	800
A-1600	Pumice-B	2.334	25.9	1600
B-50	Pumice-B	1.982	53.9	50
B-100	Pumice-B	2.018	51.0	100
B-250	Pumice-B	1.969	55.0	250
B-400	Pumice-B	2.002	52.3	400
B-800	Pumice-B	2.005	52.0	800
B-1600	Pumice-B	1.982	53.9	1600
C-50	Pumice-B	1.602	85.1	50
C-100-a	Pumice-B	1.640	82.0	100
C-100-b	Pumice-B	1.63	82.8	100
C-250	Pumice-B	1.681	78.6	250
C-400	Pumice-B	1.656	80.7	400
C-800	Pumice-B	1.646	81.5	800
C-1600	Pumice-B	1.635	82.4	1600
D-50	Pumice-A	2.354	27.9	50
D-100	Pumice-A	2.373	25.6	100
D-250	Pumice-A	2.318	32.3	250
D-400	Pumice-A	2.374	25.5	400
D-800	Pumice-A	2.357	27.5	800
D-1600	Pumice-A	2.357	27.5	1600
E-50	Pumice-A	2.159	51.6	50
E-100	Pumice-A	2.159	51.6	100

E-250	Pumice-A	2.159	51.6	250
E-400	Pumice-A	2.175	49.6	400
E-800	Pumice-A	2.133	54.7	800
E-1600	Pumice-A	2.154	52.2	1600
F-50	Pumice-A	1.915	81.2	50
F-100	Pumice-A	1.919	80.7	100
F-250	Pumice-A	1.882	85.2	250
F-400	Pumice-A	1.885	84.8	400
F-800	Pumice-A	1.907	82.2	800
F-1600	Pumice-A	1.926	79.9	1600

Table 3.3 Experimental programme for cyclic triaxial tests

Test No.	Soil Used	Initial e	Initial D_r (%)	σ_c' (kPa)	Target CSR ($\sigma_d/2\sigma_c$')
Car-1	Carrs Rd sample			72	0.30
Car-2	Carrs Rd sample			72	0.375
Car-3	Carrs Rd sample			72	0.45
Mik-3m-1	Mikkelsen Rd sample			75	0.20
Mik-3m-2	Mikkelsen Rd sample			75	0.30
Mik-6m-1	Mikkelsen Rd sample			75	0.25
Mik-6m-2	Mikkelsen Rd sample			75	0.33
Mik-6m-3	Mikkelsen Rd sample			75	0.30
Mik-12m-1	Mikkelsen Rd sample			85	0.18
Mik-12m-2	Mikkelsen Rd sample			85	0.30
Mik-12m-3	Mikkelsen Rd sample			85	0.42
L-1	Pumice-A	2.390	23.5	100	0.25
L-2	Pumice-A	2.451	16.1	100	0.22
L-3	Pumice-A	2.421	19.8	100	0.2
L-4	Pumice-A	2.290	35.7	100	0.15
L-5	Pumice-A	2.388	23.8	100	0.18
L-6	Pumice-A	2.410	21.1	100	0.21

X-1	Pumice-A	1.931	79.2	100	0.25
X-2	Pumice-A	2.026	67.7	100	0.28
X-3	Pumice-A	2.003	70.5	100	0.23
X-4	Pumice-A	2.022	68.2	100	0.18
X-5	Pumice-A	2.017	68.8	100	0.26
X-6	Pumice-A	2.011	69.5	100	0.2
A-1	Mikkelsen Rd sample	1.024	31.5	75	0.25
A-2	Mikkelsen Rd sample	1.015	33.5	75	0.15
A-3	Mikkelsen Rd sample	1.022	31.9	75	0.20
B-1	Pumice-A	2.015	69.1	35	0.20
B-2	Pumice-A	2.019	68.6	35	0.30
B-3	Pumice-A	1.981	73.2	35	0.33
B-4	Pumice-A	1.949	77.1	500	0.20
B-5	Pumice-A	1.993	71.7	500	0.223
B-6	Pumice-A	1.976	73.8	500	0.25
C-1	Pumice-C	1.329	78.9	100	0.25
C-2	Pumice-C	1.328	79.0	100	0.22
C-3	Pumice-C	1.324	79.4	100	0.20
D-1	Pumice-A	1.890	84.2	100	0.0 (N=0)
D-2	Pumice-A	1.892	84.0	100	0.10 (N=10)
D-3	Pumice-A	1.995	71.5	100	0.10 (N=100)
D-4	Pumice-A	1.963	75.4	100	0.10 (N=1000)
D-5	Pumice-A	1.992	71.8	100	0.20 (N=10)
D-6	Pumice-A	1.987	72.5	100	0.20 (N=83)
E-2	Pumice-A	1.937	78.5	100	0.25
E-4	Pumice-A	1.968	74.8	100	0.25
E-6	Pumice-A	1.964	75.2	100	0.25
YU-1	Pumice-A	1.934	78.9	100	0.229
YU-2	Pumice-A	1.958	76.0	100	0.258
YU-3	Pumice-A	1.924	80.1	100	0.240
YU-4	Pumice-A	1.994	71.6	100	0.215
YU-5	Pumice-A	2.008	69.4	100	0.283

Some explanations on the cyclic testing programme are given below. Test Series A was performed on reconstituted Mikkelsen Rd samples in order to investigate the difference in the cyclic response of undisturbed and disturbed samples. The objective of Test Series B is to investigate the effect of confining pressure, while Test Series C looks at the effect of crushed pumice (higher F_c) on the response. In Test Series D, the occurrence of particle crushing was examined by stopping the cyclic tests after a certain number of cycles, N, after which sieve analysis was performed. Finally, the tests in Series E were conducted using the same sample, with all the tests conducted under same condition (i.e., multiple cyclic tests on single specimen). Before each test, sieve analysis was performed. Series YU was performed in the Geotechnical Engineering Laboratory of Yamaguchi University (Japan) in order to confirm if the testing machine and methodology adopted in the tests were consistent with those used by Japanese researchers.

3.6 Seismic Dilatometer Test (SDMT)

In situ or field testing is a vital component of any geotechnical investigation as it allows the properties of the soil to be measured directly. Moreover, field tests do not require sampling and they measure the response of sufficiently large volume of soil and not of soil specimens. In this research, two sets of field tests were conducted: cone penetration testing (CPT) and seismic dilatometer testing (SDMT). SDMT was performed at the two sites to determine shear wave velocity profile. The tests were performed near the site where the undisturbed soil samples were obtained.

The seismic test was carried out at 500 mm depth intervals with the first reading taken at 1 m depth from the ground surface. An electrically operated Autoseis hammer was used to generate a shear wave that propagates through the ground (see Figure 3.6). The Autoseis hammer provides consistent energy for each hammer blow and optimises the shear wave generation throughout the test. The shear wave signals were recorded by the geophones in the seismic module and the signals were sent back to a computer system as seismographs for analysis purposes. The seismographs from both geophones were shown as similar waves but with the time lag due to the fact that one of the geophones is 500 mm deeper than the other. A computer program allowed the two seismographs to be re-phased and so that the actual travel time difference of the shear wave could be calculated. The shear wave velocity of the soil

layer between the two geophones was calculated from the interval between the two geophones divided by the difference in travel time.

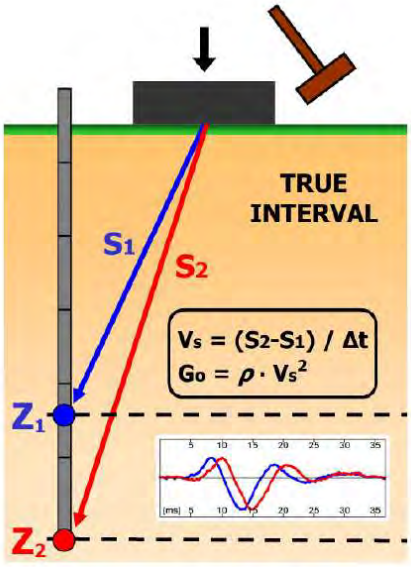

Figure 3.6: Schematic diagram of seismic test in SDMT.

The SDMT tests were carried out using a Pagani TG63-150 track mounted CPT rig. In addition, the CPT tests presented in this study were also performed with this rig. Figure 3.7 illustrates the SDMT test at Mikkelsen Rd site. Figure 3.7(a) shows the flat plate dilatometer used, while Figure 3.7(b) illustrates the SDMT set up on the rig, with the DMT blade and seismic module ready for insertion into the ground. The yellow box on the left hand side of the rig is an electrically operated Autoseis Hammer. A pressure transducer seismic box was used with the DMT control box connected to a laptop computer for automatic recording of the DMT and seismic tests using the Marchetti software, Sdmt Elab (Figure 3.7c).

Results of the CPT and SDMT tests performed in this research are summarised in Table 3.4. The approximate locations of the geotechnical investigations are discussed in Appendices A and B. As mentioned above, the undisturbed samples were obtained at the following depths: for Carrs Rd site: 8.0-8.5 m; and for Mikkelsen Rd site: 3.0-3.3 m, 6.0-6.6 m and 12.0-12.4 m. The results of the geotechnical investigations at these depths will be used in the correlation with the laboratory test results.

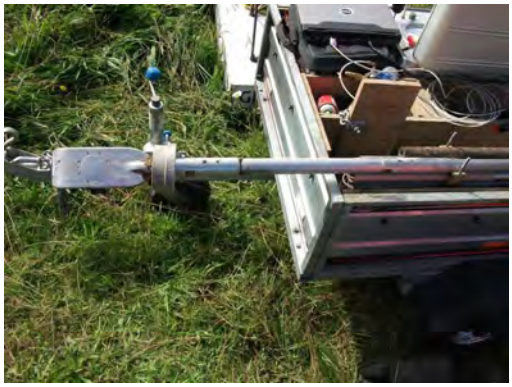

(a)

(b)

(c)

(d)

Figure 3.7: SDMT test at Waihou substation: (a) flat-plate dilatometer; (b) insertion of dilatometer into the ground; (c) equipment used in SDMT test; and (d) an overall view of the execution of SDMT.

Table 3.4 Details of Field Tests

	Depth of sounding	Location of Water Table
Carrs Rd Site		
CPT01*	15.00 m	2.2 m
CPT02*	17.40 m	4.8 m
SDMT01	16. 20 m	
SDMT02	19.00 m	
SDMT03	16.00 m	
Mikkelsen Rd site		

CPT02*	25.00m	1.8 m
CPT01a	19.61m	3.0 m
CPT02a	16.57m	3.0 m
SDMT01	16.75m	
SDMT02	16.50m	
SDMT03	16.50m	

*Data provided by AECOM

4 MONOTONIC UNDRAINED BEHAVIOUR

4.1 General Remarks

The undrained behaviour of sandy soils under monotonic shearing is conventionally used to investigate liquefaction mechanism. Monotonic shearing means the specimen in the triaxial cell, which is isotropically consolidated, is subjected to an increasing axial load until failure occurs. During shearing, the drainage valve is closed; this results in generation of excess pore water pressure.

Generally, the behaviour under monotonic shearing is characterized by three types of response, as illustrated in Figure 4.1. Very loose sand shows fully contractive behaviour where following the peak stress, the sand strain-softens until the steady state is reached at large strains. *Steady state* is the idea that sand sheared in undrained manner can attain an unlimited extent of shear deformation (> 20% strain) under a constant magnitude of shear stress and constant volume. This strain-softening phase of the response resembles a flow-type behaviour and therefore it is commonly referred to as flow or flow deformation. The shear stress at large strain, called *residual strength*, is said to be independent of the initial level of confining pressure. If the density of the sand is somewhat higher, then the strain softening is followed by strain hardening in which the sand recovers its strength and restores stability. In this case, the flow takes place over a limited range from the peak stress to the point of phase transformation where dilative behaviour is initiated (*phase transformation* is the state where the soil changes its behaviour from being contractive to dilative). This type of response is also known as flow with limited deformation or limited flow. Finally, in the case of medium dense and dense sands, a strain hardening response is observed and ever increasing shear stress is needed to induce shear strain and eventually obtain the steady state of deformation. In this case, flow is not induced.

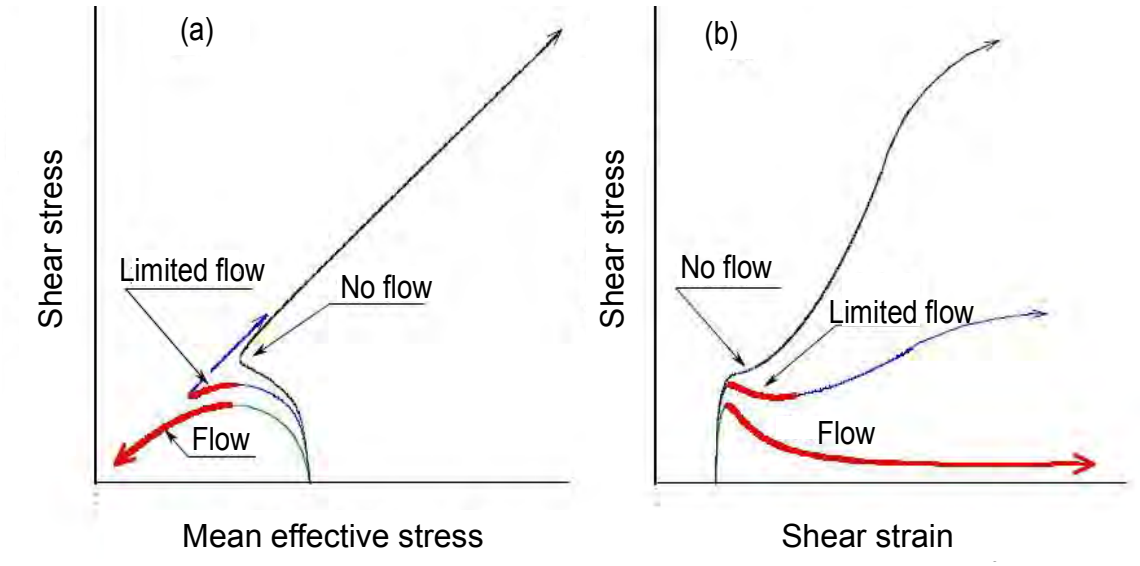

Figure 4.1: Monotonic behaviour of sand: (a) effective stress path; (b) shear stress – shear strain relation.

The results of the monotonic undrained tests on reconstituted pumice sands are expressed in terms of the effective stress path (deviator stress vs. mean effective stress) and deviator stress-axial strain relation. Taking σ_1' and σ_3' as the maximum and minimum effective principal stresses the triaxial specimen is subjected to, then the deviator stress, $q = \sigma_1 - \sigma_3$ and the mean effective stress: $p' = (\sigma_1' + 2\sigma_3')/3$. The axial strain is denoted as ε_a.

Two sets of pumice sands, each with different gradation characteristics, were used. The effects of various parameters, such as confining pressure and relative density, were investigated in the tests. Moreover, attempts to discuss the response in terms of steady state framework are presented.

4.2 Repeatability of Tests

The monotonic undrained experimental programme was conducted over a period of two years and involved two different groups of researchers. Hence, in order to confirm if the sample preparation method and testing technique adopted were consistent throughout the programme, several tests were performed under similar conditions. These are represented by "a" and "b" in the experimental programme summarised in Table 3.2. Two reproducibility tests were conducted: Test A-100 (very loose specimen at σ_c '=100 kPa) and Test C-100 (dense specimen at σ_c '=100 kPa). The stress-strain relation and effective stress paths for Test A-100a and A-100b are shown in Figure 4.2. It is observed that the stress paths are almost similar, especially after the phase transformation (transformation from contractive to dilative behaviour). Before the phase transformation, there is a slight change in the stress path, related to the pore water pressure generation during shearing. Looking at the stress-strain relation, a slight difference in the variation of axial strain with the applied deviator stress is observed after the phase transformation. This can be traced to the difference in the initial void ratio of the specimens, and the fact that the tests were done by two different research groups. Similar slight difference in response was observed in Test C-100. Hence, for practical purposes, it can be said that the test results are repeatable.

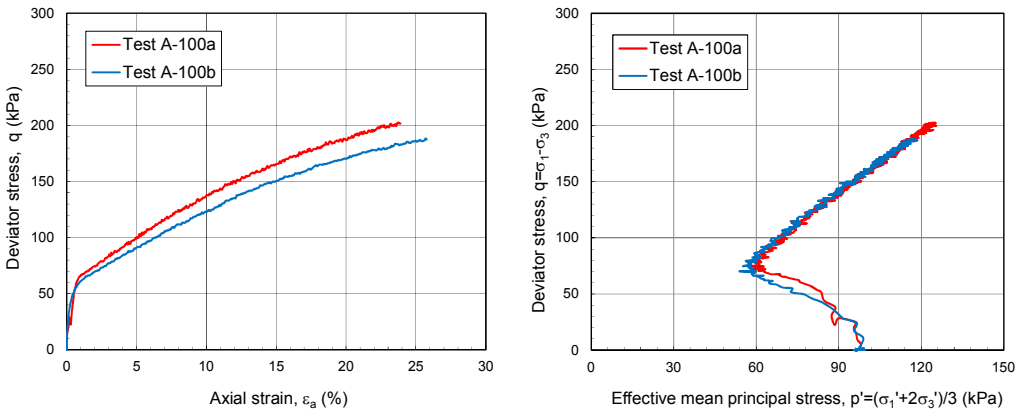

(a) (b)

Figure 4.2: Repeatability tests comparing results for similar conditions: (a) stress-strain relation; and (b) effective stress paths.

4.3 Effect of Density and Confining Pressure

It is well known that changes in density and confining pressure affect the undrained response of natural sand. The effects were therefore investigated for the pumice sandy soils by examining the respective deviator stress-axial strain curves and stress paths under different conditions. The pumice samples were reconstituted as triaxial specimen at three different states: loose (e=2.20-2.35, D_r=26-32%), medium dense (e=1.97-2.00, D_r=50-54%), and dense (e=1.63-1.68, D_r=79-85%) states. These descriptions are consistent with those used in general geotechnical engineering practice (e.g., AS1726 – 1993). Effective confining pressures ranging from 50 kPa to 1600 kPa were applied.

The results of a series of undrained triaxial compression tests on loose samples of Pumice A sand with a relative density of 26-32% are presented in Figure 4.3 for an effective confining pressure range of up to 400 kPa. It can be seen that the test results showed strain hardening response at this range of pressure, with the deviator stress q increasing with increase in axial strain. Moreover, q increases with the confining pressure and at large strain level, the plots are more or less parallel to each other. From the stress paths, the specimen under lower confining pressure was less contractive than those under higher confining pressure. The stress-strain relations show a stiffer response at small strain level, followed by development of large strains and greater dilatancy when the phase transformation state (from contractive to dilative) is reached. Compared to natural sands where the stress-strain curves appear to merge

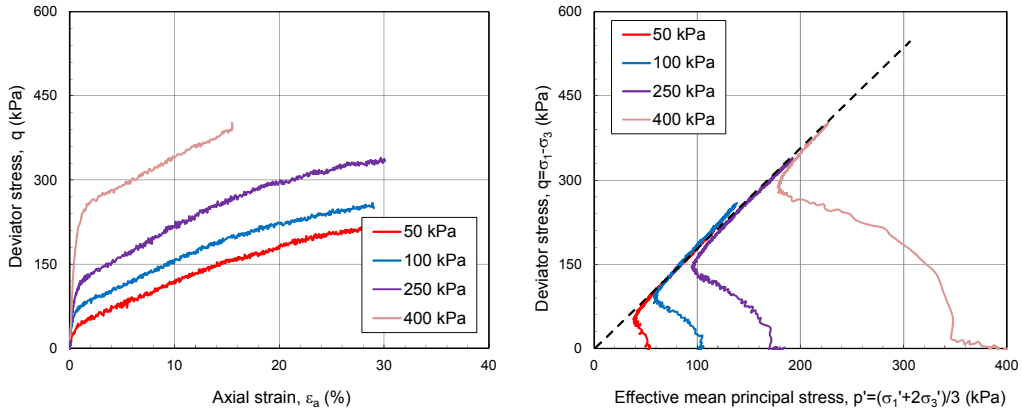

(a) (b)

Figure 4.3: Test results for loose Pumice A sands – test series D: (a) stress-strain relation; and (b) effective stress paths.

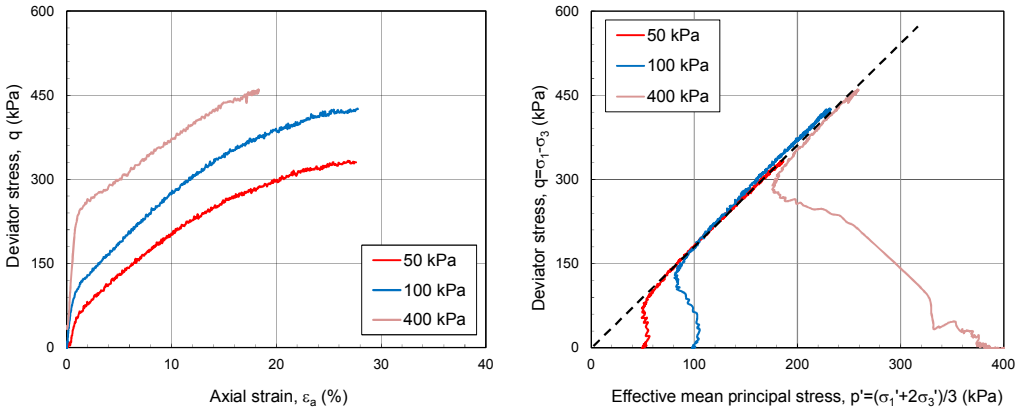

(a) (b)

Figure 4.4: Test results for medium Pumice A sands – test series E: (a) stress-strain relation; and (b) effective stress paths

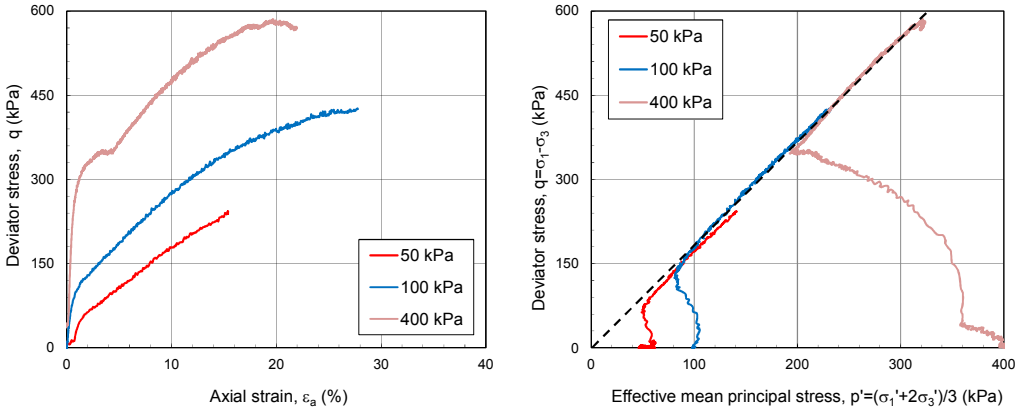

(a) (b)

Figure 4.5: Test results for dense Pumice A sands – test series F: (a) stress-strain relation; and (b) effective stress paths

at large strain range (i.e., steady state of deformation), the curves for pumice sand do not converge, at least within the strain level shown, which was limited by the capability of the testing apparatus.

The results for two other series of tests, this time on medium dense (D_r=50-54%) and dense (D_r=79-85%) states are presented in Figures 4.4 and 4.5, respectively. Considering the influence of initial confining pressure on the stress-strain relation and pore water pressure response, similar tendencies are observed in the overall behaviour of dense and loose pumice

specimens. This observation indicates that relative density is not a good parameter to differentiate the response of pumice sands. Moreover, all the tests showed similar of tendency of stiff response at small strain level, followed by large straining when the phase transformation state is reached.

Tests were conducted at very high confining pressure; however, problems were encountered in some cases because of the limitation of the apparatus. Nevertheless, a clear trend was observed in the tests which were successful. Figure 4.6 shows the monotonic undrained test results for dense Pumice B sands subjected to σ_c'=400, 800 and 1600 kPa. Whereas the results for 400 kPa showed strain hardening behaviour, those at higher pressures manifested strain softening response, especially at large strain level. This behaviour is similar to those observed in Toyoura sand (Ishihara 1996). However, it can be seen from the figure that even at strain levels as large as 40%, the stress-strain curves did not converge to the steady state. Also noticeable is the stiff response of pumice at small strain range, followed by large deformation after the phase transformation was reached.

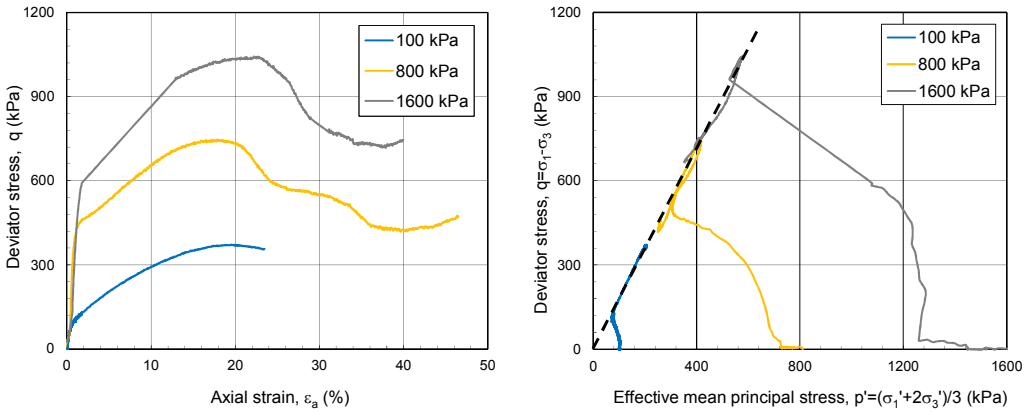

(a) (b)

Figure 4.6: Test results for dense Pumice B sands – test series C: (a) stress-strain relation; and (b) effective stress paths

4.4 Effect of soil gradation

Next, the monotonic undrained response of Pumice A and Pumice B sand specimens are compared. Figure 4.7 shows the comparison of results for the two specimens at σ_c'=100 kPa and 400 kPa. It can be observed that while the stress-strain curves are more or less similar, the development of excess pore water pressure appears to be faster for Pumice B sands. Similar general tendencies were also observed in the other test comparisons. Thus, the finer-grained Pumice B sand appears to be more liquefiable when compared to Pumice A sand.

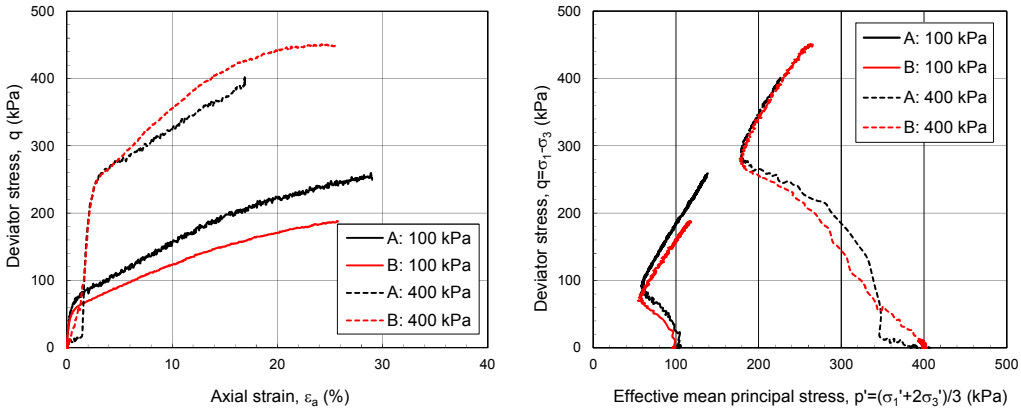

(a) (b)

Figure 4.7: Test results for dense Pumice B sands – test series C: (a) stress-strain relation; and (b) effective stress paths

For the cases shown in Figures 4.3-4.5, it can be observed that for the specimen of particular density, the effective stress paths become asymptotic to the failure line, indicated by the dashed lines in the figures. The slope of the line, M_f, can be correlated to the angle of inter-particle friction ϕ_f using the following equation:

$$M_f = \left(\frac{q}{p'}\right) = \frac{6\sin\phi_f}{3-\sin\phi_f} \qquad (4.1)$$

For all the densities considered, the values of the inter-particle friction angle were calculated for both Pumice A and B sands and the results are summarised in Table 4.1. Regardless of the

density, the angle ϕ_f for each type of pumice sand appears to be constant, with values of 42° and 44° for pumice B and A, respectively. Thus, pumice A has higher ϕ_f and therefore a little bit higher shear resistance than pumice B.

Table 4.1 Values of inter-particle friction angle at failure, ϕ_f, for pumice

	Pumice A sand	Pumice B sand
Loose	44	42
Medium dense	44	42
Dense	44	42

For comparison purposes, typical values for loose natural sands are in the order of ϕ_f=30°. The higher frictional angle of pumice may be attributed to their crushable nature as well as the particle's very angular shape.

Using the same concept, the locus of points in the *p'-q* plane representing the phase transformation state (from contractive to dilative behaviour) can be obtained for each test condition. Results indicate that the friction angle at phase transformation, ϕ_{pt}, ranges from 34-36° for Pumice B and 36-37° for pumice A sand. Again, these values are much larger than those typically observed for natural sands.

4.5 Investigation of Particle Crushing

In order to investigate whether particle breakage occurred during monotonic shearing, sieve analyses were conducted after most of the tests. A comparison of the grain size distribution before and after the undrained shear test for dense Pumice B sand at σ_c'=400 kPa is shown in Figure 4.8. For the level of shearing the specimen was subjected to, considerable particle crushing occurred.

As pointed out by Kikkawa et al. (2011b), pumice particles are very fragile not only because they are porous but also because they are angular in shape; it is the combination of these two factors that makes the particles highly crushable. It is postulated that the axial strain measured during the test is the result of both load-induced compression of the specimen and

particle crushing; as a result, the structure of pumice specimen becomes more stable with continuous shearing, accounting for the predominantly strain-hardening response observed in the tests. In addition, the changing particle size distribution during the course of undrained test makes the pumice soil more resistant to deformation when compared to specimens consisting of hard-grained sands.

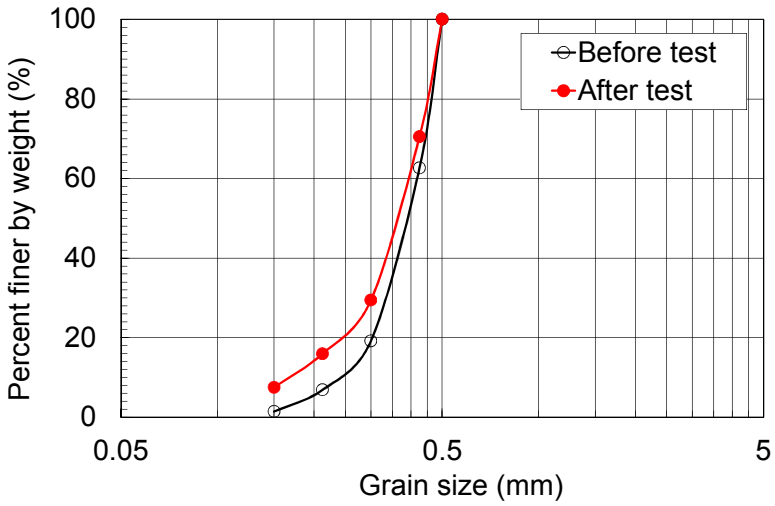

Figure 4.8: Grain size distribution curves of dense Pumice B specimen before and after test (σ_c'=400 kPa).

4.6 Steady State Concept

Numerous studies that have investigated the undrained monotonic behaviour of sand have used the steady state concept to discuss the response. The steady state of deformation, also known as critical state, is defined as the state at which a sandy soil deforms under constant shear stress, constant effective stress and constant volume (Casagrande, 1976; Castro and Poulos, 1977). The strength and mean effective stresses which occur at the steady state of deformation change as the density of sand is varied, enabling a 'steady state line' to be defined in $e - q - p'$ space. The projection of this line in the $e - p'$ plane is often presented to discuss the response of sand at the steady state of deformation. Initial states with densities lower than those of the steady state line tend to result in contractive soil response during monotonic loading, whilst initial states with densities higher than the steady state line tend to dilate during loading. Note however that the steady state line only provides an approximation for division between initial states that contract or dilate (Cubrinovski and Ishihara, 2000) –

the initial dividing line (Ishihara, 1993) actually marks the boundary between contractive and dilative initial states.

Looking again at the test results presented in Figures 4.3-4.5, it is seen that the steady state condition was not reached in the tests. The deviator stress continues to increase even when large deformation was reached ($\varepsilon_a > 25\%$). The breakage of the particles does not allow for the pumice sand to deform under constant shear stress, constant effective stress and constant volume. In fact, at large deformation, the specimens tend to deform irregularly, as shown by typical deformation modes illustrated in Figure 4.9. Thus, meaningful data at the end of the tests were not obtained.

Although limited in scope, the monotonic undrained tests on pumiceous specimens presented herein showed that the steady state was not reached in the tests. Because the particles are crushed as the deviator stress is applied, the soil structure becomes more stable and resistance increases; as a result the condition of constant deformation under constant shear stress (and constant volume) was not achieved, at least within the strain range allowed by the triaixal apparatus used. It follows that the framework of crticial soil mechanics may not be applicable to crushable sands like pumice. More experiments are recommended to confirm this.

(a) (b)

Figure 4.9: Deformed shape of Pumice B specimens after monotonic undrained tests: (a) σ_c'=100 kPa; (b) σ_c'=400 kPa.

4.7 Summary

Under monotonic undrained loading, specimens reconstituted under loose and dense states practically showed similar response, indicating that relative density did not have significant effect on the behaviour of pumice. Within the range of effective confining pressures investigated, pumice specimens showed contractive response followed by dilative behaviour. The contractive response was more significant at high confining pressure. The stress-strain relations showed a stiffer response at small strain level, followed by development of large strains and greater dilatancy when the phase transformation (from contractive to dilative) state is reached.

Pumice sands have angles of internal friction at failure of about 42-44^{o}, and these values were not affected by relative density. It was noted that these were far greater than those for natural hard-grained sands. The friction angles at phase transformation were between 34-37^{o}, which were again much higher than those of natural sands. Even under large strain level, pumice sands did not reach steady state of deformation. This can be attributed to breakage of particles during shearing, which resulted in more resistant soil structure that did not allow deformation at constant shear stress to occur. As a result, it can be surmised that critical state soil mechanics may not be applicable to crushable soils like pumice.

5 CYCLIC UNDRAINED BEHAVIOUR

5.1 General Remarks

The resistance of sand to soil liquefaction is evaluated by performing cyclic undrained test on sand specimen using either triaxial or torsional shear apparatus. In the tests, samples of saturated sand are consolidated under a specified confining pressure and subjected to a sequence of constant amplitude cyclic stress until the specimen either deforms to a certain amount of strain, or the excess pore water pressure reaches a value close to the initial confining pressure. At this stage, it can be considered that the specimen is in a state of cyclic instability, and liquefaction has occurred. In essence, liquefaction can be defined in two ways: (a) development of high pore water pressure, usually 95% of initial confining pressure; or (2) development of high strain, typically expressed as *5% double amplitude axial strain* for triaxial tests and *7.5% double amplitude shear strain* for simple shear tests (see Figure 5.1)

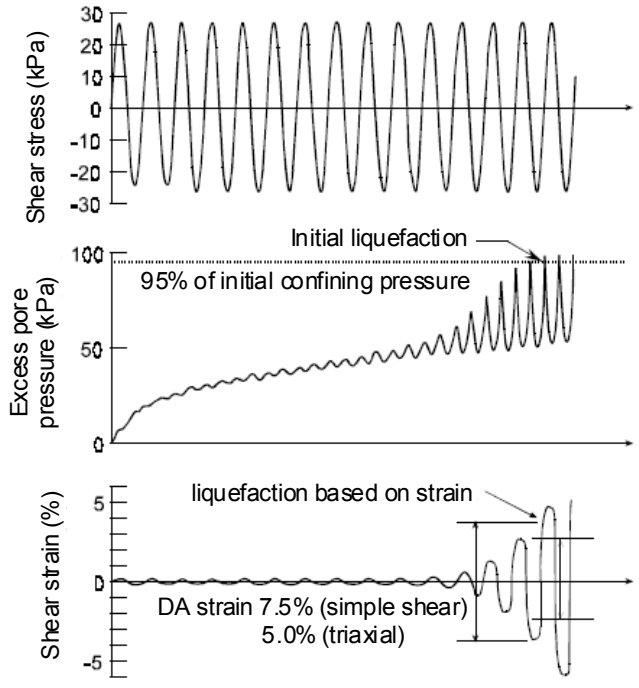

Figure 5.1: Response of saturated sand under cyclic loading in undrained condition.

In order to specify the onset of liquefaction (development of 95% pore water pressure of 5% double amplitude axial strain), the number of cycles needs to be specified for a given constant-amplitude uniform cyclic loading. In practice, three or four tests are performed, with varying amplitudes of shear stress, and the number of cycles to attain liquefaction is noted (see Figure 5.2). Then, each of the shear stress ratios, obtained by normalizing the shear stress by the initial confining pressure, is plotted against the number of cycles required to achieve either 95% pore pressure ratio or 5% double amplitude axial strain. The locus of points defining each state is called the *liquefaction resistance curve*. Note that the attainment of liquefaction as defined in terms of 95% pore pressure ratio or 5% double amplitude axial strain may not occur simultaneously, and therefore, two separate curves can be drawn; however, the latter is usually preferred in many cases. In principle, it is customary to consider 15 cycles in view of the typical number of significant cycles present in many time histories of accelerations recorded during past earthquakes. Thus, the *liquefaction resistance* (or *cyclic strength*) is specified in terms of the magnitude of cyclic stress ratio required to produce 5% double amplitude axial strain in 15 cycles of uniform load application.

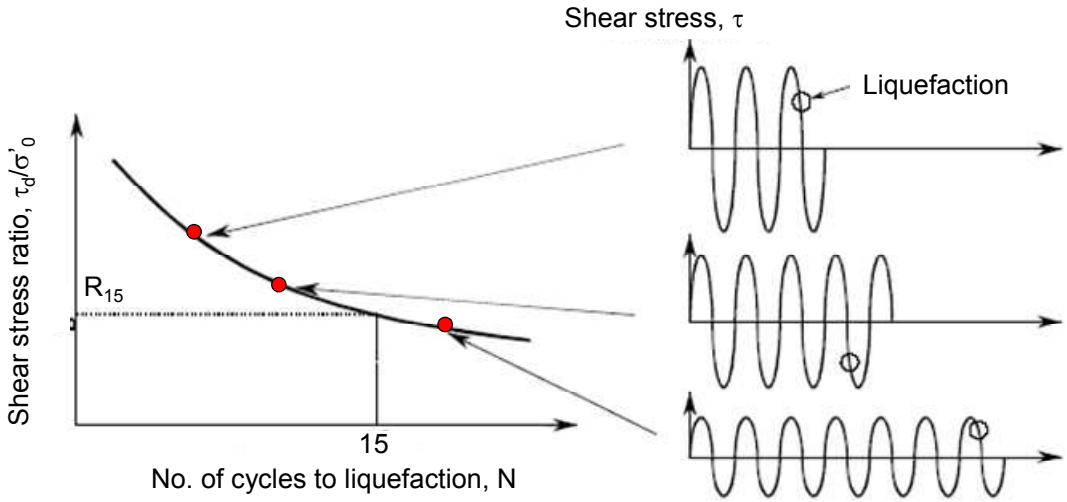

Figure 5.2: Determination of liquefaction resistance curve.

Several series of undrained cyclic triaxial tests were conducted on both undisturbed and reconstituted pumiceous soil specimens to investigate the cyclic shear characteristics of pumice. Overall, 11 tests were performed on undisturbed samples, 3 tests on specimens reconstituted after the tests on undisturbed samples, and 36 tests on reconstituted pumice

sands, for a total of 50 tests. Five of the tests on reconstituted specimens were performed at Yamaguchi University to independently verify if the sample preparation and testing procedure adopted in the tests here at the University of Auckland were consistent with international standards.

The test specimens were prepared using the procedures outlined in Chapter 3, and were loaded in a stress-controlled manner at a frequency of 0.1 Hz or 10 sec for every load cycle. The targeted cyclic shear stress ratio ($CSR=\sigma_d/2\sigma_c'$) was fully-reversed, applying the same amplitude deviator stress (σ_d) in both compression and extension. Considering σ_1' and σ_3' as the major and minor effective principal stresses, respectively, in a triaxial specimen, it follows that $\sigma_1'=\sigma_c'+\sigma_d$ and $\sigma_3'=\sigma_c'$. All the results were expressed in terms of the time histories of the cyclic shear stress ratio, CSR, axial strain, ε_a, and excess pore water pressure ratio, r_u (defined as the excess pore water pressure, u, normalised by the initial confining pressure, σ_c'). In addition, the deviator stress-axial strain curves, the effective stress paths

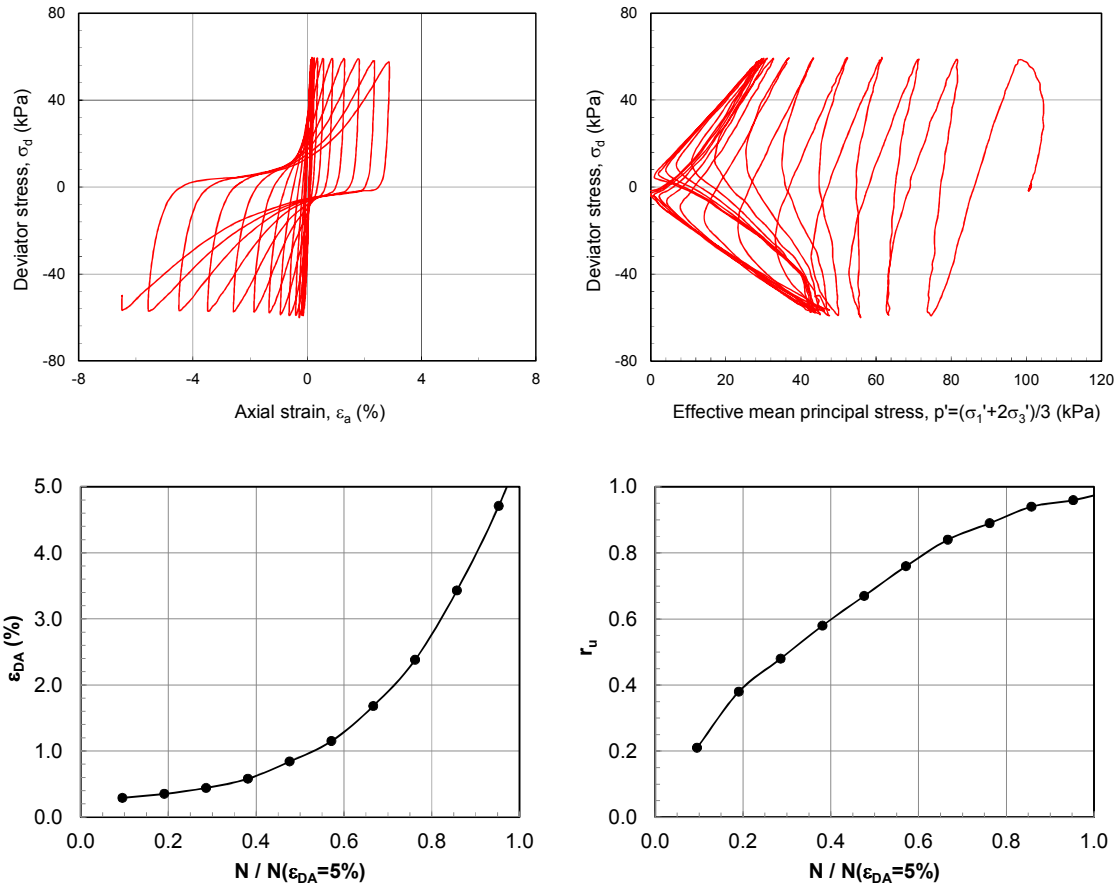

Figure 5.3: Typical plots of cyclic triaxial test results (Test X-2).

(i.e., plots of effective mean principal stress, $p' = (\sigma_1' + 2\sigma_3')/3 = \sigma_c' + \sigma_d/3$ and deviator stress $\sigma_d = \sigma_1' - \sigma_3'$) and the relationships between r_u and ε_a plotted against the number of cycles, N, normalised by the number of cycles required to induce liquefaction, N_l, were also examined. Typical plots of the cyclic triaxial test results are shown in Figure 5.3.

5.2 Verification of Testing Procedure

Before presenting the cyclic test results, it is best to show that the sample preparation technique and testing procedure adopted are in agreement with international standards. For this purpose, the same pumice sand samples used in the tests were brought to Japan and cyclic triaxial tests were performed at the Geotechnical Engineering Laboratory of Yamaguchi University, considered as one of the best soil dynamic testing laboratories in Japan, where many research projects focusing on the liquefaction behaviour of soils have been conducted.

At Yamaguchi University, test specimens using Pumice A samples were prepared in the same manner done at the Geomechanics Laboratory, University of Auckland (see Series X tests in Table 3.3). The only differences between the tests were: the type of loading machine employed, the size of specimen used (50 mm diameter and 100 mm high in Japan) and the use of carbon dioxide to ensure full saturation. For comparison purposes, dense specimens (target initial void ratio, e_i=1.90-2.10) were prepared and consolidated at σ_c'=100 kPa. Five tests were performed on different specimens with *CSR* ranging from 0.20-0.30 (Series YU tests in Table 3.3).

A comparison of the deviator stress-axial strain relationships obtained at the two research laboratories for a typical test condition is shown in Figure 5.4. Both hysteresis curves show larger axial strains in the tension side than in compression side, with the Yamaguchi University results showing smaller axial strain in compression. Figure 5.5 compares the effective stress paths from the two tests where again, almost perfectly similar plots were obtained.

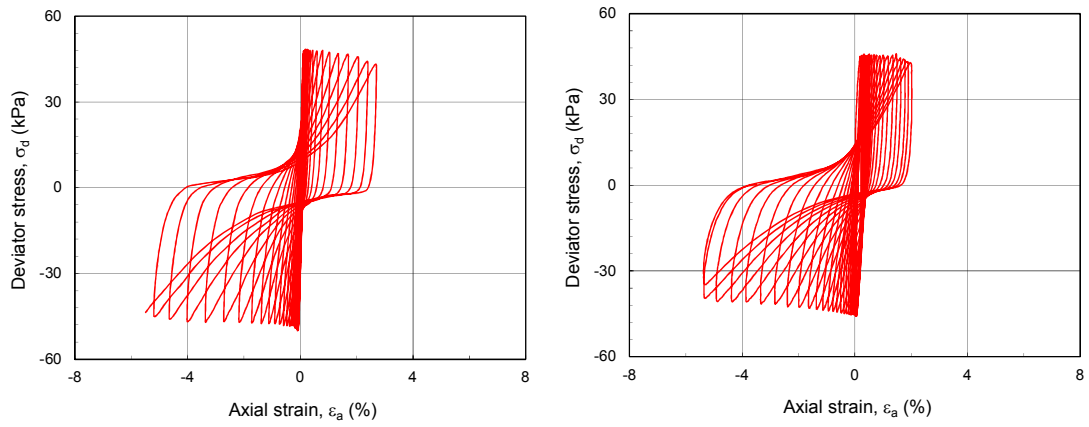

(a) (b)

Figure 5.4: Comparison of shear stress-strain relations for *CSR*=0.23: (a) test at University of Auckland (e_i=2.003); and (b) test at Yamaguchi University (e_i=1.934)

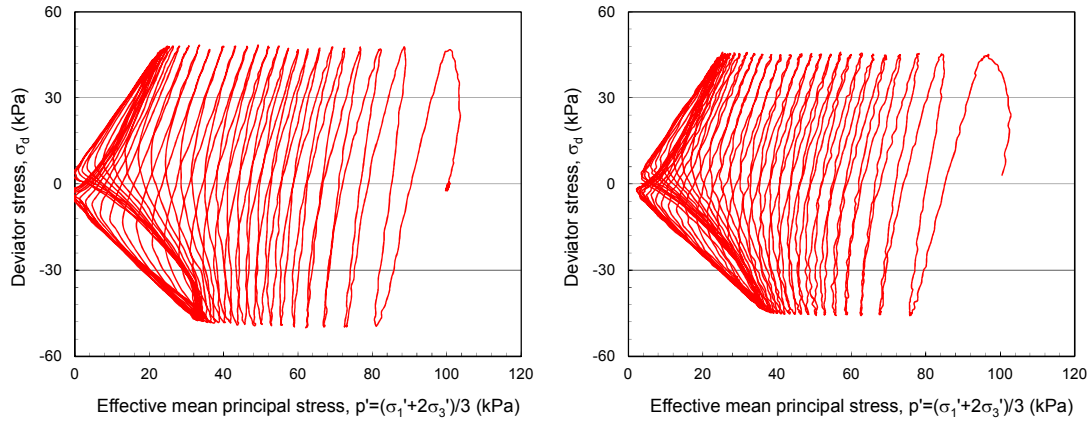

(a) (b)

Figure 5.5: Comparison of stress paths for *CSR*=0.23: (a) test at University of Auckland (e_i=2.003); and (b) test at Yamaguchi University (e_i=1.934)

Finally, the number of cycles required to induce 5% double amplitude axial strains for the given *CSR* is plotted for the 6 tests at University of Auckland (Tests X-1 to X-6) and the 5 tests at Yamaguchi University (tests YU-1 to YU-5), and the plot is shown in Figure 5.6. The data points for all 11 tests are consistent with the liquefaction resistance curve drawn, indicating the similarity between the two series of tests.

Therefore, these confirmed that the sample preparation method and experimental procedure adopted in this research are consistent with international standards and the results can be treated with high accuracy.

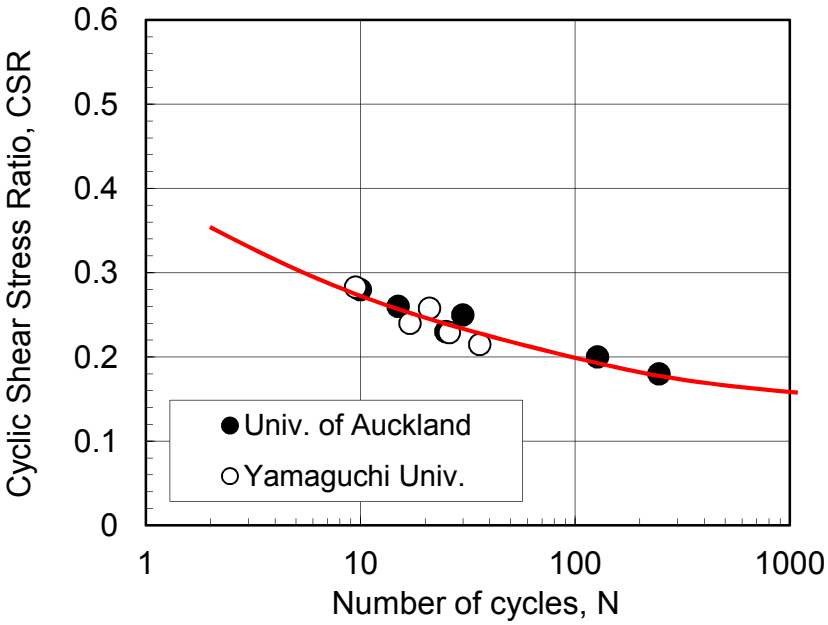

Figure 5.6: Comparison of liquefaction strength curves.

5.3 Cyclic Behaviour of Undisturbed Specimens

5.3.1 *Carrs Rd Samples*

Cyclic triaxial tests were performed on the undisturbed soil samples obtained from Carrs Rd site in Hamilton. Three levels of *CSR* were considered, *CSR*=0.30, 0.375 and 0.45 under a confining pressure of σ_c'=72 kPa. Figure 5.7 illustrates the stress-strain relations for the last two, while Figure 5.8 depicts the corresponding stress paths. It can be observed that for the largest *CSR*, liquefaction-like response was observed immediately after the first extension and the MTS machine became unstable; hence the test was terminated. For *CSR*=0.375, there was continuous build-up of axial strain and excess pore water pressure over a significant number of cycles; however, the condition of initial liquefaction (i.e., r_u=0.95 or ε_{DA}=5%) was not observed. It therefore appears that this particular sample, taken from a depth of 8.0-8.5 m has high liquefaction potential.

Several factors may be behind this behaviour, but it appears that the main factor is the high fines content ($F_c > 60$). The soil sample consists of weathered ignimbrite whose fines are of medium plasticity (Plasticity Index, PI=20). This type of soil is generally not susceptible to liquefaction, but as the test results show, cyclic softening can occur as a result of cyclic load application.

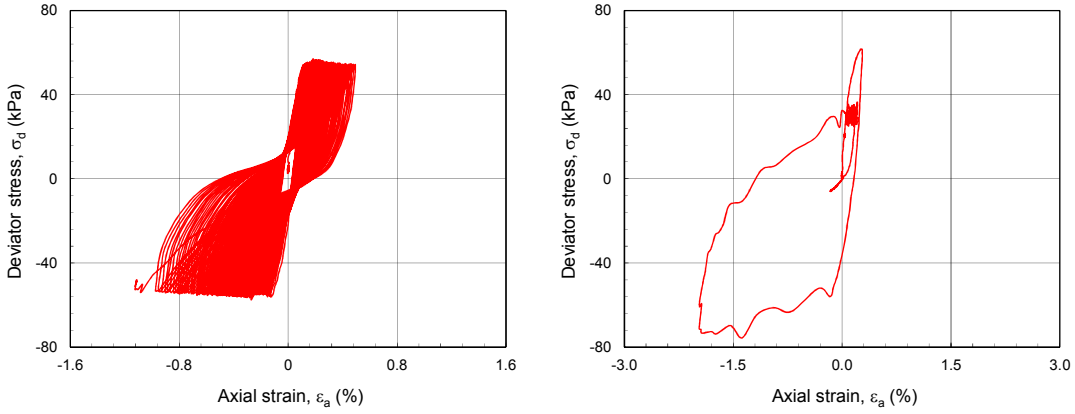

(a) (b)

Figure 5.7: Deviator stress-axial strain relations for Carrs Rd undisturbed samples: (a) *CSR*=0.375; and (b) *CSR*=0.45.

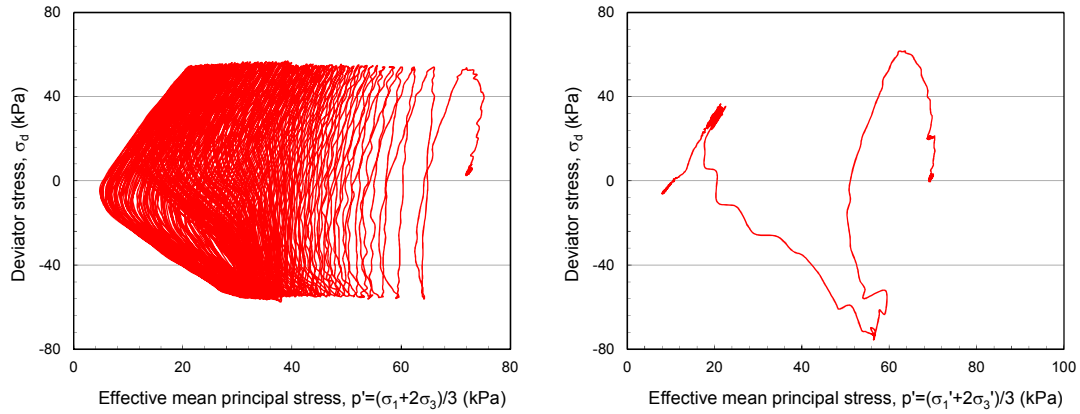

(a) (b)

Figure 5.8: Effective stress paths for Carrs Rd undisturbed samples: (a) *CSR*=0.375; and (b) *CSR*=0.45.

5.3.2 *Mikkelsen Rd Samples*

Eight cyclic tests were performed on the undisturbed samples taken from the Mikkelsen Rd site – 2 specimens from 3 m depth, 3 specimens from 6 m depth and 3 specimens from 12 m depth. The samples from shallower depths (3 m and 6 m) were subjected to effective confining pressure of 75 kPa while the deeper sample (12 m) was subjected to 85 kPa. Moreover, the shallower specimens were observed to crumble upon extraction from the tubes; hence the tubes with the soil inside were placed first in a freezer and then the samples were extracted in frozen state, after which they were thawed prior to testing. On the other hand, the specimens from 12 m depth were able to stand unsupported when they were extracted.

Typical stress-strain relations and effective stress paths are shown in Figures 5.9 and 5.10, respectively, for 3 m depth and 12 m depth samples subjected to *CSR*=0.30. It can be seen that although the cyclic shear stress ratios were similar, the deeper sample appears to be more resistant to liquefaction. The generation of excess pore water pressure for each cyclic load application is much faster for the shallower specimen.

To highlight this, a comparison of the liquefaction resistance curves for the three samples is shown in Figure 5.11. Since a 5% double amplitude axial strain was not achieved in all the tests, the curves were obtained by taking the number of cycles required for the specimen to achieve 4% double amplitude axial strain. These were almost coincident with the condition of r_u=95%. The curves for the 3 m and 6 m depth specimens are parallel and there is an obvious difference; however, the 12 m depth specimens show steeper curves than the other two. Such difference is due to the nature of the specimens themselves, as described above. These are also reflected in the boring log where the shallower samples from 3 m and 6 m depths were described as “loose” while the 12 m depth samples were described as “dense” (see Appendix B). It is also interesting to note that the tip resistance at these three depths were the same, about q_c=10 MPa; this indicates that penetration resistance does not reflect the in-situ degree of packing in pumiceous deposits. Further discussion of this is presented in Section 6.3.

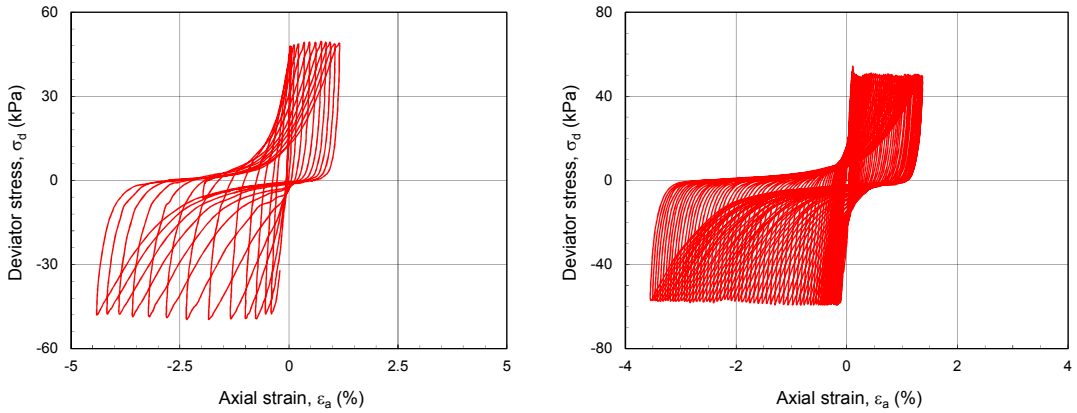

(a) (b)

Figure 5.9: Deviator stress-axial strain relations for Mikkelsen Rd undisturbed samples for *CSR*=0.30: (a) specimen from 3 m depth (σ_c'=75 kPa); and (b) specimen from 12 m depth (σ_c'=85 kPa).

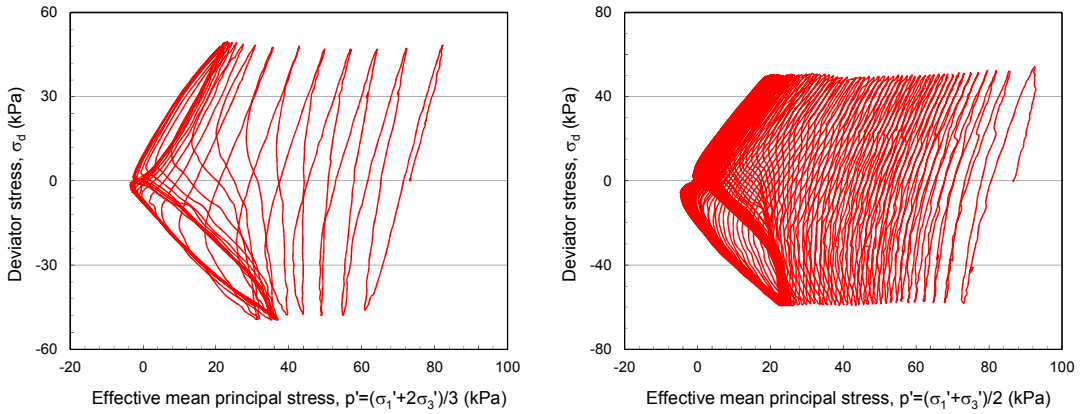

(a) (b)

Figure 5.10: Effective stress paths for Mikkelsen Rd undisturbed samples for *CSR*=0.30: (a) specimen from 3 m depth (σ_c'=75 kPa); and (b) specimen from 12 m depth (σ_c'=85 kPa).

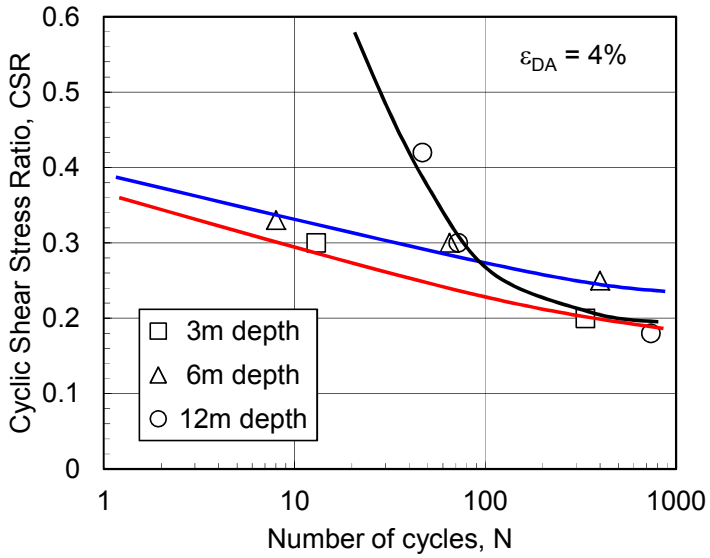

Figure 5.11: Liquefaction resistance curves for Mikkelsen Rd undisturbed samples.

In order to investigate the effect of soil fabric and history, the specimens from the 3 m depth sampling tubes were re-used to form a reconstituted specimen by water pluviation technique. Based on the mass and volume of the undisturbed specimens, the density of the reconstituted specimens were made similar to those of the undisturbed specimens, i.e., D_r=31-34%. An effective confining pressure of 75 kPa was also used.

Figure 5.12 compares the stress-strain relations for the disturbed and reconstituted specimens at *CSR*=0.20. Obviously, the reconstituted specimen has lower resistance, with larger axial strains occurring during cyclic load applications. Figure 5.13 shows the liquefaction resistance curves for the two sets of samples. Again, the curves were drawn for 4% double amplitude axial strain. The reconstituted specimens show lower liquefaction resistance by about 50%, due to the fact that the soil fabric and stress history were totally erased during the specimen preparation.

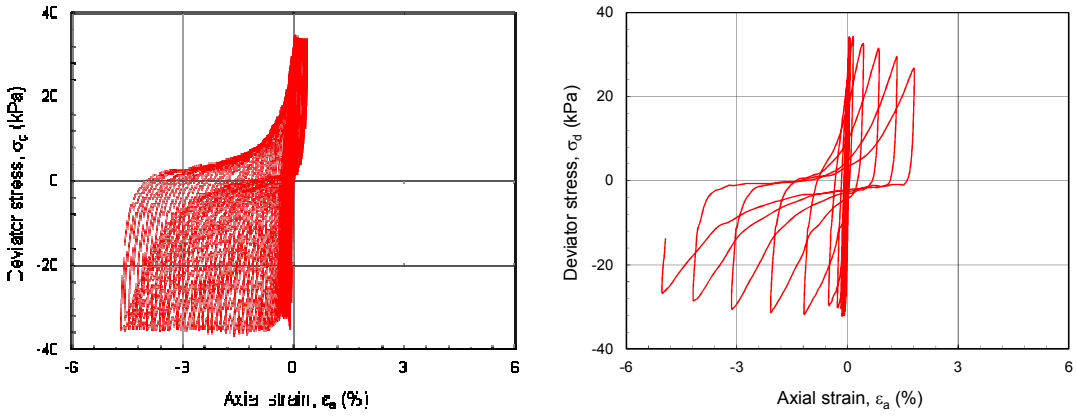

(a) (b)

Figure 5.12: Deviator stress-axial strain relations for Mikkelsen Rd samples at *CSR*=0.20: (a) undisturbed specimen; and (b) reconstituted specimen.

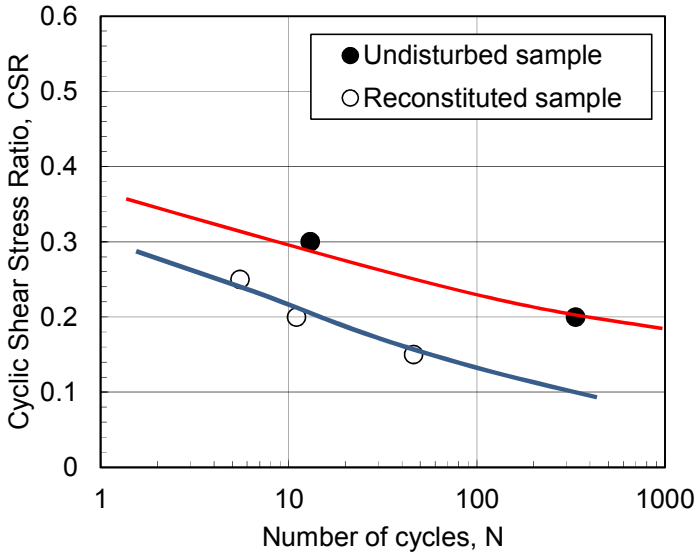

Figure 5.13: Liquefaction resistance curves for Mikkelsen Rd samples: (a) undisturbed specimen; and (b) reconstituted specimen.

5.4 Cyclic Behaviour of Reconstituted Specimens

Although it is best to investigate the behaviour of undisturbed pumiceous specimens, the limited availability of undisturbed samples puts constraints on the number of tests that can be studied. In addition, it is difficult to investigate other conditions, such as the degree of packing, in undisturbed specimens of particular state. For this purpose, testing of reconstituted specimens is adopted in order to investigate the cyclic response under different conditions.

In this section, the effects of degree of packing (or density), confining pressure and gradation characteristics on the undrained cyclic response of pumice sands are presented.

5.4.1 *Effect of Density*

Figures 5.14 show the plots of double amplitude axial strain ε_{DA} and excess pore water pressure ratio, $r_u=u/\sigma_c$' against normalized number of cycles N/N(at ε_{DA}=5%) obtained from undrained cyclic shear tests on reconstituted loose pumice specimens (D_r=25%) corresponding to different cyclic shear stress ratio, $CSR=\sigma_d/2\sigma_c$' (Series L tests in Table 3.3). The curves for each double amplitude axial strain ε_{DA} are dispersed, with the variation dependent on the level of applied cyclic shear stress while the curves for the corresponding

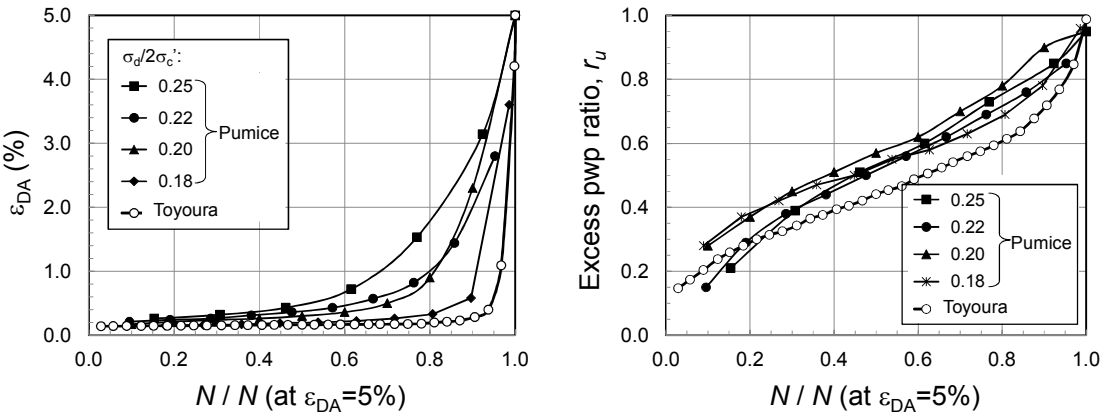

(a) (b)

Figure 5.14: Double amplitude axial strain ε_{DA} and (b) excess pore water pressure ratio $r_u=u/\sigma_c'$ plots against normalized number of cycles N/N(at ε_{DA}=5%) for loose pumice specimens.

excess pore water pressure ratio, u/σ_c', show practically similar behaviour. Comparison of the two plots indicate that while the development of excess pore water pressure with cyclic loading is more or less linear, the development of ε_{DA} starts only after significant number of cycles of load application.

Also plotted in the figure is the cyclic shear behaviour of medium dense (D_r=50%) Toyoura sand (a quartz-based sand), as reported by Yoshimoto et al. (2008). It is seen that for Toyoura sand, axial strain did not occur at the early stage of cyclic loading; however, it suddenly increased to almost the maximum values at N/N(at ε_{DA}=5%) of about 0.9 to 0.95. Similarly, the magnitude of excess pore water pressure ratio for Toyoura sand is lower than pumice, but the rate increases at a much faster rate just prior to liquefaction (development of ε_{DA}=5%).

A comparison of the cyclic shear behaviour of loose (Series L tests) and dense (Series X tests) reconstituted pumice sands, as well as that of undisturbed Mikkelsen Rd samples (at 6 m depth) is performed next. Similar behaviour as in loose samples was noted in dense and undisturbed samples, i.e., while the curves for double amplitude axial strain ε_{DA} are dependent on the level of applied cyclic shear stress, the corresponding curves for excess pore water pressure ratio, u/σ_c', show practically similar trend. Thus, for comparison purposes, the results for the three specimens subjected to cyclic shear stress ratio $\sigma_d/2\sigma_c'$=0.25 are compared and these are shown in Figure 5.15. It is observed that as far as the development of axial strain is concerned, the response of undisturbed pumice appears to be delayed when compared to the reconstituted specimens; however, the development of excess pore water pressure is similar for undisturbed sample and loose reconstituted sample while the dense reconstituted specimen shows slower response. Note that as discussed below, the three types of materials have different liquefaction resistance, and this may have affected the trends shown in the figure.

The cyclic resistance curves of the three pumice materials corresponding to double amplitude axial strain ε_{DA}=5% are shown in Figure 5.16. The curve for loose samples is gentle when compared to that of dense sand, with the later having higher cyclic resistance. On the other hand, the curve for undisturbed sample is as gentle as the loose reconstituted samples, but the cyclic deviator stress ratio is about three times higher.

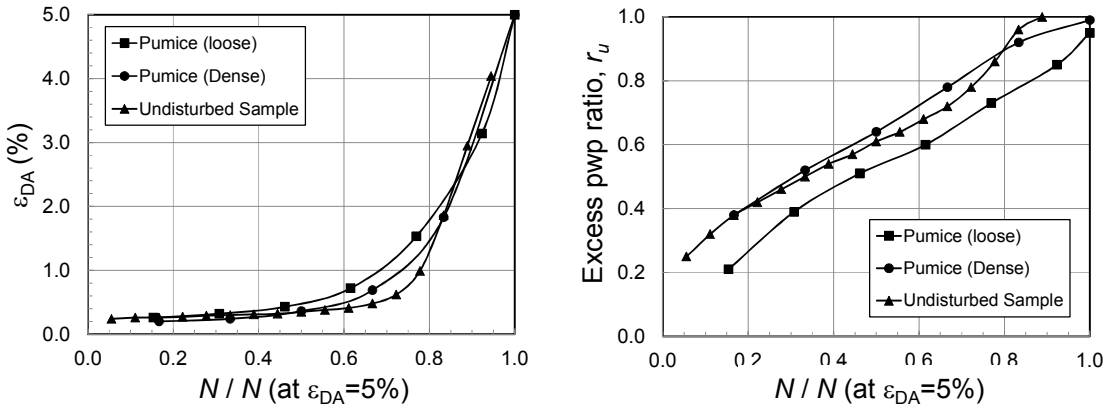

(a) (b)

Figure 5.15: (a) Double amplitude axial strain ε_{DA} and (b) excess pore water pressure ratio $r_u=u/\sigma_c'$ plots against normalized number of cycles N/N(at ε_{DA}=5%) for loose and dense reconstituted pumice sands and undisturbed specimens for $\sigma_d/2\sigma_c'$=0.25.

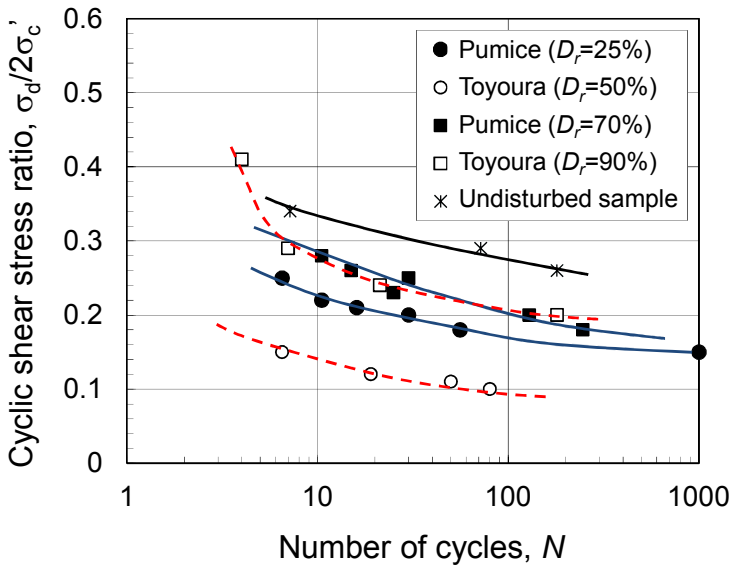

Figure 5.16: Comparison of liquefaction resistance curves for loose and dense pumice and Toyoura sand specimens and undisturbed Mikkelsen Rd samples.

Also plotted in the figure are the cyclic resistance curves for medium dense (D_r=50%) and very dense (D_r=90%) Toyoura sand, as reported by Yamamoto et al. (2009). Comparing the curves for Toyoura sand and for reconstituted pumice sands, two things are clear: (1) loose specimens have gentle cyclic resistance curves, while dense specimens have resistance curves rising sharply as the number of cycles decreases; and (2) while the effect of relative density is

very pronounced for Toyoura sand, the difference between loose and dense pumice specimens appear to be not as remarkable.

If the liquefaction resistance is defined in terms of the cyclic deviator stress ratio corresponding to 15 cycles, then very dense Toyoura sand (with D_r =90%) and dense pumice sand (D_r =70%) practically have the same resistance. On the other hand, the cyclic resistance of loose pumice sand (D_r =25%) is about twice of that of medium dense Toyoura sand (D_r =50%). The undisturbed pumice sand has cyclic resistance of about three times that of loose pumice. Aside from its finer particles, the undisturbed samples maintained its soil structure and fabric, accounting for its higher strength.

5.4.2 *Effect of Confining Pressure*

During triaxial testing, sand specimens are typically subjected to an effective confining pressure equivalent to the effective overburden pressure it is subjected to in-situ. Thus, the influence of effective confining pressure on the liquefaction resistance of reconstituted pumice sands was investigated. For this purpose, dense sand specimens (e_i=1.90-2.00) were subjected to three different levels of effective confining pressure, σ_c'=35, 100 and 500 kPa under different levels of cyclic shear stress ratio, *CSR* (Series B tests in Table 3.3).

Figure 5.17 compares the effective stress paths of sand specimens under the three levels of σ_c' and *CSR*=0.20. It is clear from the plots that the specimen subjected to higher σ_c' requires less number of cyclic loading for liquefaction to occur (zero effective confining pressure) while the specimen subjected to low σ_c' did not even liquefy after hundreds of cyclic load applications. This indicates that the effective confining pressure has significant effect on the development of excess pore water pressure during cyclic loading.

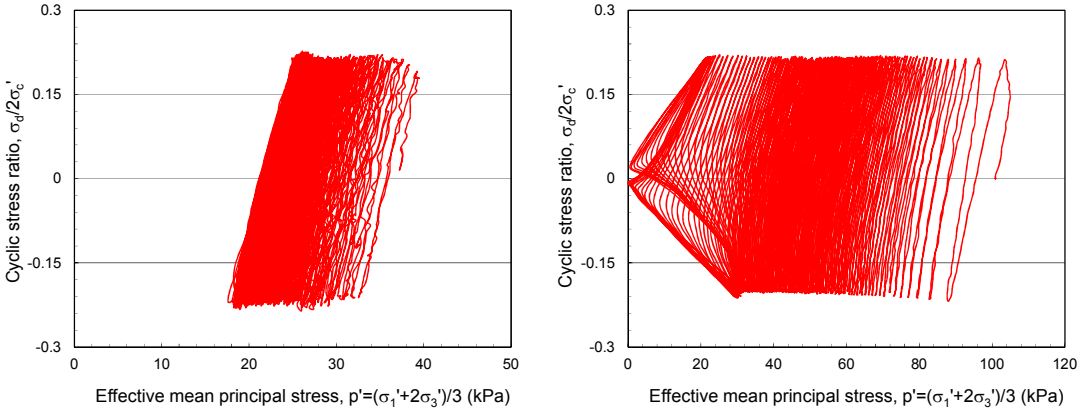

(a) (b)

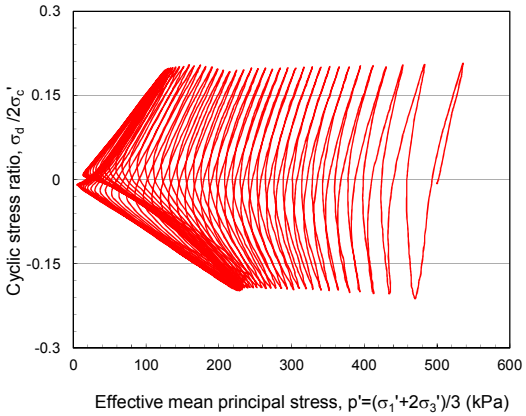

(c)

Figure 5.17: Effective stress paths of reconstituted pumice sands at *CSR*=0.20: (a) σ_c'=35 kPa; (b) σ_c'=100 kPa; and (c) σ_c'=500 kPa.

To investigate the confining pressure dependency of liquefaction resistance, the curves for the three samples are illustrated in Figure 5.18. It can be seen that the curves are almost parallel to each other, with the liquefaction resistance increasing as the confining pressure decreases, consistent with the observations made on natural sands (Rollins and Seed, 1988; Seed and Harder, 1990). The value of the correction factor K_σ (cyclic stress ratio causing 5% double amplitude axial strain in 15 cycles under any confining pressure normalised to the corresponding value of *CSR* at σ_c'=100 kPa) is equal to 1.16 for σ_c'=35 kPa and 0.88 for σ_c'=500 kPa. These values appear to coincide with those reported for reconstituted natural sands (Ishihara 1996; Boulanger and Idriss, 2004).

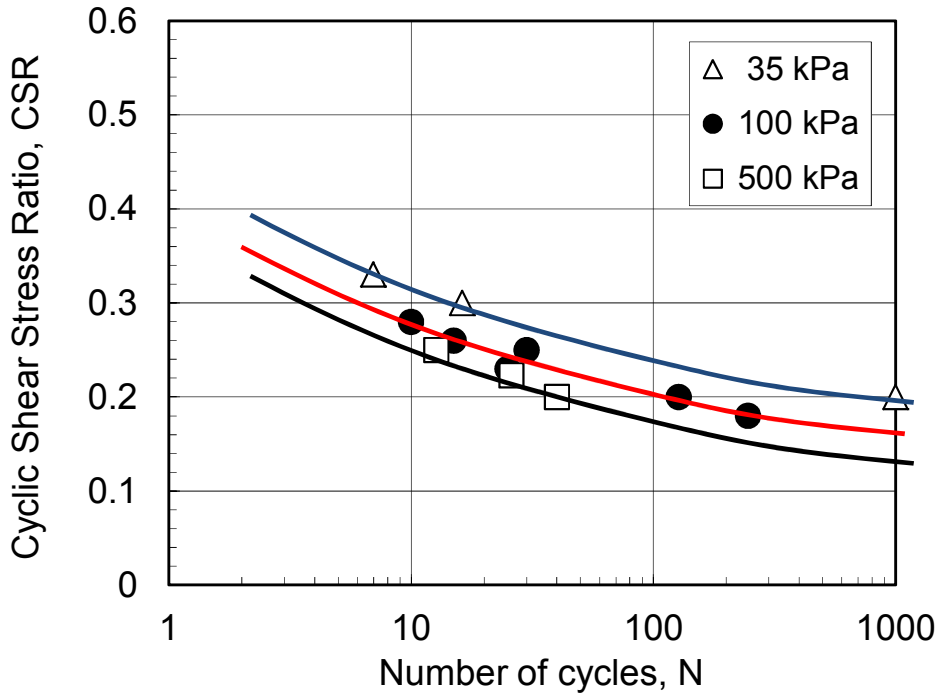

Figure 5.18: Comparison of liquefaction resistance curves for reconstituted dense pumice sands under different effective confining pressures.

5.4.3 *Effect of Crushed Particles*

Since pumice sands are crushable, there is a strong possibility that the particles may be crushed during the deposition process. Hence, it is worthwhile to investigate the effect of grading properties on the liquefaction behaviour of pumice. Samples of Pumice A sands were crushed using mortar and pestle to derive a new set of samples, referred to as Pumice C

sands, whose properties and grain size distribution curve are shown in Table 3.1 and Figure 3.1, respectively. Although Pumice A samples can be considered as clean sand (negligible fines content), Pumice C samples have fines content, F_c=52%.

Undrained cyclic tests were performed on Pumice C sand specimens with initial void ratio range of e_i=1.32-1.33 under an effective confining pressure of σ_c'=100 kPa (Series C tests in Table 3.3). Attempts were made to form specimens similar to dense Pumice A specimens (e_i=1.9-2.0); however, it was very difficult to make such loose specimens. In any case, the initial relative density of the Pumice C specimens were D_r=74-76%, whereas those of dense Pumice A specimens were D_r=68-74%.

Figures 5.19 and 5.20 compare the stress-strain curves and effective stress paths, respectively, of Pumice A and Pumice C sands with *CSR*=0.20. Both plots indicate higher development of excess pore water pressure as well as strain for Pumice C sands than Pumice A sands. Also, it can be observed that although the tests were performed under constant stress condition, there was a reduction in the deviator stress as the Pumice C specimen reaches failure condition.

A comparison of the liquefaction resistance curves obtained for the two samples is shown in Figure 5.21. It is obvious that there is a reduction in liquefaction resistance as the fines content, F_c, increases. Based on previous experiments on soil mixtures, there has been conflicting opinion regarding the effect of increasing fines content on the liquefaction resistance of the sands. Some results showed increase in strength while others indicate a

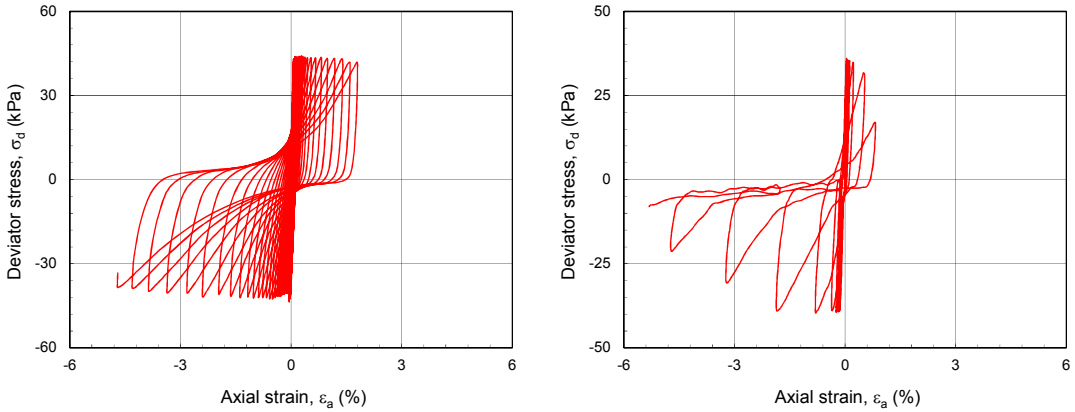

(a) (b)

Figure 5.19: Deviator stress-axial strain relations at *CSR*=0.20: (a) Pumice A sands; and (b) Pumice C sand.

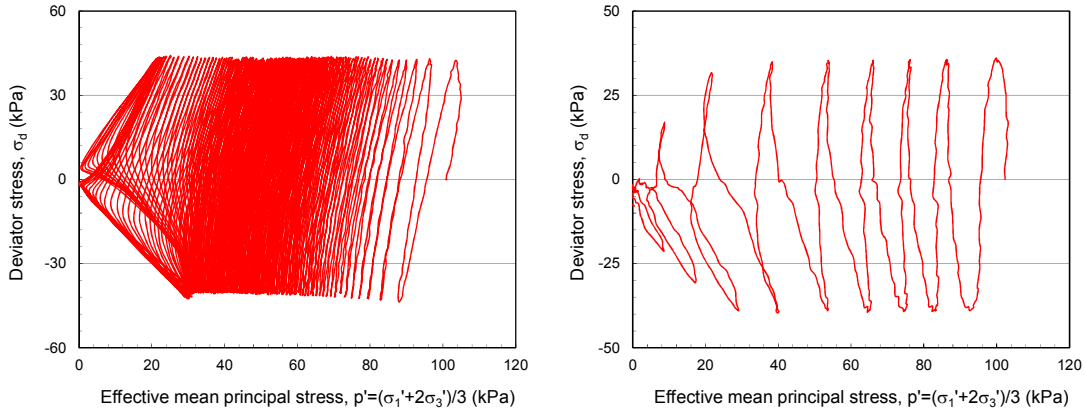

(a) (b)

Figure 5.20: Effective stress paths at *CSR*=0.20: (a) Pumice A sands; and (b) Pumice C sand.

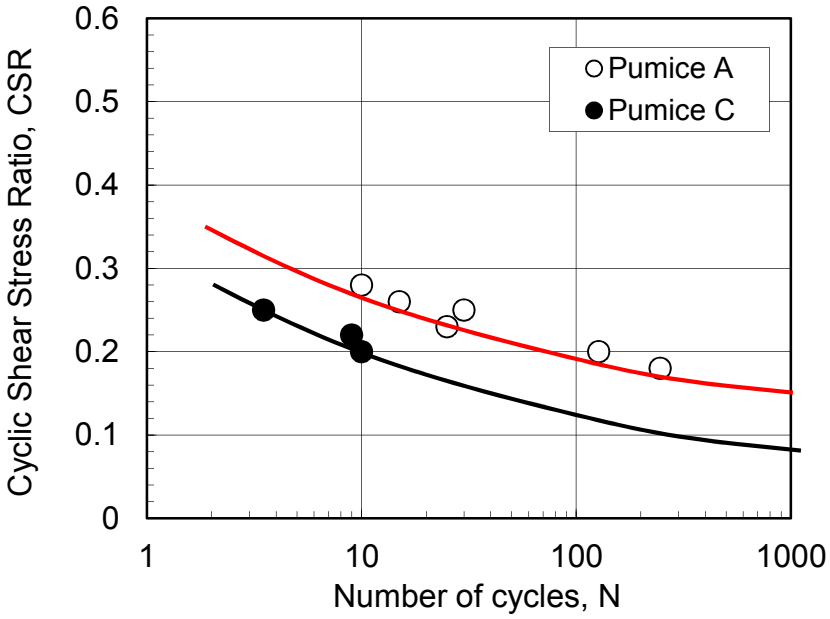

Figure 5.21: Comparison of liquefaction resistance curves for reconstituted Pumice A and Pumice C sands.

decrease in strength. However, recent studies (e.g., Matsumoto et al., 1999) have shown that the difference in effect can be attributed to the activity of fines; i.e., non-plastic fines decrease the liquefaction resistance of sands while plastic fines increase the resistance. Investigation of the activity of the fine particles in Pumice C sands revealed that they are non-plastic; hence, the results presented herein are consistent with the results obtained for natural sands.

5.5 Investigation of Particle Crushing

5.5.1 *Particle Crushing during Tests*

Previous investigations have shown that pumice grains are crushable when sheared (Kikkawa, 2008; Kikkawa et al., 2011a). Thus it is important to pay attention to particle breakage during the cyclic tests and to investigate how this can affect the cyclic shear behaviour of pumice. For this purpose, sieve analyses were carried out after the end of most of the cyclic shear tests performed herein. A typical comparison is shown in Figure 5.22 for the original (virgin) sample of Pumice A sand and for two other samples – loose (L4 test) and dense (X6 dense) after the tests. Note that the specimens in these tests were subjected to the lowest cyclic shear stress ratio and consequently, the most number of cycles. It can be seen that the particle size distributions of the two samples after the cyclic tests are almost similar to each other, and when compared to that of the original sample, there is obvious increase in percentage of smaller particles (< 1.10 mm) and decrease in percentage of bigger particles (> 1.70 mm). Thus, particle breakage is quite significant after the shearing stage, with the degree of breakage appearing to be similar for dense and loose samples.

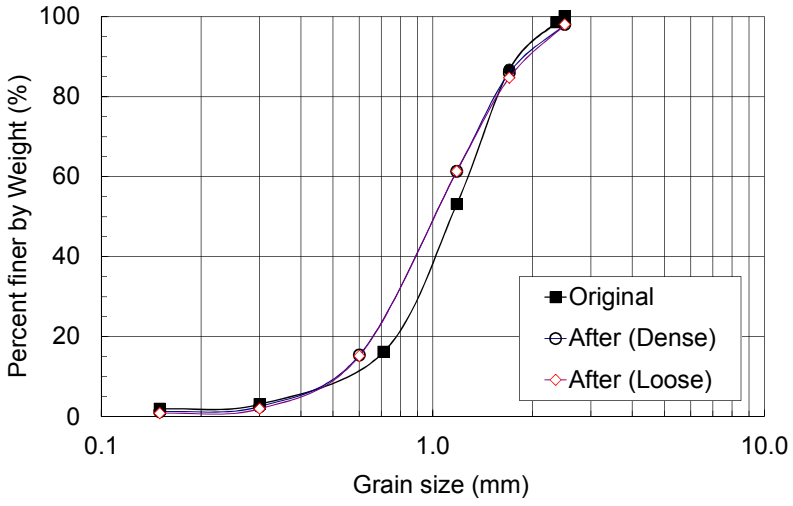

Figure 5.22: Comparison of grain size distribution curves after cyclic tests of reconstituted Pumice A sand.

Under the confining pressure (σ_c'=100 kPa) considered and number of cycles applied (N > 250 cycles), pumice undergoes remarkable particle crushing when subjected to cyclic shear. As cyclic shearing and particle crushing occur, the soil structure is gradually stabilized,

resulting in higher cyclic shear resistance, even exceeding that of Toyoura sand, as indicated in Figure 5.16. Because the degree of particle crushing appears to be similar for loose and dense reconstituted pumice specimens, cyclic shearing and the associated particle breakage resulted in stable soil structure for both cases, which was not be substantially different from each other but was quite different when compared to the original soil sample. This is the reason why the effect of density on cyclic resistance is not as remarkable in pumice when compared to the cyclic resistance of Toyoura sand.

5.5.2 *Re-testing of Specimen*

In all the tests performed on reconstituted specimens, virgin samples were used, that is, after each test, the specimens were not re-used. In order to further investigate the effect of particle crushing on the cyclic response, series E tests was performed where a single specimen was subjected to three cyclic tests one after the other. In the test series, sieve analysis was performed after the first cyclic test then the same sample was reconstituted to form a specimen of almost similar void ratio. The second cyclic test was conducted followed by sieve analysis. The sequence was followed for a third time, with the gradation checked after each test.

Figure 5.23 compares the axial strain and excess pore water pressure time histories for the 1st, 2nd and 3rd cyclic tests. It can be seen from Figure 5.23(a) that the development of axial strain for each cycle of loading is more significant for the 3rd test than for the 1st test. Similar response can be observed in Figure 5.23(b) where the generation of pore water pressure is more significant in the 3rd test than in the 1st test. It follows therefore that the liquefaction resistance of the specimen decreases when re-used.

A comparison of the grain size distribution curves taken after each test is shown in Figure 5.24. For the level and duration of cyclic loading the specimens were subjected to, it appears that particle crushing occurred after each test, with increase in percentage of smaller particles (< 0.5 mm) and decrease in percentage of larger particles (> 1.10 mm). However, the degree of particle breakage is not as significant when compared to Figure 5.22, where the specimens were subjected to higher *CSR* and larger number of cycles.

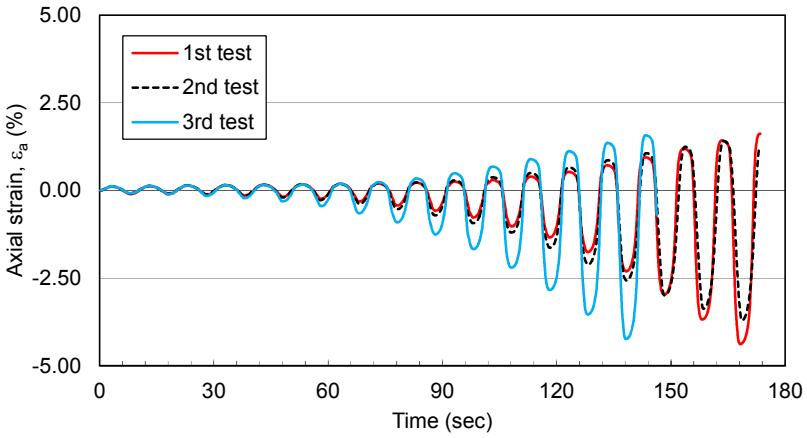

(a) Axial strain time history

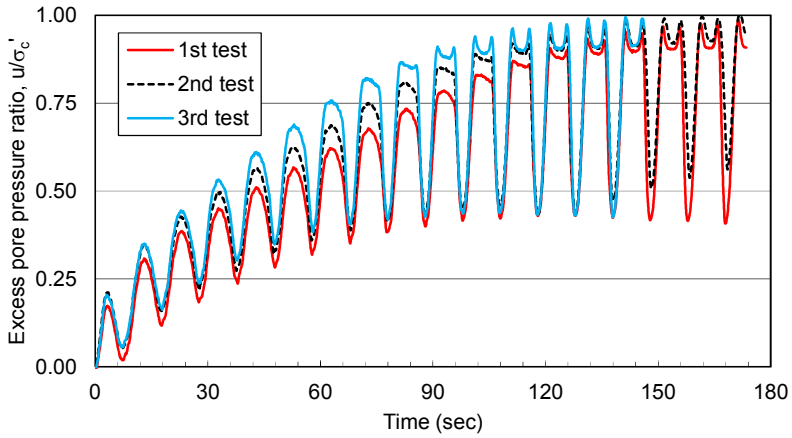

(b) Excess pore water pressure time history

Figure 5.23: Comparison of test results on a reconstituted Pumice A sand specimen subjected to multiple cyclic tests

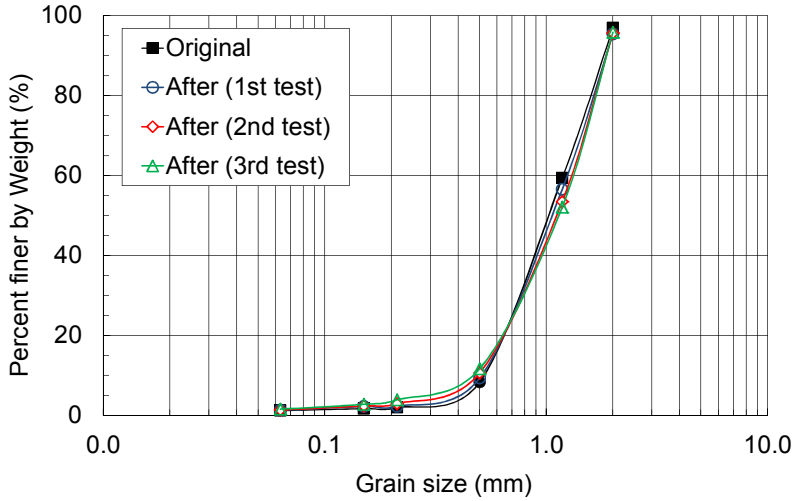

Figure 5.24: Comparison of grain size distribution curves after multiple cyclic tests on the same reconstituted Pumice A sand.

Thus, there is a strong correlation between the decrease in liquefaction resistance and the occurrence of particle breakage in pumice sand specimens. Although the amount of crushed particles is much smaller than the one shown in Section 5.4.3 (where the crushed particles are represented by Pumice C sand), the results are consistent with the observations that fines content decreases the liquefaction potential. This may appear to counter the observation made earlier that particle crushing is the reason for the higher liquefaction resistance of pumice when compared to hard-grained sands. It should be noted that in each test, the specimen was reconstituted using the same sample and therefore, whatever stable soil structure has been formed as a result of particle breakage is destroyed when the new specimen was formed.

5.5.3 *Effect of Number of Cyclic Loading*

In order to observe the development of particle crushing during a cyclic loading test, the tests were terminated after a specified number of cycles and sieve analyses were performed (Series D tests in Table 3.3). For these tests, virgin samples were used at each test. A confining pressure of σ_c'=100 kPa was considered, with the void ratio set at e_i=1.90-2.00. For *CSR*=0.10, the sieve analyses were carries out: (1) on the virgin samples; (2) after the end of consolidation stage; (3) after *N*=10 cycles; (4) after *N*=100 cycles; and (5) after *N*=1000 cycles. On the other hand, for *CSR*=0.20, sieving was done (1) after *N*=10 cycles; and (2) after *N*=83 cycles where initial liquefaction (r_u=100%) occurred. The effective stress paths for the tests at *CSR*=0.10 are shown in Figure 5.25. Such small amplitude of cyclic loading did not induce development of large strain nor generation of high excess pore water pressure; hence, liquefaction did not occur at this level of *CSR*.

The grain size distributions of the specimens after the tests were determined. Particle crushing occurred, but with the level of *CSR* and the number of cycles applied, it was difficult to use the grading curves to make reasonable comparison. Instead, a method of evaluating particle crushing originally proposed by Miura and Yamanouchi (1971) was used which involves the quantification of the surface area of the particles. The specific surface of the particles was measured by first sieving the soil using 2.5 mm, 2.0 mm, 1.18 mm, 0.5 mm, 0.212 mm, 0.15 mm and 0.063 mm sieve sizes. For this range of particle sizes, the specific surface area (in mm^2/mm^3) is calculated using the following equation:

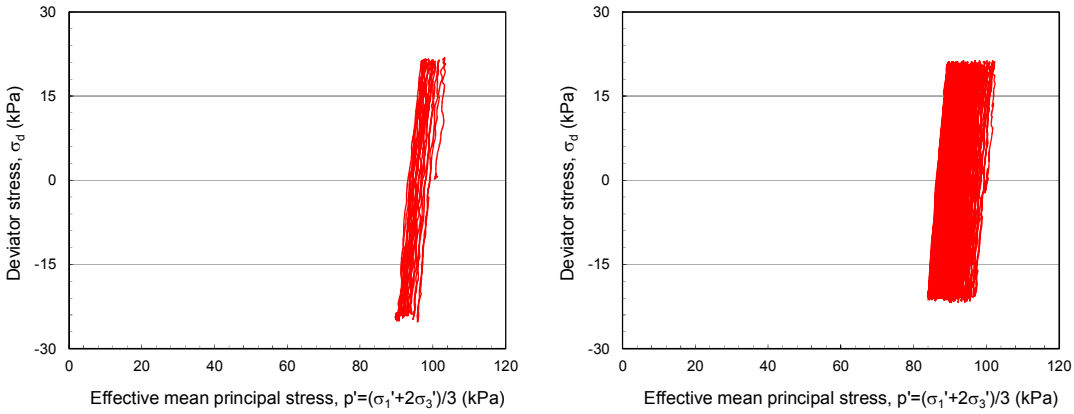

(a) (b)

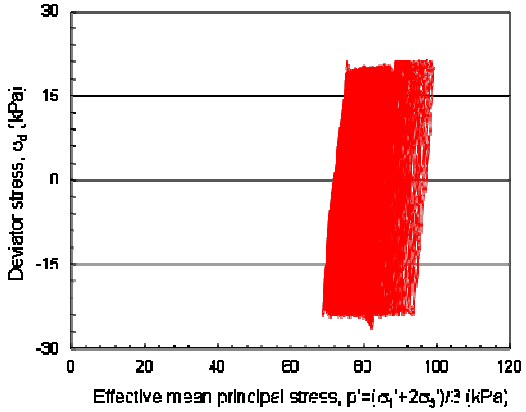

(c)

Figure 5.25: Effective stress paths at *CSR*=0.10: (a) *N*=10 cycles; (b) *N*=100 cycles; and (c) *N*=1000 cycles.

$$S = \sum \frac{F}{100} \cdot \frac{4\pi (d_m / 2)^2}{(4/3)\pi (d_m / 2)^3 G_s \gamma_w} \cdot \gamma_d \tag{5.1}$$

where $d_m = \sqrt{d_1 d_2}$, d_1 and d_2 are adjacent sieve sizes (e.g., 0.50 mm and 0.212 mm), F is the % by weight retained on the sieve, G_s is the specific gravity of the particles, γ_w is the unit weight of water and γ_d is the dry unit weight of the specimen.

Figure 5.26 shows the development of the surface area *S* for the different tests described above. Firstly, it was observed that consolidation at 100 kPa effective confining pressure did not induce appreciable particle breakage to the pumice particles; however, the cyclic shearing did. Secondly, the degree of particle crushing increased with the amplitude of applied *CSR*. For the test with *CSR*=0.20, the increase in surface area during the initial stage of cyclic loading was small; however, as the liquefaction stage was reached (*N*=83), the surface area increased remarkably because large strains occurred with associated translation and rotation of particles causing the higher degree of crushing. For *CSR*=0.10, the state of liquefaction did not occur even when *N*=1000 cycles. Particle breakage was more or less gradual, with almost linear variation with the logarithm of *N*.

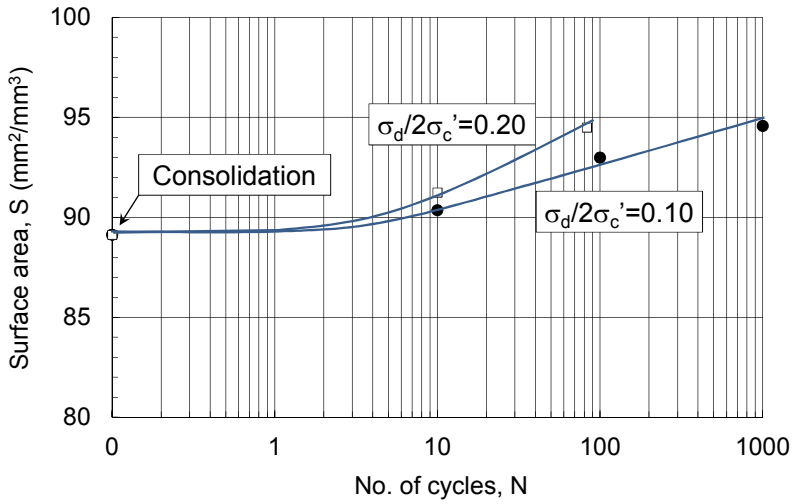

Figure 5.26: Relationships between specific surface area and number of cycles during cyclic undrained tests.

5.6 Summary

The cyclic tests on the undisturbed soil samples indicated higher liquefaction resistance than specimens reconstituted to the same density. This is because the soil structure (fabric, stress history, cementation, etc.) was totally erased when the reconstitution was made. Although dense reconstituted pumice specimens have higher liquefaction resistance than loose ones, the difference was not as remarkable as that observed on hard-grained Toyoura sand, where relative density affected the response significantly. Specimens with reduced grain size (and higher fines content) showed slower development of excess pore water pressure and lower

liquefaction resistance, similar to the behaviour of natural sand with non-plastic fines. The higher liquefaction resistance of pumice when compared with natural sands is a result of particle crushing which occurred during cyclic shearing. As cyclic shearing and particle crushing occurred, the soil structure was gradually stabilized, resulting in higher cyclic shear resistance.

Within the level of confining pressure used in the tests, particle crushing in pumice occurred during cyclic shearing and not during consolidation. In addition, the degree of particle crushing increased with the amplitude of applied cyclic shear stress ratio. During the initial stage of shearing, the increase in surface area (as a result of particle crushing) was small; however, as the liquefaction stage was reached, the surface area increased remarkably because large strains occurred with associated translation and rotation of particles causing the higher degree of crushing. For the sample that did not liquefy, particle breakage during cyclic shearing was more or less gradual, with almost linear variation with the logarithm of the number of cycles applied.

6 CRR EVALUATION BASED ON FIELD TESTS

6.1 General Remarks

As mentioned in Section 2.3, most conventional liquefaction potential evaluation methods are based on empirical correlations between the cyclic resistance and the relative density of the soil. However, for sands like pumice which are susceptible to particle breakage, these methods may not be applicable. The cyclic undrained test results presented in Chapter 5 showed a dependency of cyclic resistance with relative density which is less than that of Toyoura sand, a hard-grained sand. This was supplemented by the observation on Mikkelsen Rd samples where the samples taken at 3 m and 6 m depth were in loose condition, while those obtained from 12 m depth was dense, although similar cone penetration resistances were recorded at these points. Thus, method other than those involving penetration testing may be suitable for crushable pumiceous soils.

Cone penetration tests (CPT) and seismic dilatometer tests (sDMT) were performed at the Mikkelsen Rd site and Carrs Rd site to supplement the undrained cyclic triaxial tests conducted on the undisturbed samples taken from these sites. The field tests were performed as near as possible to the sampling site. Correlations between the cyclic resistance obtained from the laboratory tests and the in-situ parameters were performed to confirm which method was appropriate for pumice. Note that undisturbed soil samples were obtained at 3 elevations in Mikkelsen Rd site, while samples from Carrs Rd site were taken only at a single depth; hence, emphasis is placed on the former. In addition, the results presented herein may be appropriate only for the two sites investigated and further tests are necessary to confirm their applicability to other pumiceous sites.

6.2 Correlation between Field and Laboratory *CRR*

As discussed in Chapter 5, the results of undrained cyclic triaxial tests are summarised in the form of liquefaction resistance curve. Moreover, it is customary to consider 15 cycles in view

of the typical number of significant cycles present in many time histories of accelerations recorded during past earthquakes. Thus, the liquefaction resistance (or cyclic strength) is specified in terms of the magnitude of cyclic stress ratio required to produce 5% double amplitude axial strain in 15 cycles of uniform load application; herein, this is referred to as $(CRR)_{triaxial}$.

However, the conditions the laboratory specimens were subjected to are different from those in-situ. Hence, in order to estimate the in-situ liquefaction resistance, $(CRR)_{field}$, corrections need to be applied to the laboratory-obtained values. The corrections are typically written as

$$(CRR)_{field} = C_1 \cdot C_2 \cdot C_3 \cdot C_4 \cdot C_5 \cdot (CRR)_{triaxial} \tag{6.1}$$

where, according to Towhata (2008):

C_1 – correction due to difference in consolidation stress. $C_1=(1+2K_0)/3$ where $K_0=0.5$ for normally consolidated soils;

C_2 – correction due to difference in loading condition, where earthquake loading is irregular while laboratory specimens are subjected to sinusoidal waves. $C_2=1/0.65$ or $(=1/0.55$-$0.70)$.

C_3 – correction due to sample disturbance. $C_3>1$, but not clearly understood yet.

C_4 – correction due to densification during handling. $C_4<1$, but not clearly understood yet.

C_5 – correction due to loading direction, where earthquake loading is at least two components, E-W and N-S. $C_5=0.80$-0.90.

The Japanese Design Code for Highway Bridges (JRA 1996), which is one of the most important codes addressing liquefaction, states that when $K_0=0.5$, then $C_1 \cdot C_2 \approx 1$. Moreover, $C_3 \cdot C_4 \approx 1$ is assumed, although the quality of the samples is unpredictable. By further assuming $C_5 \approx 1$, it follows that $C_1 \cdot C_2 \cdot C_3 \cdot C_4 \cdot C_5 \approx 1$ and

$$(CRR)_{field} \approx (CRR)_{triaxial} \tag{6.2}$$

Thus, in liquefaction potential evaluation, the laboratory-derived cyclic resistance ratio can be taken directly as the representative of the in-situ cyclic resistance ratio.

6.3 CPT-based Approach

Several cone penetration tests were performed at Carrs Rd site and Mikkelsen Rd site in this research. The cone tip resistance, q_c, obtained in the test is normalised as follows:

$$Q_{tn} = \left(\frac{q_c - \sigma_v}{P_a} \right) \left(\frac{P_a}{\sigma_v'} \right)^n \tag{6.3}$$

where Q_{tn} is the normalised cone resistance, σ_v and σ_v' are the total and effective overburden pressures, P_a is the atmospheric pressure and n is a stress component which is taken as 1.0 for clay, 0.5 for sand and between 0.5 and 1.0 for silts and sandy silts. The equivalent clean sand cone penetration resistance, $Q_{tn,cs}$ is then estimated as

$$Q_{tn,cs} = K_c \cdot Q_{tn} \tag{6.4}$$

In the above equation, K_c is a correction factor that is a function of grain characteristics (combined influence of fines content and plasticity) of the soil. Details of calculating K_c are presented by Robertson (2009) and Robertson and Cabal (2010).

The locations of the CPT soundings are shown in Appendices A & B. For the purpose of the analysis, the CPT results close to the sampling site were considered. For Mikkelsen Rd site, the result from CPT-02 (provided by AECOM which was nearest borehole DH-01 from where the samples were obtained) was used, although two other tests (CPT-01a and CPT-02a) were also performed at the site; however, there is not much difference between the results of CPT-02 and CPT-01a. For Carrs Rd site, tests were not performed adjacent to BH-03 where the sample was obtained; nevertheless, comparisons of the CPT data obtained at the site showed more or less similar stratigraphy. Hence, in this analysis, CPT-01 data was used. Note that the tip resistance, q_c, sleeve friction, f_s and dynamic pore pressure, u_2, were

measured at 0.1 m interval. The effective overburden pressure σ_v' at each specified elevation was estimated based on the measured depth of water table, the assumed unit weights of soil at each layer (inferred from the borehole log) and depth of the target point from the ground surface.

Figure 6.1 shows the plot of the *CRR* vs $Q_{tn.cs}$ relationship for the undisturbed samples used in this study, together with the boundary line separating liquefaction/no-liquefaction as proposed by Robertson and Wride (1998). Note that the cyclic tests were conducted at effective confining pressures less than 100 kPa; hence, appropriate correction factor, K_σ, must be considered when comparing laboratory results with $Q_{tn,cs}$ which is normalized at σ_v'=100 kPa. Considering the results shown in Section 5.4.2 and the findings of Boulanger and Idriss (2004), a value of K_σ=1.10 is assumed for all four values. Moreover, the $(CRR)_{triaxial}$ do not correspond to ε_{DA}=5%; rather, the liquefaction resistance curves shown in Chapter 5 were obtained for ε_{DA}=2% for Carrs Rd site sample and ε_{DA}=4% for Mikkelsen Rd samples. However, no studies have been conducted to date to determine the equivalent *CRR* when the reference double amplitude axial strain is not equal to ε_{DA}=5%. To simplify the analysis and considering that ε_{DA}=4% and 5% are not that much different, it is assumed that the increase in *CRR* for Mikkelsen Rd samples required for ε_{DA}=5% is similar to the magnitude of decrease in *CRR* when K_σ is applied; i.e., the *CRR* that will be used in the analysis is the same as those obtained in the laboratory tests. However, for Carrs Rd site sample, the required *CRR* for ε_{DA}=5% is difficult to estimate from the *CRR* obtained for ε_{DA}=2%; hence, for the purpose of the comparison, it is simply assumed that the corresponding *CRR* must be much higher, even with the incorporation of K_σ, and this is indicated in the figure by an arrow sign directed upward (i.e., inferred value > indicated).

It can be observed that majority of the data points underestimate the cone penetration required for the specified *CRR*. This is consistent with the chamber test results obtained by Wesley et al. (1999) and shown in Figure 2.2 which indicates that cone penetration resistance on pumice sand is only marginally influenced by the density of the material. It is hypothesized that the shear stresses imposed by the cone penetrometer are so severe that particle breakage forms new finer grained materials, the mechanical properties of which are nearly independent of the initial state of the sand. This behaviour is very different from that

observed on typical hard-grained sands. Thus, conventional relationships between cone resistance, relative density, and liquefaction resistance are not valid for pumice.

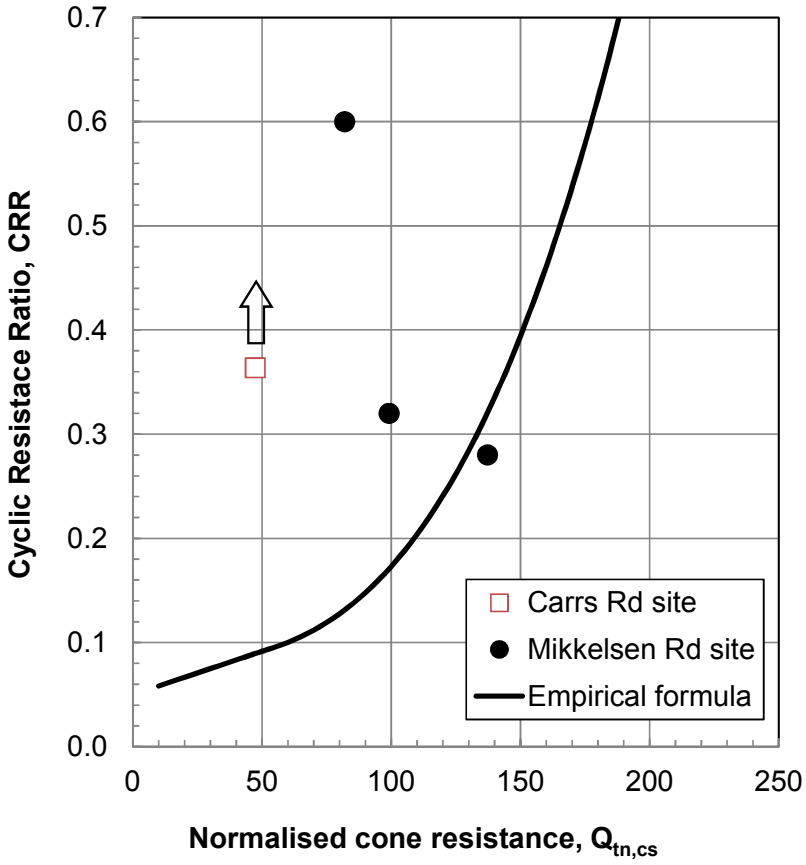

Figure 6.1: Relationships between *CRR* of undisturbed specimens and normalised cone resistance from CPT tests.

6.4 SDMT-based Approach

Seismic dilatometer tests (SDMT) were also performed adjacent to the boreholes where the undisturbed samples were performed. As discussed in Sections 2.3 and 3.6, three independent parameters can be obtained in SDMT, all of which can be correlated with the liquefaction resistance of sands: shear wave velocity (V_s), dilatometer modulus (E_D) and horizontal stress index (K_D). The values of CRR estimated from these three parameters at the elevations where the undisturbed samples were obtained are compared with the laboratory-obtained liquefaction resistance of the samples.

For the purpose of the analysis, the result of SDMT-03 (see Appendix A) is used for Carrs Rd site, and SDMT-03 (see Appendix B) is employed for Mikkelsen Rd site.

6.4.1 *V_s-based Method*

The shear wave velocity was measured at an interval of 0.5 m. The value normalised for an overburden pressure of σ_v'=1 kg/cm^2 (or 98 kPa) were obtained at each elevation where the samples were obtained, and compared with the *CRR* obtained from the cyclic tests (considering the effects of K_σ and ε_{DA} used, as described above). The result is shown in Figure 6.2, together with the *CRR* versus V_{s1} curve recommended for engineering practice by Andrus and Stokoe (2000) for magnitude 7.5 earthquakes and uncemented Holocene-age soils with fines contents F_c>35%. It can be observed that there is a very good correlation between $(CRR)_{triaxial}$ and V_{s1}, indicating that shear wave velocity-based approach may better

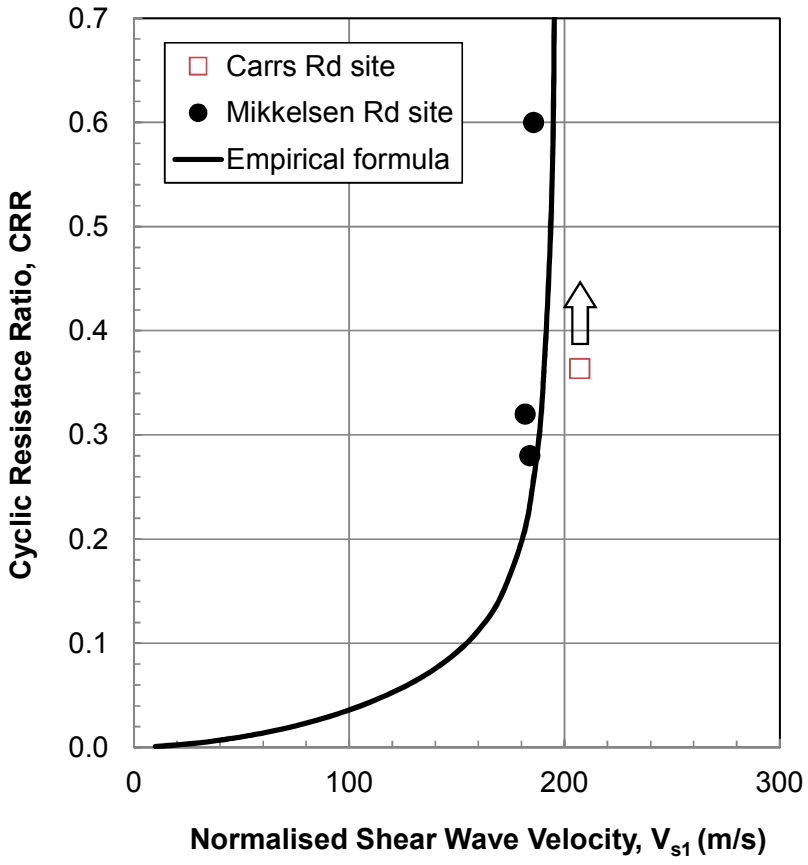

Figure 6.2: Relationships between *CRR* of undisturbed specimens and normalised shear wave velocity from SDMT tests.

suited to crushable sands like pumice. Although the penetrating rod during the SDMT may have induced particle breakage in the adjacent zone, the shear wave travelled faster through the more intact grains rather than the crushed ones; hence, we can say that the measured shear wave velocity represents the true velocity in the pumice deposit.

Non-destructive methods of measuring V_s, such as through spectral analysis of surface waves (SASW) or multi-channel analysis of surface waves (MASW), are therefore better alternatives since they will not induce breakage of pumice particles.

6.4.2 *E_D- and K_D-based Methods*

The dilatometer consists of a flat, 15 mm thick and 95 mm wide blade and has a length of 220 mm. A flexible, stainless steel membrane, 60 mm in diameter, is located on one face of the blade. Inside the steel membrane there is a pressure chamber and a distance gauge for measurement of the movements of the membrane when the pressure inside is changed. The probe is pushed into the soil with the aid of hollow sounding rods and does not require drilling of a hole. When the membrane is inflated, the pressure required to just lift the membrane off the sensing device (p_0) and to cause 1.10 mm deflection (p_1) are recorded. As the pressure is released and the membrane returns to its initial lift-off position, another reading can be taken. The pressure values p_0 and p_1 can be used to define three index parameters. Marchetti (1980) referred to these parameters as the material index (I_D), the horizontal stress index (K_D) and the dilatometer modulus (E_D), respectively. These are calculated as follows:

$$I_D = \frac{p_1 - p_0}{p_0 - u_0} \tag{6.5a}$$

$$K_D = \frac{p_0 - u_0}{\sigma_{v0}'} \tag{6.5b}$$

$$E_D = 34.7(p_1 - p_0) \tag{6.5c}$$

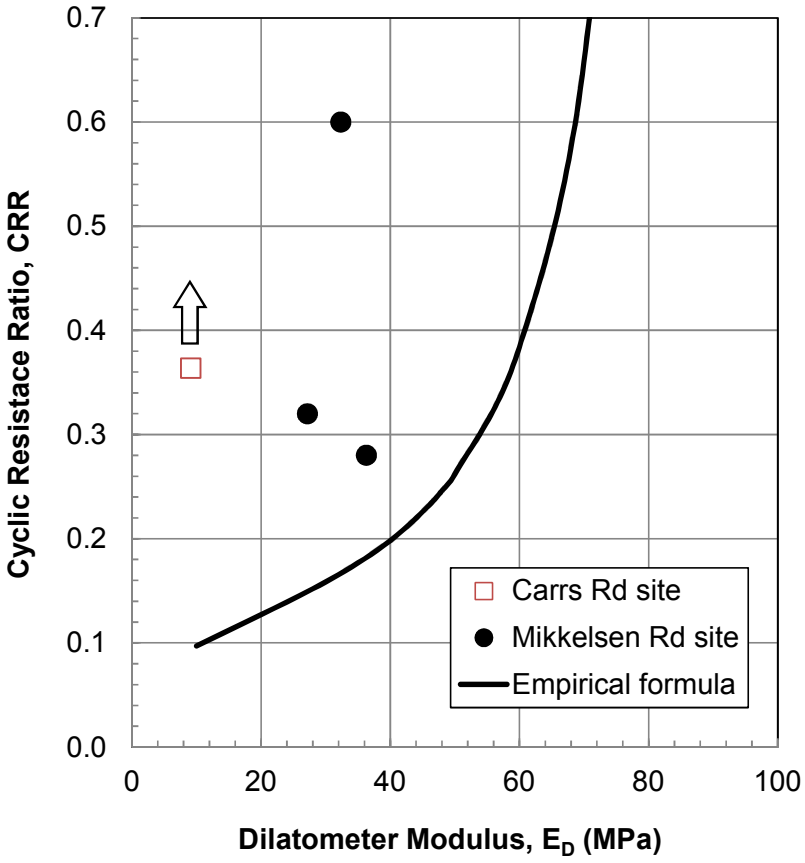

Figure 6.3: Relationships between CRR of undisturbed specimens and dilatometer modulus from SDMT tests.

where u_0 and σ_{v0}' are the in-situ initial pore water pressure and initial effective overburden pressure, respectively. The tests were performed at 0.2 m interval and the values from SDMT tests at the specified elevations were compared to the *CRR*-values of the appropriate undisturbed samples. Figures 6.3 and 6.4 show the relations between *CRR* and the K_D and E_D values, respectively. Also shown in the figures are the boundary curves proposed by Tsai et al. (2009). It can be seen that in both plots, the data points overestimate the *CRR* required for the indicated parameters (or underestimate the required E_D and K_D values). Although several researchers have shown good correlations between *CRR* and the SDMT-obtained parameters, it appears that it is not the case for crushable soils. The penetration of the dilatometer may have crushed the adjacent soils, and the pressures measured when the membrane is displaced (either to lift the membrane or to inflate it to 1.1mm distance) actually indicate the stresses on the crushed zone, not on the intact pumice grains. Since both of these parameters (more notably K_D) are affected by soil fabric (aging, prestressing, cementation and structure, etc.),

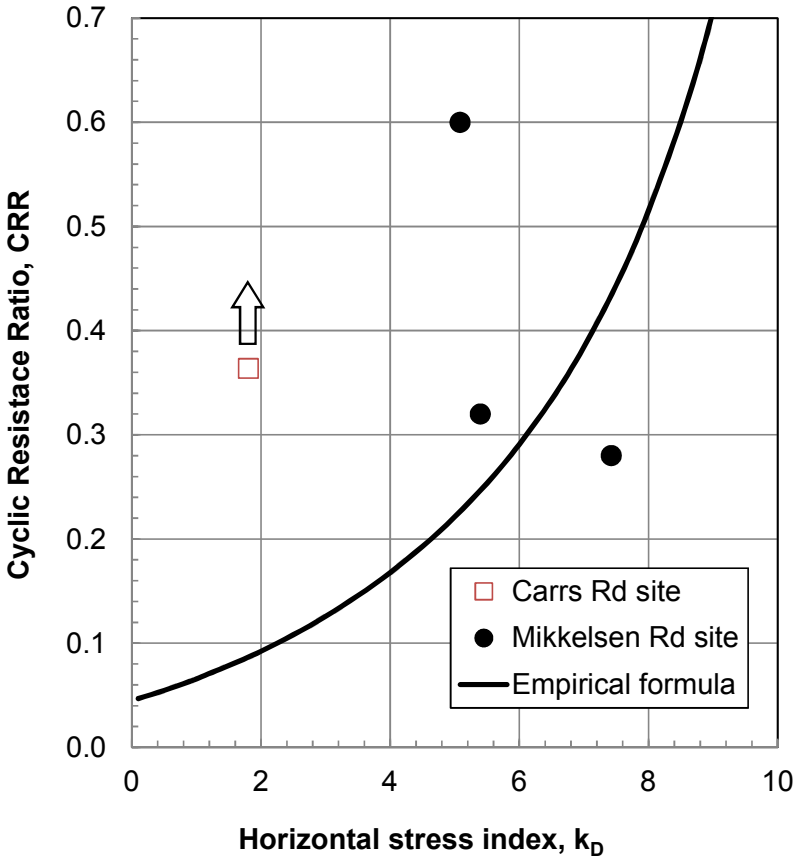

Figure 6.4: Relationships between *CRR* of undisturbed specimens and horizontal stress index from SDMT tests.

the crushing induced by the penetration may have affected the actual values and therefore these do not reflect those of the original pumice soils.

Although very few data points were presented in this research, it seems that the degree of scatter for the K_D- and E_D-based boundary curves to delineate liquefaction is similar to that of the CPT-based curve. Thus, the penetration-induced crushing of the pumice grains can underestimate the liquefaction resistance of the soil. When evaluating the liquefaction potential of pumiceous deposits, a V_s-based approach may be more appropriate.

6.5 Summary

A comparison of laboratory-obtained cyclic resistance and those estimated from conventional liquefaction potential evaluation procedures showed that penetration-based approaches, such as cone penetration tests and seismic dilatometer tests, underestimated the value of *CRR*. It is hypothesized that the shear stresses during penetration were so severe that particle breakage formed new finer grained materials, the mechanical properties of which were very different from the original pumice sand. Thus, any procedure where the liquefaction resistance is correlated with density will not work on pumiceous deposits.

On the other hand, empirical method based on shear wave velocity seemed to produce good correlation with liquefaction resistance of pumiceous soils. Although the shear wave velocity in this research was obtained from SDMT where the penetrating rod may have induced particle breakage in the adjacent zone, the shear waves travelled through the intact grains and not on the crushed ones. It follows that non-destructive methods of measuring shear wave velocity, such as through spectral analysis of surface waves (SASW) or multi-channel analysis of surface waves (MASW), may be better alternatives in estimating the in-situ liquefaction resistance of pumiceous deposits.

7 CONCLUSIONS AND RECOMMENDATIONS

In order to investigate the liquefaction characteristics of pumice sands, a comprehensive testing programme was implemented, consisting of several series of undrained monotonic and cyclic triaxial tests, mostly on reconstituted pumice specimens and on several undisturbed specimens, and geotechnical investigations at sites of pumiceous deposits. The following sections summarize the main conclusions drawn, and the significant contributions made, by this study.

7.1 Conclusions from Monotonic Undrained Tests

1. Specimens reconstituted under loose and dense states showed similar response under monotonic undrained shearing, indicating that relative density did not have significant effect on the behaviour of pumice.
2. Within the range of effective confining pressures investigated, pumice specimens showed contractive response followed by dilative behaviour. The contractive response was more significant at higher confining pressure.
3. The stress-strain relations of pumice showed a stiff response at small strain level, followed by the development of large strains and larger dilatancy when the phase transformation (from contractive to dilative) state was reached.
4. Pumice A sands, characterised by larger grain size, had an angle of internal friction at failure of about 44^o while Pumice B sands, with smaller grain size, had about 42^o. These friction angles, which were not affected by density, were far greater than those obtained in hard-grained sands.
5. The friction angle at phase transformation was about $36\text{-}37^o$ for Pumice A sands and $34\text{-}36^o$ for Pumice B sands; again, these values were much higher than those of hard-grained sands.
6. Even under large strain level, pumice sands did not reach the steady state of deformation. This can be attributed to breakage of particles during shearing, which resulted in more resistant soil structure that did not allow deformation at constant shear stress to occur.

7. Critical state soil mechanics may not be applicable to crushable soils like pumice.

7.2 Conclusions from Cyclic Undrained Tests

1. The undisturbed soil samples taken at Mikkelsen Rd site have higher liquefaction resistance than specimens reconstituted to the same density. This is because the soil structure (fabric, stress history, cementation, etc.) was totally erased when the reconstitution was done. The Carrs Rd site undisturbed samples have much higher liquefaction resistance, possibly because of the high fines content and high plasticity.
2. Dense reconstituted pumice specimens have higher liquefaction resistance than loose ones. However, the difference in resistance was not remarkable when compared with the behaviour of Toyoura sand, where relative density affected the response significantly.
3. Defining liquefaction resistance as the cyclic deviator stress ratio corresponding to 15 cycles, it was observed that very dense Toyoura sand (with D_r =90%) and dense pumice sand (D_r =70%) have practically the same resistance. On the other hand, the cyclic resistance of loose pumice sand (D_r =25%) is about twice of that of medium dense Toyoura sand (D_r =50%).
4. As the confining pressure was increased, the liquefaction resistance curve of reconstituted pumice specimens was shifted downward, consistent with the observations made on hard-grained sands. The values of the correction factor K_σ (cyclic stress ratio causing 5% double amplitude axial strain in 15 cycles under any confining pressure normalised to the corresponding value of *CSR* at σ_c'=100 kPa) coincided with those reported for reconstituted hard-grained sands.
5. Specimens with reduced grain size (and higher fines content) showed slower development of excess pore water pressure and lower liquefaction resistance.
6. The higher liquefaction resistance of pumice when compared with hard-grained sands was the result of particle crushing which occurred during cyclic shearing. As cyclic shearing and particle crushing occurred, the soil structure was gradually stabilized, resulting in higher cyclic shear resistance.
7. When the same specimen was subjected to cyclic shear and then re-tested, a decrease in resistance was observed. This was because some of the particles were crushed, resulting in increase in fines content. Whatever stable soil structure has been formed as a result of

particle breakage was destroyed when the new specimen was formed. Hence, consistent with Conclusion (5) above, this resulted in decrease in liquefaction resistance.

8. Within the level of confining pressure used in the tests, particle crushing in pumice occurred during cyclic shearing, not during the consolidation stage. In addition, the degree of particle crushing increased with the amplitude of applied cyclic shear stress ratio.
9. During the initial stage of shearing, the increase in surface area (as a result of particle crushing) was small; however, as the liquefaction stage was reached, the surface area increased remarkably because large strains occurred with associated translation and rotation of particles causing the higher degree of crushing.
10. Prior to liquefaction, particle breakage during cyclic shearing was more or less gradual, with almost linear variation with the logarithm of the number of cycles applied.

7.3 Conclusions from Geotechnical Investigations

1. CPT-based empirical methods of estimating the cyclic resistance ratio (*CRR*) underestimated the in-situ values, which were taken to be similar to those obtained from the cyclic triaxial tests. It was hypothesized that the shear stresses imposed by the cone penetrometer were so severe that particle breakage formed new finer grained materials, the mechanical properties of which were nearly independent of the initial state of the sand. This showed that conventional relationships between cone resistance, relative density, and liquefaction resistance were not valid for pumice.
2. Similarly, parameters obtained from SDMT, such as the dilatometer modulus and horizontal stress index, did not correlate well with liquefaction resistance. The penetration of the dilatometer may have crushed the adjacent soils, and the pressures measured when the membrane was displaced (either to lift the membrane or to inflate it to 1.1mm distance) actually indicated the stresses on the crushed zone, not on the intact pumice grains.
3. On the other hand, the empirical method based on shear wave velocity seemed to produce good correlation with liquefaction resistance of pumiceous soils. Although the penetrating SDMT rod may have induced particle breakage in the adjacent zone, the shear wave travelled faster through the more stable grains rather than the crushed ones;

hence, the measured shear wave velocity represented the true velocity in the pumiceous soil medium.

4. Non-destructive methods of measuring V_s, such as through spectral analysis of surface waves (SASW) or multi-channel analysis of surface waves (MASW), may be better alternatives to estimate the liquefaction resistance of pumice since they will not induce breakage of the particles.

7.4 Recommendations for Future Work

Whilst this study has made a number of contributions to the knowledge about the liquefaction characteristics of pumice through laboratory testing and field investigations, much more research can be performed to clarify some of the issues raised in this research. Some suggestions for future studies are the following:

1. More laboratory tests (i.e. both monotonic and cyclic undrained tests) are recommended to be undertaken on other types of pumiceous soils. Samples taken from sites other those presented in this research are preferred, both in undisturbed and disturbed states. This will provide more opportunities to investigate the liquefaction characteristics of other varieties of pumice.
2. More field tests at other pumiceous sites are encouraged. These will not only confirm which other empirical method is better suited for pumice, but will also provide larger database to calibrate the results. In addition, the relationships between various in-situ parameters, such as between q_c of CPT and K_D of SDMT, can be investigated when more data are available. This may also provide an opportunity to estimate important in-situ properties of pumiceous soils, such as relative density, which are difficult to assess with conventional procedures.

REFERENCES

Andrus, R.D. & Stokoe, K.H., II. (2000). “Liquefaction resistance of soils from shear-wave velocity,” *J. Geotech. Geoenv. Engrg.*, ASCE, 126(11), 1015-1025.

Boulanger, R.W & Idriss, I.M. (2004). “State normalization of penetration resistances and the effect of overburden stress on liquefaction resistance,” *Proc., 11th International Conference on Soil Dynamics and Earthquake Engineering and 3rd International Conference on Earthquake Geotechnical Engineering*, Vol. 2, 484-491.

Casagrande, A. (1976). “Liquefaction and cyclic deformation of sands: A critical review,” *Harvard Soil Mechanics Series*, 88.

Castro, G. & Poulos, S. J. (1977). “Factors affecting liquefaction and cyclic mobility,” *J Geotech Eng Div*, ASCE, 103, 501 - 516.

Creinarz (2010). “Soil liquefaction,” *EERI Chile Earthquake Clearinghouse*, http://www.eqclearinghouse.org/20100227-chile/reports-from-the-field/soil-liquefaction-3

Cubrinovski, M. & Ishihara, K. (2000). “Flow potential of sandy soils with different grain compositions,” *Soils and Foundations*, 40, 103 - 119.

Cubrinovski, M. & Ishihara, K. (2002). “Maximum and minimum void ratio characteristics of sands,” *Soils and Foundations*, 42, 65 - 78.

Cubrinovski, M, Green, R, Allen, J, Ashford, S, Bowman, E, Bradley, B, Cox, B., Hutchinson, T., Kavazanjian, E., Orense, R., Pender, M., Quigley, M, & Wotherspoon, L.M. (2010). “Geotechnical reconnaissance of the 2010 Darfield (Canterbury) Earthquake,” *Bulletin of the New Zealand Society for Earthquake Engineering*, 43 (4), p243-320.

Franks, C.A.M. (1988). "Engineering geological aspects of the Edgecumbe, New Zealand earthquake of 2 March 1987". *Quarterly Journal of Engineering Geology* 21 (4): 337–345.

Hatanaka, M., Sugimoto, M. & Yoshio, S. (1985). “Liquefaction resistance of two alluvial volcanic soils sampled by in-situ freezing,” *Soils and Foundations*, Vol. 25, No. 3, 49-63.

Ishihara, K. (1993). “Liquefaction and flow failure during earthquakes,” *Geotechnique*, 43, 351 - 415.

Ishihara, K., (1996). *Soil Behaviour in Earthquake Geotechnics*, Oxford Science.

Ishihara, K. & Harada, K. (1996). “Cyclic behaviour of partially saturated collapsible soils subjected to water permeation,” *Ground Failures under Seismic Conditions*, ASCE, Geotechnical Special Publication No. 44, 34-50.

Japan Road Association, JRA (1996). *Specifications for Highway Bridges, Part V, Seismic Design* (in Japanese).

Japan Society of Civil Engineers-Japanese Geotechnical Society (2003). *Damage Investigation Report of the 26 May 2003 off Miyagi Prefecture Earthquake* (in Japanese).

Kikkawa, N. (2008). “Stress relaxation during Ko compression of pumice sand,” *Proc. 8th ANZ Young Geotechnical Professionals Conference 2008*, Wellington, NZ, 5-8 November, 97-102.

Kikkawa, N., Pender, M.J., Orense, R.P. & Matsushita, E. (2009). “Behaviour of pumice sand during hydrostatic and Ko compression,” *Proceedings, 17th International Conference on Soil Mechanics and Geotechnical Engineering,* Alexandria (Egypt), 5-9 October 2009, Vol. 1, 812-815.

Kikkawa, N., Orense, R.P. & Pender, M.J. (2011a). ”Mechanical behaviour of loose and heavily compacted pumice sand,” *Proc., 14th Asian Regional Conference on Soil Mechanics and Geotechnical Engineering*, Hong Kong, 23-27 May 2011, Paper 214. 6pp.

Kikkawa, N., Orense, R.P. & Pender, M.J. (2011b). “Observations on microstructure of pumice particles using computed tomography,” *Geotechnical Testing Journal* (submitted).

Marchetti, S. (1980). “In situ tests by flat dilatometer," *J. Geotech. Engrg. Div.*, ASCE, 106(GT3), 299-321.

Marchetti, S., Monaco, P., Totani, G. & Marchetti, D. (2008). “In situ tests by seismic dilatometer (SDMT),” *ASCE Geotecnical Special Publication GSP No. 170*, 20pp.

Matsumoto, K., Hyodo, M. & Yoshimoto, N. (1999). “Cyclic shear properties of intermediate soils subjected to initial shear,” *Proc., 34h Japan National Conference on Geotechnical Engineering*, 637-638 (in Japanese).

Mishima, S. & Kimura, H. (1970). “Characteristics of landslides and embankment failures during the Tokachi-oki earthquake,” *Soils and Foundations*, Vol. 10, No. 2, 39-51.

Miura, N. & Yamanouchi, T. (1971). “Drained shear characteristics of Toyoura sand under high confining stress,” *Proc. of Japanese Society of Civil Engineers*. 260: 69-79 (in Japanese).

Miura, S. & Yagi, K. (1995). "The effect of stress history on the dynamic characteristics of a coarsed-grained volcanic soil," *Proc. Symposium on Properties of Volcanic Ash Soils related to Design and Construction*, Japanese Geotechnical Society, 229-236 (in Japanese).

Monaco, P., Marchetti, S., Totani, G. & Calabrese, M. (2005). "Sand liquefiability assessment by flat dilatometer test (DMT)," *Proc. XVI ICSMGE*, Osaka, 4, 2693-2697.

New Zealand Standard (1986). *NZS 4402 : 1986 - Methods of Testing Soils for Civil Engineering Purposes*. Part 2 Soil classification tests. 2.7 Determination of the solid density of soil particles. Test 2.7.2 Method for medium and fine soils

Okabayashi, T., Hyodo, M., Murata, H., Yamamoto, T., Nakata, Y., Kitamura, R., Kobayashi, T., Fujii, T. & Kusakabe, S. (1998). "Geotechnical property of the 1997 Kagoshimaken-hokuseibu and Daini-hokuseibu earthquakes," *Western Regional Division Report of Japan Group for the Study of Natural Disaster*, (22), 21-28 (in Japanese).

Orense, R., Vargas-Monge, W. & Cepeda, J. (2002). "Geotechnical aspects of the January 13, 2001 El Salvador Earthquake," *Soils and Foundations*, Vol. 42, No. 4, 57-68.

Orense, R., Pender, M., Wotherspoon, L. & Cubrinovski, M. (2011a). "Geotechnical aspects of the 2010 Darfield (New Zealand) Earthquake," I*nvited Lecture, 8th International Conference on Urban Earthquake Engineering, Tokyo (Japan)*, 7 - 8 March, 2011, 407-416.

Orense, R.P., Kiyota, T., Yamada, S., Cubrinovski, M., Hosono, Y., Okamura, M. & Yasuda, S. (2011b). "Comparison of liquefaction features observed during the 2010 and 2011 Canterbury earthquakes," *Seismological Research Letters, 82* (6), p905-918. DOI: 10.1785/gssrl.82.6.905

Orense, R.P., Larkin, T., & Chouw, N. (2011c). "Bridge performance during the 2010/2011 Canterbury Earthquakes," *Proc., Australian Earthquake Engineering Society Annual Conference*, Barossa Valley, South Australia, 18-20 November 2011, 8pp.

Pender, M.J. & Robertson, T.W., Editors. (1987). "Edgecumbe Earthquake: Reconnaissance Report," *Bull. New Zealand Society for Earthquake Engineering*, Vol. 20(3), September 1987, p. 201-249.

Pender, M. J. (2006). "Stress relaxation and particle crushing effects during Ko compression of pumice sand," *Proc. International Symposium on Geomechanics and Geotechnics of Particulate Media*, Yamaguchi, Japan, Vol.1, 91-96.

Pender, M.J., Wesley, L.D., Larkin, T.J. & Pranjoto, S. (2006). "Geotechnical properties of a pumice sand," *Soils and Foundations*, 46, (1), 69-81.

Robertson, P.K. & Wride, C.E. (1998). "Evaluating cyclic liquefaction potential using the cone penetration test," *Canadian Geotechnical Journal*, 35(3), 442-459.

Robertson, P.K. (2009). "Performance-based earthquake resistant design using the CPT," *Keynote Lecture, Performance-based Design in Earthquake Geotechnical Engineering*, 3-20.

Robertson, P. K. & Cabal, K. L. (2010) *Guide to Cone Penetration Testing for Geotechnical Engineering*, Gregg Drilling & Testing, 4th Edition.

Robinson, K., Cubrinovski, M., Kailey, P. & Orense, R. (2011). "Field measurements of lateral spreading following the 2010 Darfield Earthquake", *Proc. 9th Pacific Conference on Earthquake Engineering*, Auckland, 14 April - 16 April, 2011, Paper 052, 8pp.

Rollins, K.M. & Seed, H. B. (1988). "Influence of buildings on potential liquefaction damage," *Journal of Geotechnical Engineering, ASCE*, 116, GT2, 165-185.

Seed, H.B. & Idriss, I.M. (1971). "Simplified procedure for evaluating soil liquefaction potential," *Journal of Soil Mechanics and Foundation Division, ASCE,* Vol. 97, No. 9, 1249-1273.

Seed, R.B. & Harder, I.F. (1990). "SPT-based analysis of cyclic pore pressure generation and undrained residual strength," *Proceedings of the B. Seed Memorial Symposium*, Vol. 2, 351-376.

Suzuki, M. & Yamamoto, T. (2004). "Liquefaction characteristic of undisturbed volcanic soil in cyclic triaxial test," *Proc., 13th World Conference on Earthquake Engineering*, Vancouver, B.C., Canada, Paper No. 465.

Towhata, I. (2008). *Geotechnical Earthquake Engineering*, Springer Series in Geomechanics and Geoengineering, Springer Verlag.

Tsai, P.H., Lee, D.H., Kung, G.T.C. & Juang, C.H. (2009). "Simplified DMT-based methods for evaluating liquefaction resistance of soils," *Engineering Geology*, Vol. 103, No. 102, 13-22.

Uzuoka, R., Sento, N., Kazama, M. & Unno, T. (2005). "Landslides during the earthquakes of May 26 and July 26, 2003 in Miyagi," *Soils and Foundations*, Vol. 45, No. 4, 149-164.

Wesley, L. D., Meyer, V. M., Pronjoto, S., Pender, M. J., Larkin, T. J. & Duske, G. C. (1999). "Engineering properties of pumice sand," *Proc. 8th Australia-NZ Conference on Geomechanics*, Hobart, Vol. 2, 901-908.

Wesley, L. D. (2001). "Determination of specific gravity and void ratio of pumice materials," *Geotechnical Testing Journal*, 24 (4), 418-422.

Yamada, S., Orense, R.P., & Cubrinovski, M. (2011). “Geotechnical damage due to the 2011 Christchurch. New Zealand Earthquake,” *ISSMGE Bulletin*, Vol. 5, Issue 2, April 2011, pp. 27-45, 2011

Yamamoto, T., Okabayashi, T. & Matsumoto, N. (1997). “Earthquake disaster in the 1997 Kagoshimaken-hokuseibu and Daini-hokuseibu earthquakes,” *Japan Society for Earthquake Engineering Promotion News*, (157), 31-41 (in Japanese).

Yamamoto, Y., Hyodo, M. & Orense, R. (2009). “Liquefaction resistance of sandy soils under partially drained condition,” *Journal of Geotechnical and Geoenvironmental Engineering, ASCE*, Vol. 135, No. 8, 1032-1043.

Yamanouchi, T. (1968). “Ground failure due to the Ebino earthquake,” Report of the JSSMFE Technical Committee on Shirasu, *Tsuchi-to-Kiso, JSSMFE*, 16(9), 47-59 (*in Japanese*).

Yoshimi, Y., Hatanaka, M. & Oh-oka, H. (1978). “Undisturbed sampling of saturated sands by freezing,” *Soils and Foundations*, Vol. 18, No. 3, 59-73.

Yoshimoto, N., Hyodo, M., Nakata, Y., Orense, R. & Murata, H. (2006). “Cyclic shear strength characteristics of granulated coal ash,” *Soil and Rock Behavior Modeling: Proceedings of Sessions of Geo-Shanghai, June 6-8, 2006, Shanghai, China (ASCE Geotechnical Special Publication No. 150),* 474-481.

Youd, T.L. Idriss, I.M. Andrus, R.D. Arango, I., Castro, G., Christian, J.T., Dobry, R., Liam Finn, W.D.L., Harder, L.F., Jr., Hynes, M.E., Ishihara, K., Koester, J.P., Liao, S.S.C., Marcuson, W.F., III, Martin, G.R., Mitchell, J.K., Moriwaki, Y., Power, M.S., Robertson, P.K., Seed, R.B. & Stokoe, K.H., II (2001). “Liquefaction resistance of soils: Summary report from the 1996 NCEER and 1998 NCEER/NSF Workshops on Evaluation of Liquefaction Resistance of Soils,” *Journal of Geotechnical and Geoenvironmental Engineering, ASCE*. 127 (10), p 817–833.

APPENDIX A

Carrs Rd Site

(Wairere Drive, Waikato)

A – 1: Location Map

A – 2: Approximate locations of geotechnical investigations

A – 3: Drillhole Log

A – 4: CPT Soundings

A – 5: SDMT Results

A – 1: Location Map

A – 2: Approximate locations of geotechnical investigations

A – 3: Drillhole Log

BH-03

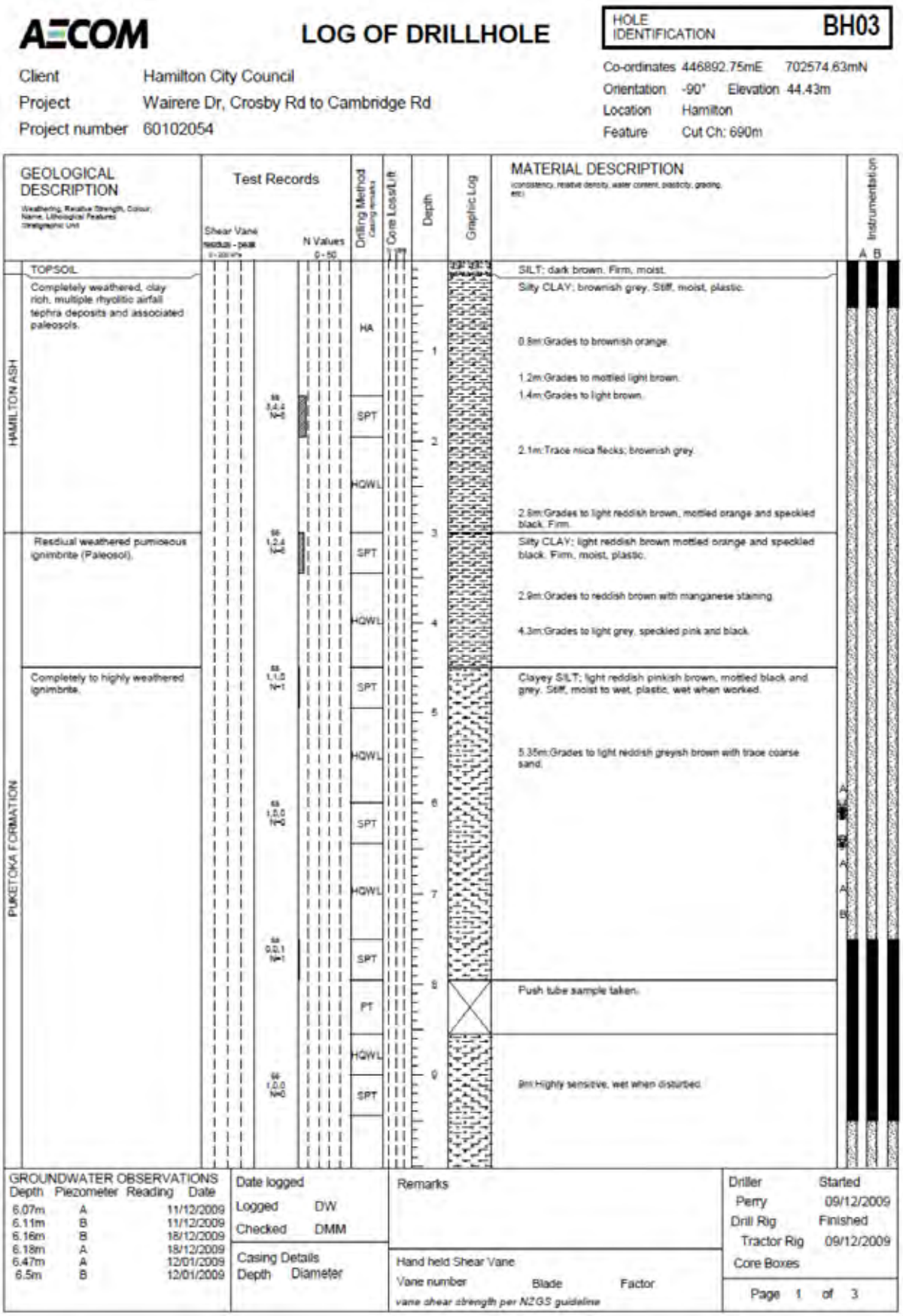

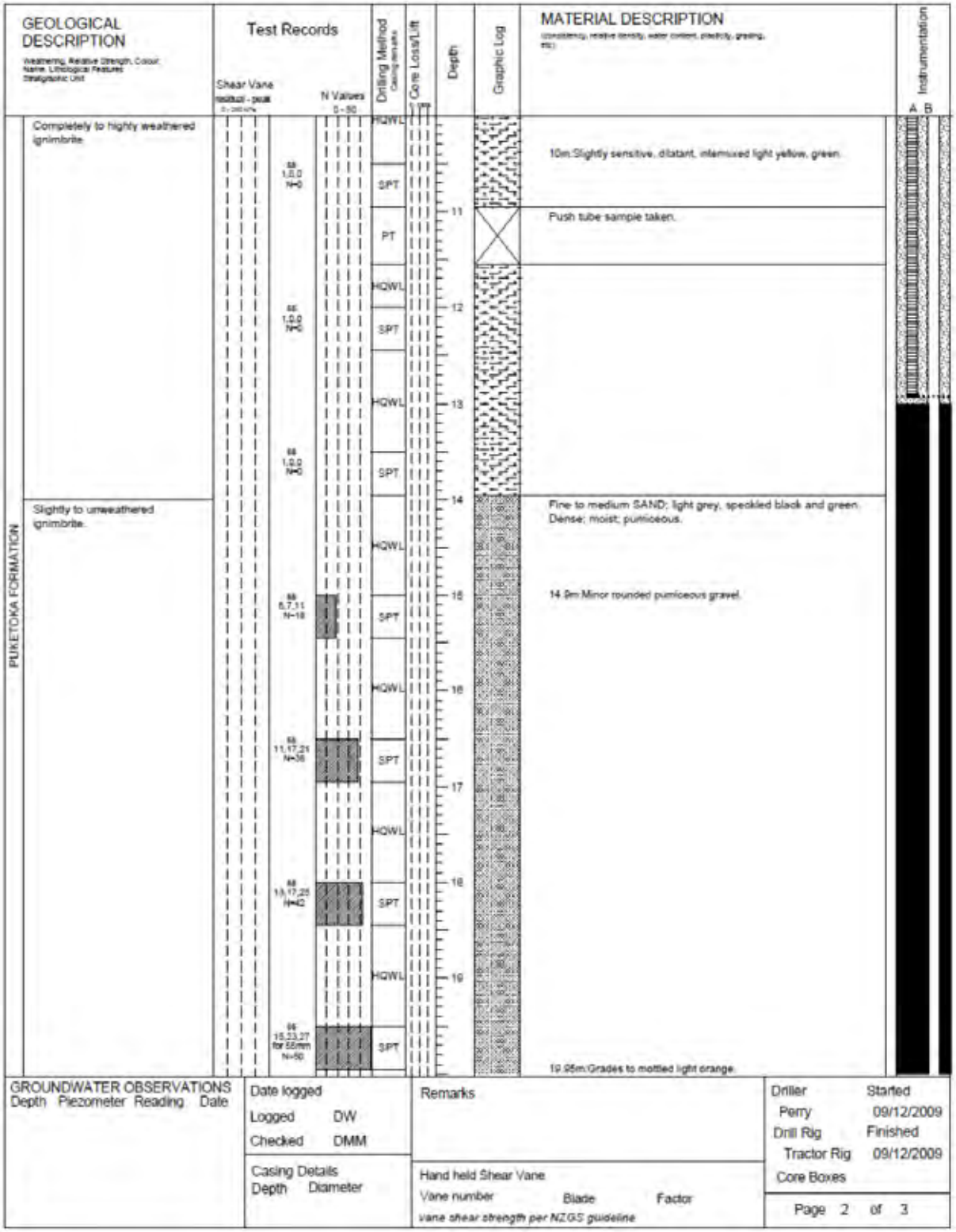
GEOLOGICAL DESCRIPTION
Test Records
Shear Vane
N Values
Drilling Method
Core Loss/Lift
Depth
Graphic Log
MATERIAL DESCRIPTION
Instrumentation
A B
Completely to highly weathered ignimbrite.
Slightly to unweathered ignimbrite.
PUKETOKA FORMATION
10m:Slightly sensitive, dilatant, interfixed light yellow, green.
Push tube sample taken.
Fine to medium SAND; light grey, speckled black and green. Dense; moist; pumiceous.
14.9m Minor rounded pumiceous gravel.
19.95m:Grades to mottled light orange.
HQWL
SPT
PT
11
12
13
14
15
16
17
18
19
GROUNDWATER OBSERVATIONS
Depth Piezometer Reading Date
Date logged
Logged DW
Checked DMM
Casing Details
Depth Diameter
Remarks
Hand held Shear Vane
Vane number Blade Factor
vane shear strength per NZGS guideline
Driller Started
Perry 09/12/2009
Drill Rig Finished
Tractor Rig 09/12/2009
Core Boxes
Page 2 of 3

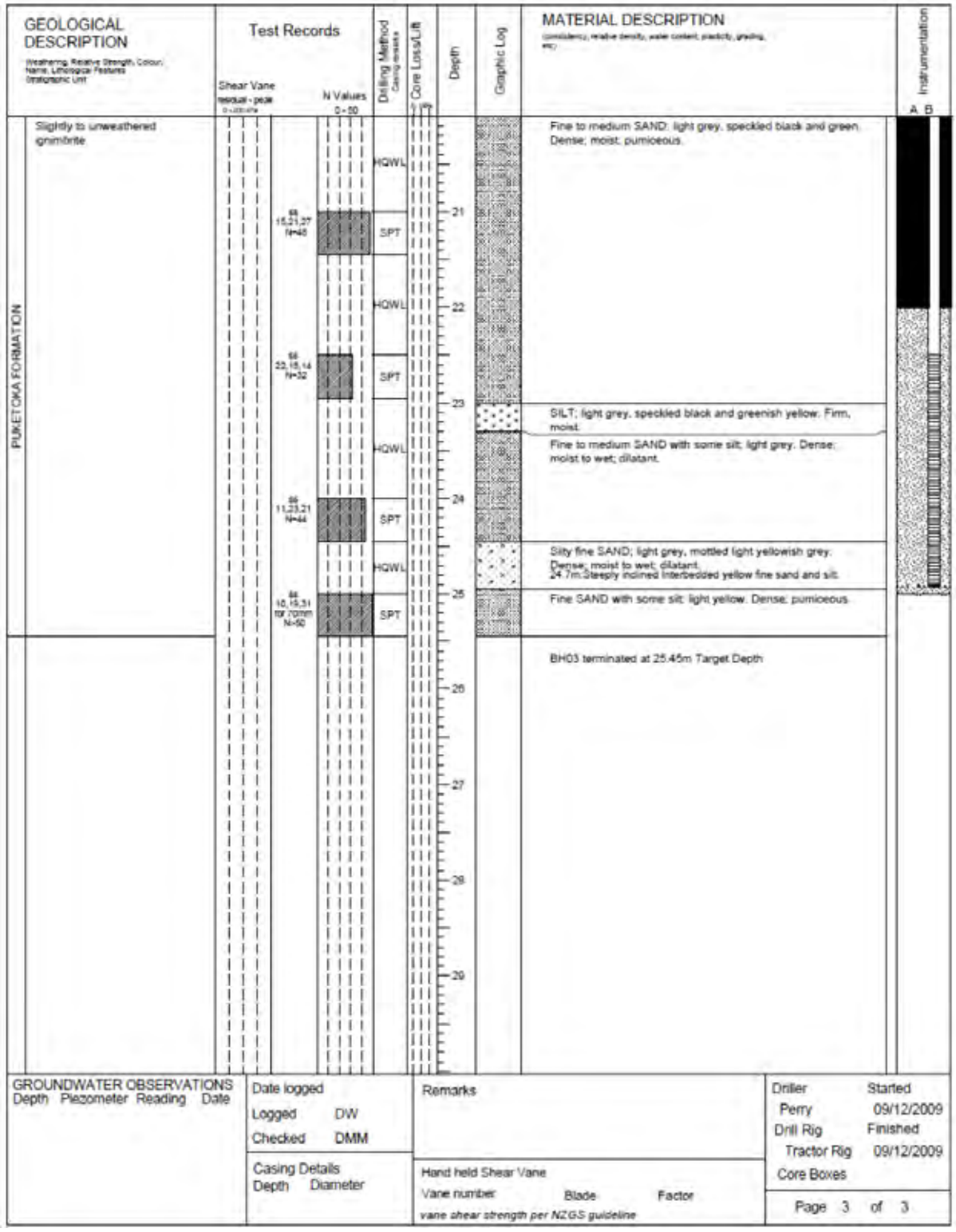
GEOLOGICAL DESCRIPTION
Weathering, Relative Strength, Colour, Name, Lithological Features, Stratigraphic Unit
Test Records
Shear Vane residual - peak
N Values 0 - 50
Drilling Method
Core Loss/Lift
Depth
Graphic Log
MATERIAL DESCRIPTION
(consistency, relative density, water content, plasticity, grading, etc)
Instrumentation
A B
PUKETOKA FORMATION
Slightly to unweathered ignimbrite
HQWL
SPT
15,21,27 N=48
HQWL
SPT
33,15,14 N=32
HQWL
SPT
11,23,21 N=44
HQWL
SPT
16,15,31 for 70mm N=50
Fine to medium SAND: light grey, speckled black and green. Dense; moist; pumiceous.
SILT: light grey, speckled black and greenish yellow. Firm, moist.
Fine to medium SAND with some silt; light grey. Dense; moist to wet; dilatant.
Silty fine SAND; light grey, mottled light yellowish grey. Dense; moist to wet; dilatant.
24.7m:Steeply inclined interbedded yellow fine sand and silt.
Fine SAND with some silt; light yellow. Dense; pumiceous.
BH03 terminated at 25.45m Target Depth
21
22
23
24
25
26
27
28
29
GROUNDWATER OBSERVATIONS
Depth Piezometer Reading Date
Date logged
Logged DW
Checked DMM
Casing Details
Depth Diameter
Remarks
Hand held Shear Vane
Vane number Blade Factor
vane shear strength per NZGS guideline
Driller Perry
Started 09/12/2009
Drill Rig Tractor Rig
Finished 09/12/2009
Core Boxes
Page 3 of 3

A – 4: CPT Soundings

CPT01

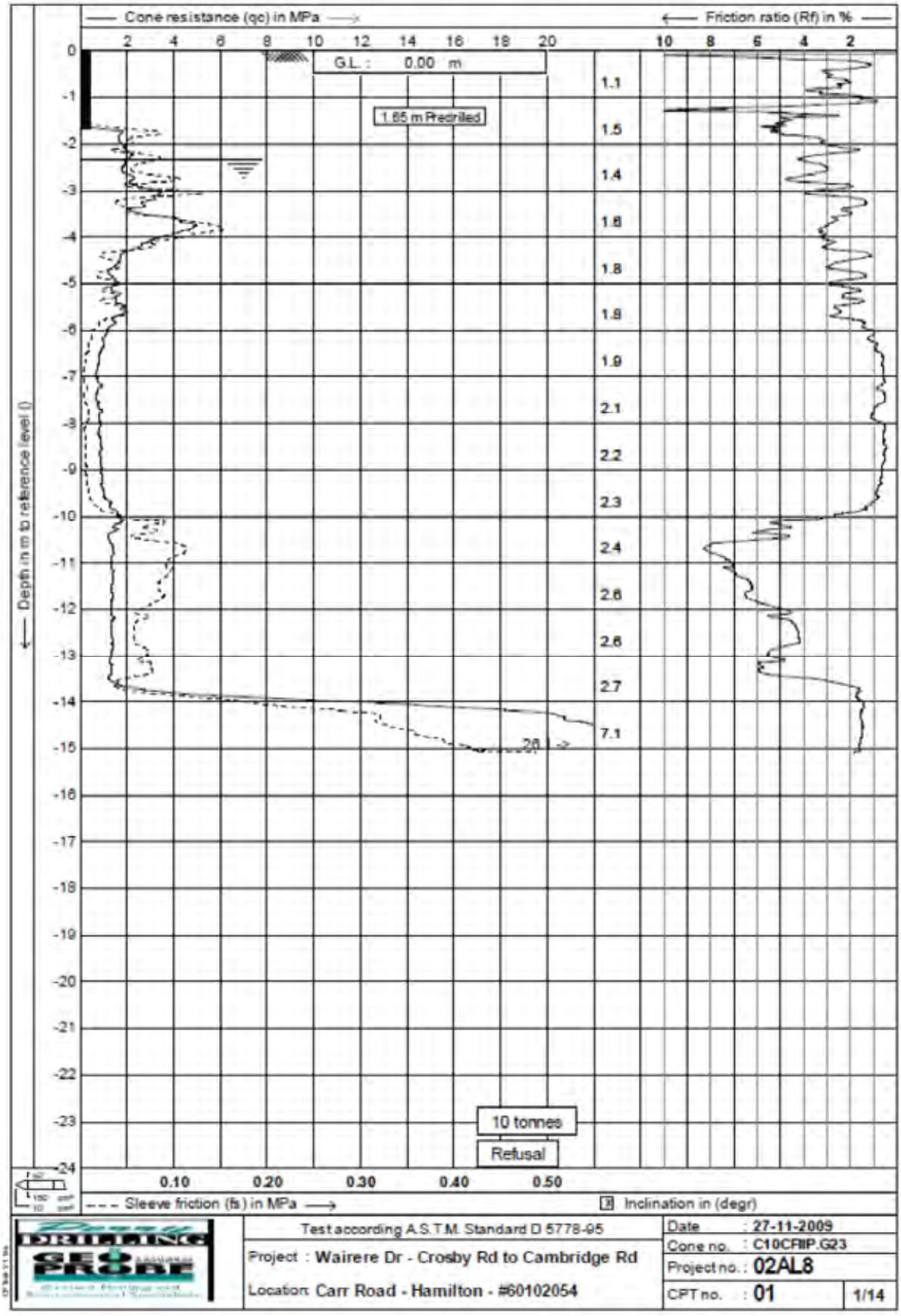

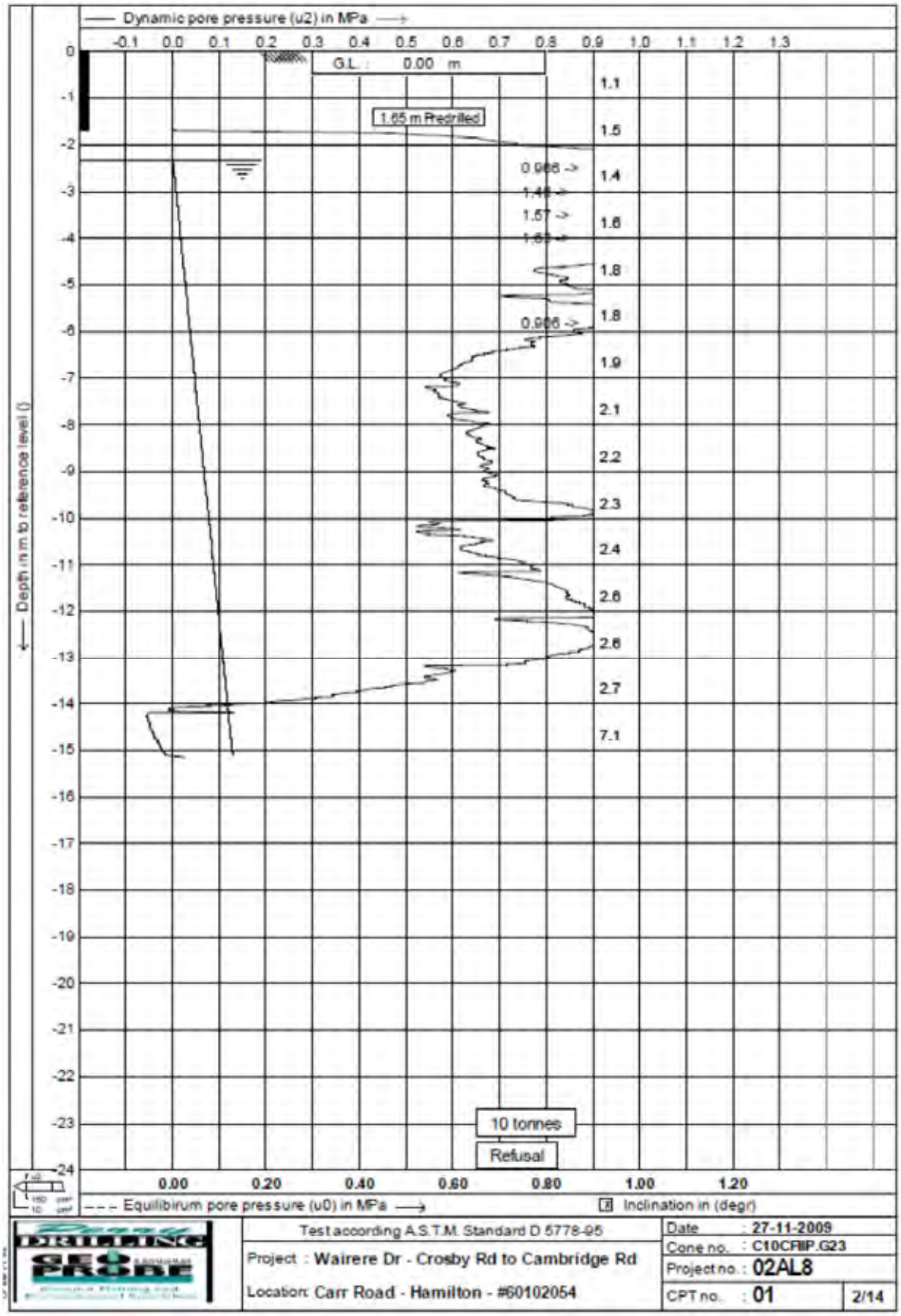
Dynamic pore pressure (u2) in MPa
-0.1 0.0 0.1 0.2 0.3 0.4 0.5 0.6 0.7 0.8 0.9 1.0 1.1 1.2 1.3
G.L. : 0.00 m
1.65 m Predrilled
0.966 ->
1.48 ->
1.57 ->
1.63 ->
0.966 ->
1.1
1.5
1.4
1.6
1.8
1.8
1.9
2.1
2.2
2.3
2.4
2.6
2.6
2.7
7.1
10 tonnes
Refusal
Depth in m to reference level ()
0.00 0.20 0.40 0.60 0.80 1.00 1.20
Equilibirum pore pressure (u0) in MPa
Inclination in (degr)
Test according A.S.T.M. Standard D 5778-95
Project : Wairere Dr - Crosby Rd to Cambridge Rd
Location: Carr Road - Hamilton - #60102054
Date : 27-11-2009
Cone no. : C10CFIIP.G23
Project no. : 02AL8
CPT no. : 01
2/14

CPT02

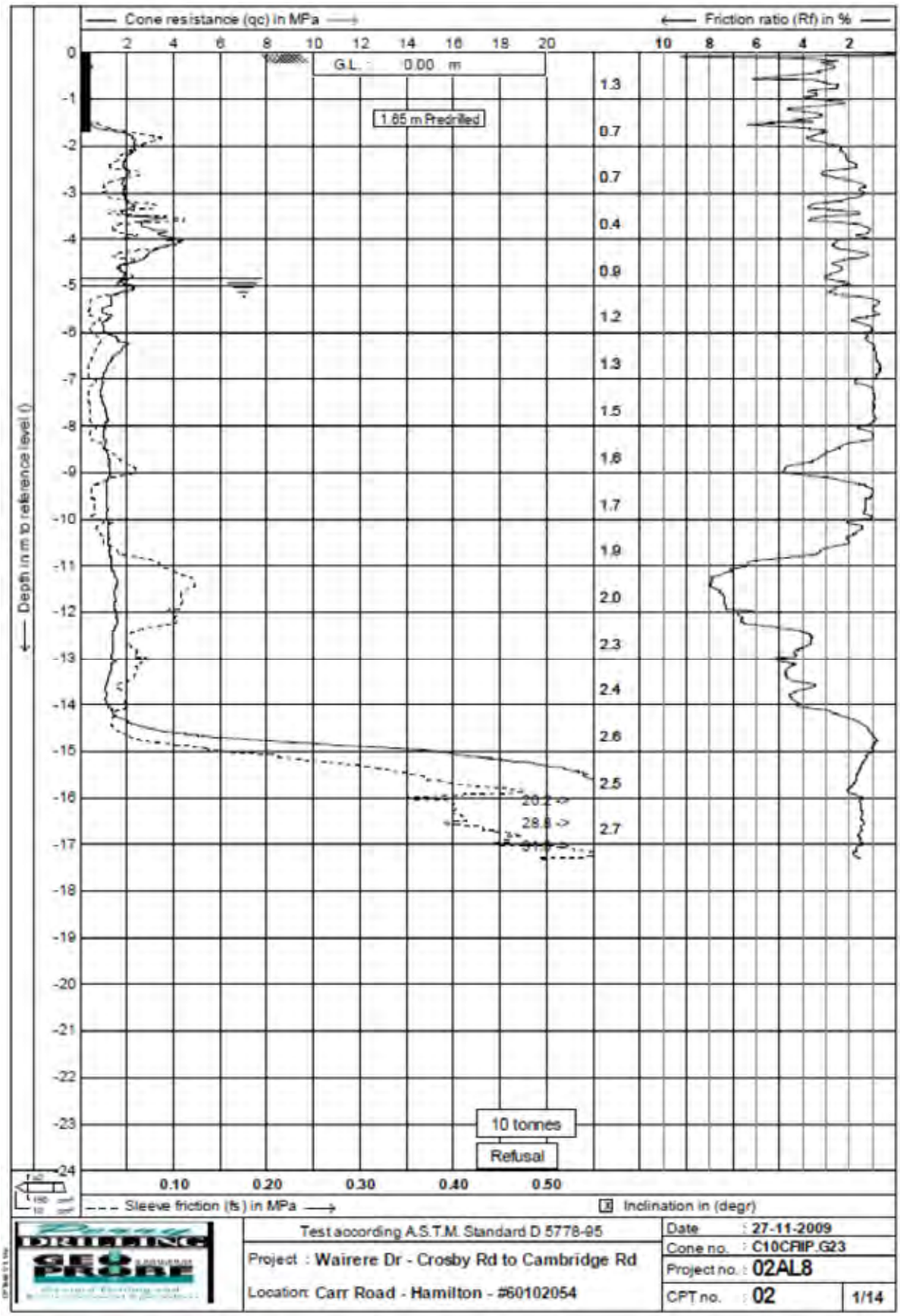
Cone resistance (qc) in MPa
Friction ratio (Rf) in %
G.L. : 0.00 m
1.65 m Predrilled
Depth in m to reference level (-)
10 tonnes
Refusal
Sleeve friction (fs) in MPa
Inclination in (degr)
Test according A.S.T.M. Standard D 5778-95
Project : Wairere Dr - Crosby Rd to Cambridge Rd
Location: Carr Road - Hamilton - #60102054
Date : 27-11-2009
Cone no. : C10CFIIP.G23
Project no. : 02AL8
CPT no. : 02
1/14

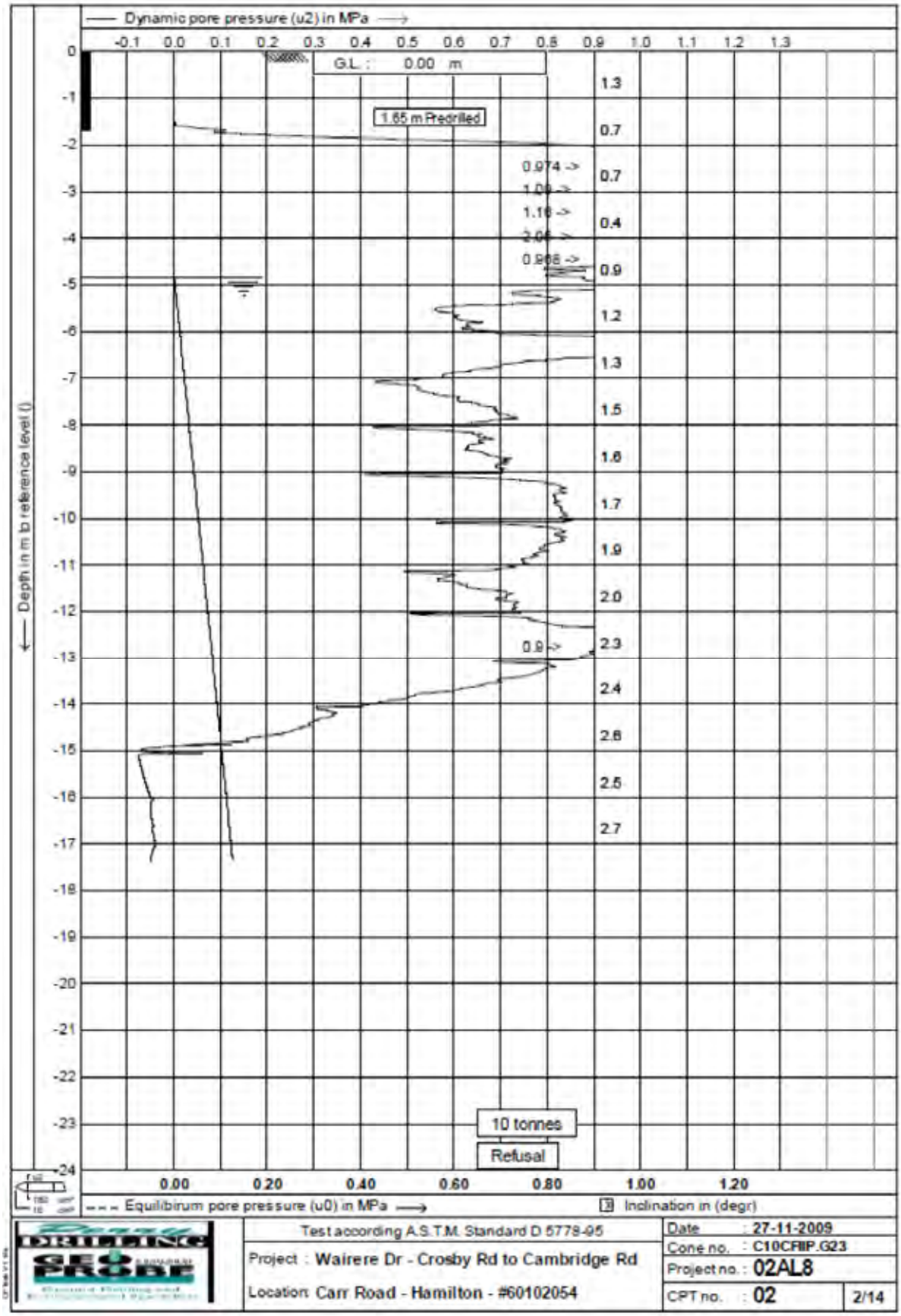
Dynamic pore pressure (u2) in MPa
-0.1 0.0 0.1 0.2 0.3 0.4 0.5 0.6 0.7 0.8 0.9 1.0 1.1 1.2 1.3
G.L. : 0.00 m
1.65 m Predrilled
0.974 ->
1.09 ->
1.16 ->
2.06 ->
0.966 ->
0.9 ->
10 tonnes
Refusal
Depth in m to reference level ()
0.00 0.20 0.40 0.60 0.80 1.00 1.20
Equilibirum pore pressure (u0) in MPa
Inclination in (degr)
Test according A.S.T.M. Standard D 5778-95
Project : Wairere Dr - Crosby Rd to Cambridge Rd
Location Carr Road - Hamilton - #60102054
Date : 27-11-2009
Cone no. : C10CFIIP.G23
Project no. : 02AL8
CPT no. : 02
2/14

A – 5: SDMT Results

SDMT-01

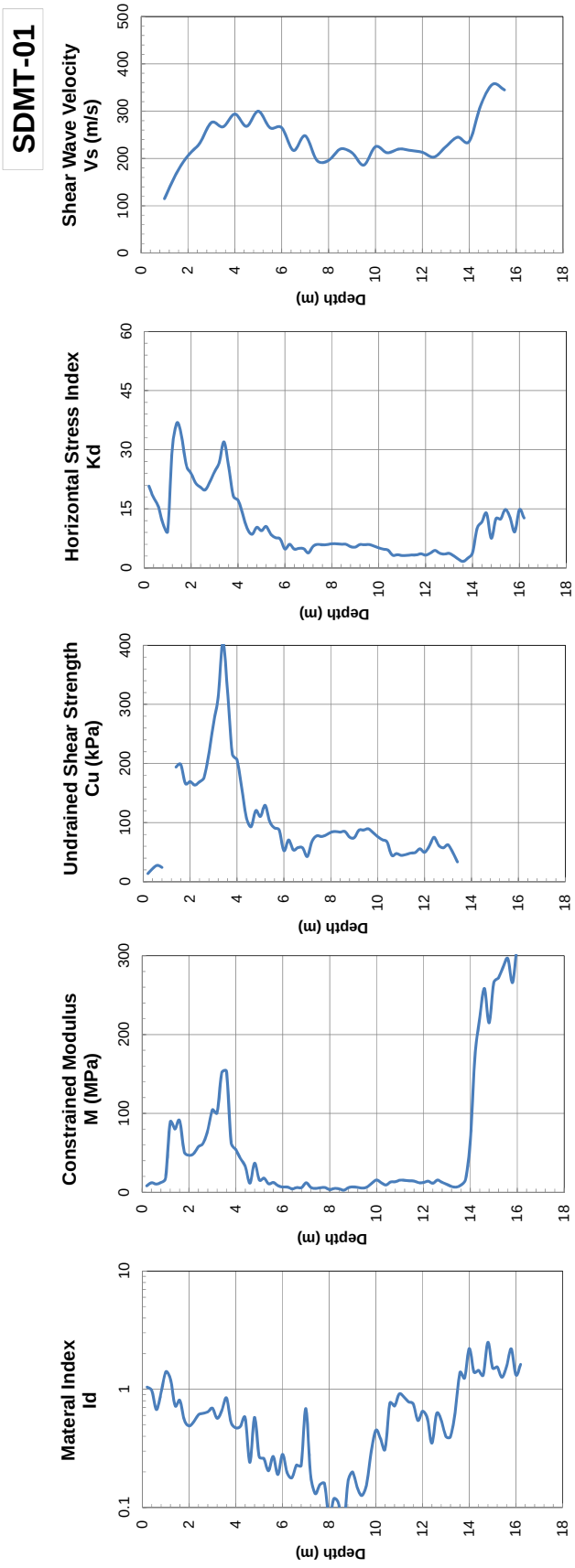

SDMT-02

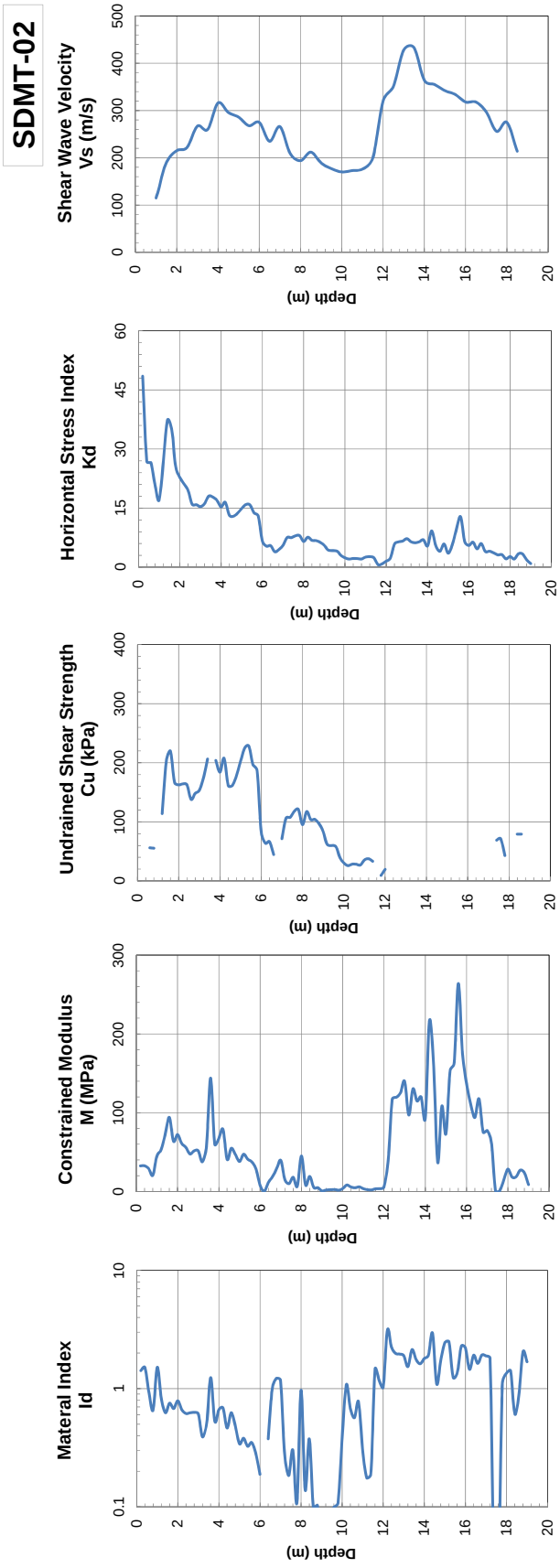
SDMT-02
Shear Wave Velocity Vs (m/s)
0
100
200
300
400
500
Depth (m)
0
2
4
6
8
10
12
14
16
18
20
Horizontal Stress Index Kd
0
15
30
45
60
Depth (m)
Undrained Shear Strength Cu (kPa)
0
100
200
300
400
Depth (m)
Constrained Modulus M (MPa)
0
100
200
300
Depth (m)
Materal Index Id
0.1
1
10
Depth (m)

SDMT-03

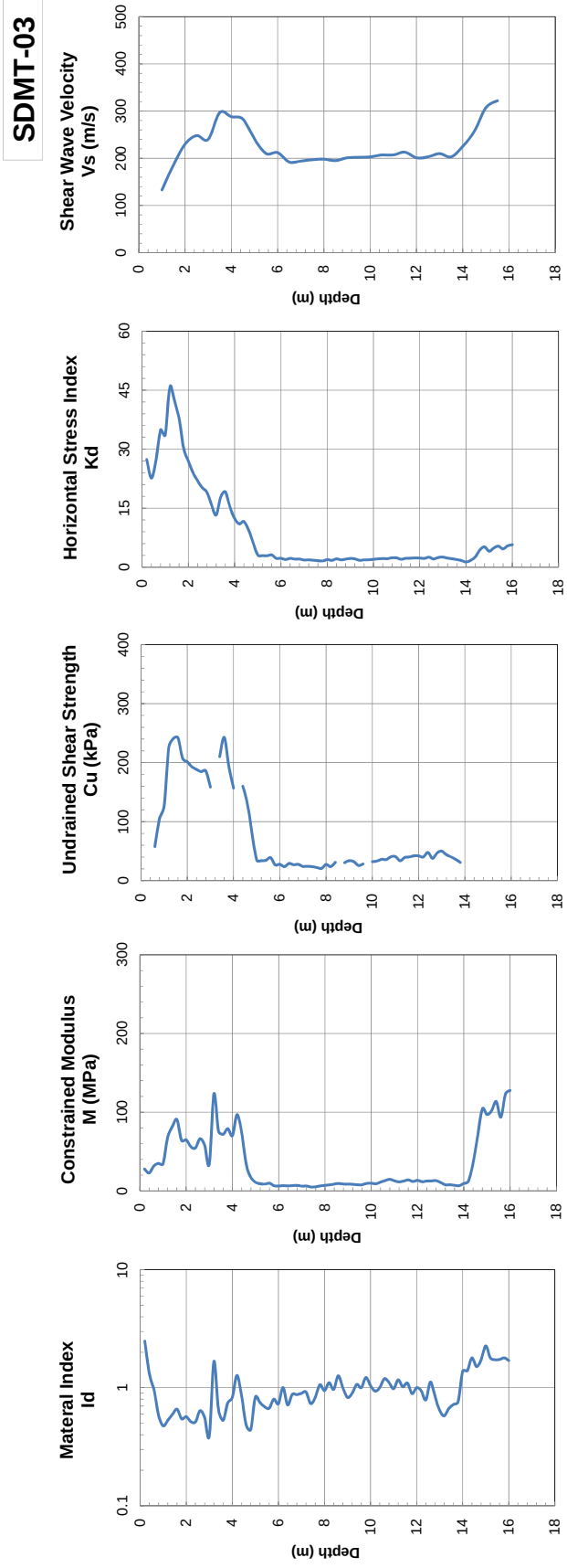
SDMT-03
Shear Wave Velocity Vs (m/s)
0
100
200
300
400
500
Depth (m)
0
2
4
6
8
10
12
14
16
18
Horizontal Stress Index Kd
0
15
30
45
60
Undrained Shear Strength Cu (kPa)
Constrained Modulus M (MPa)
Materal Index Id
0.1
1
10

APPENDIX B

Mikkelsen Rd Site

(Waihou Substation)

B – 1: Location Map

B – 2: Approximate locations of geotechnical investigations

B – 3: Drillhole Log

B – 4: CPT Soundings

B – 5: SDMT Results

B – 1: Location Map

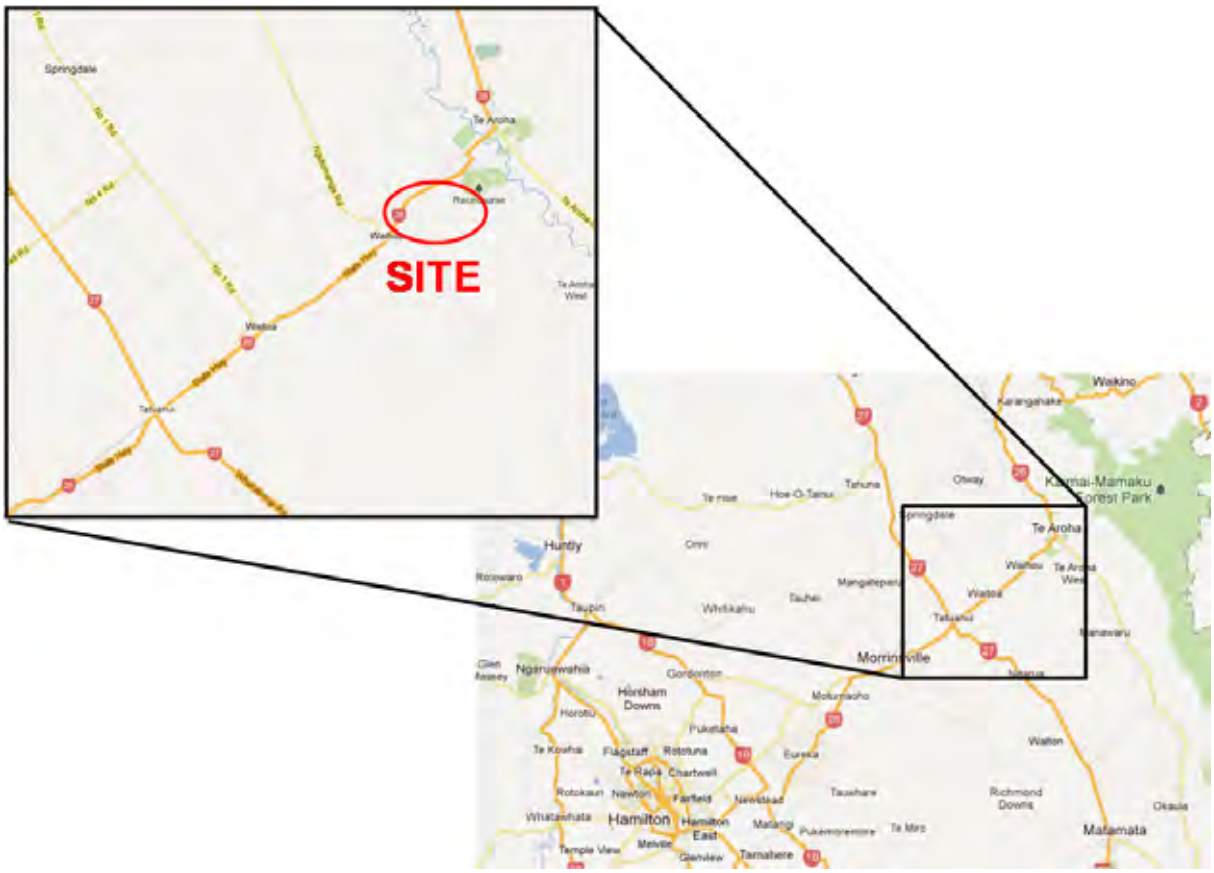

B – 2: Approximate locations of geotechnical investigations

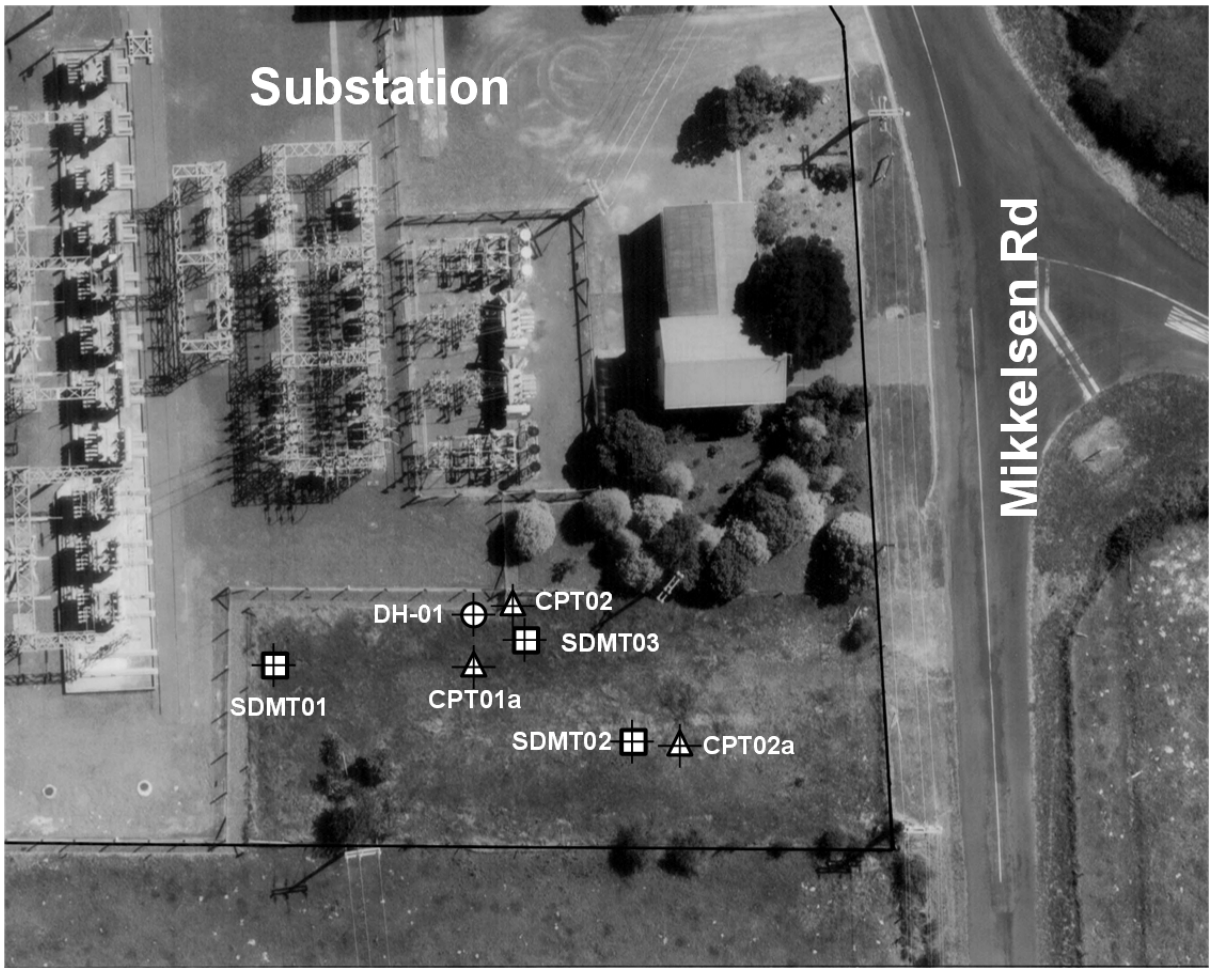

B – 3: Drillhole Log

DH-01

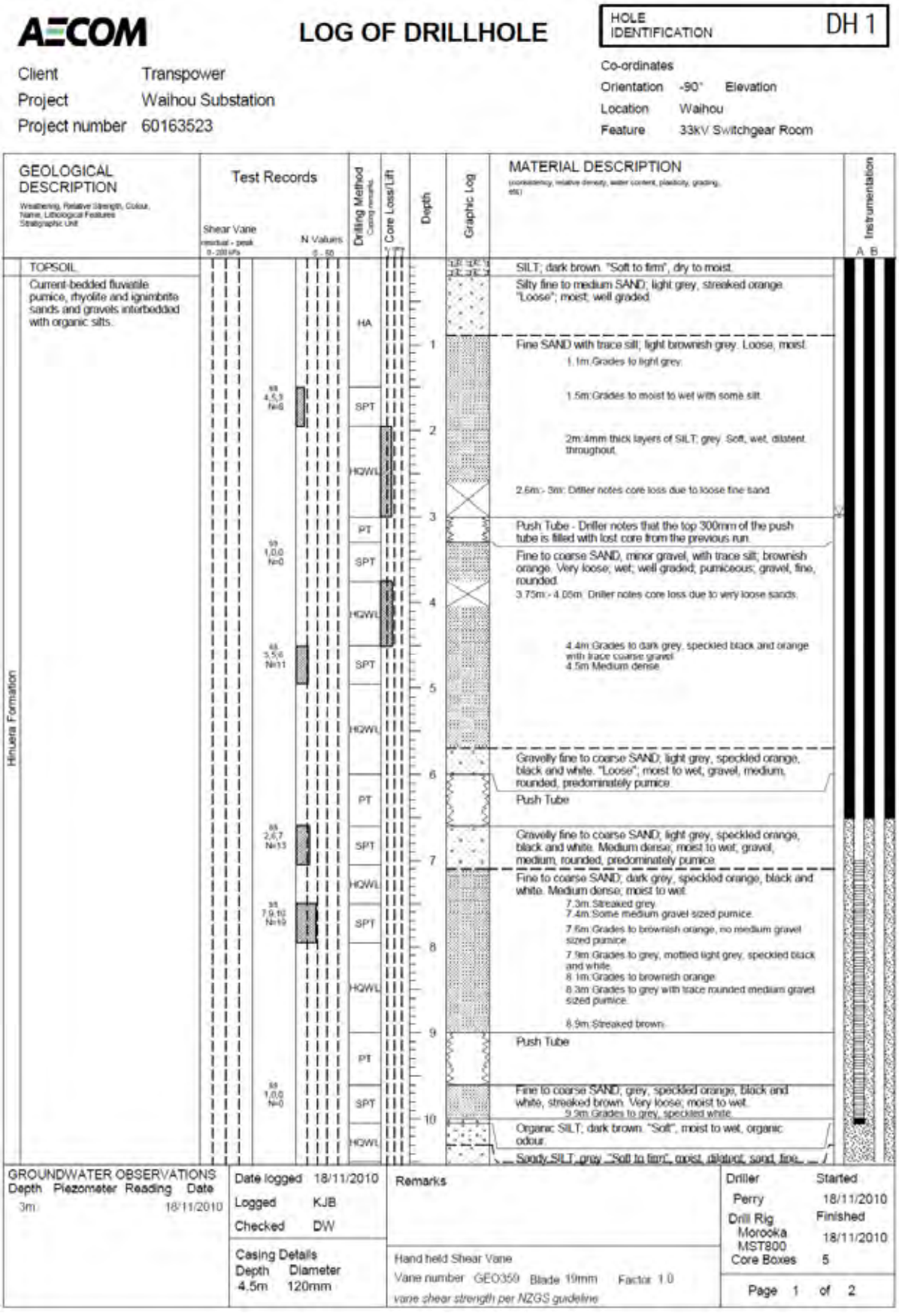

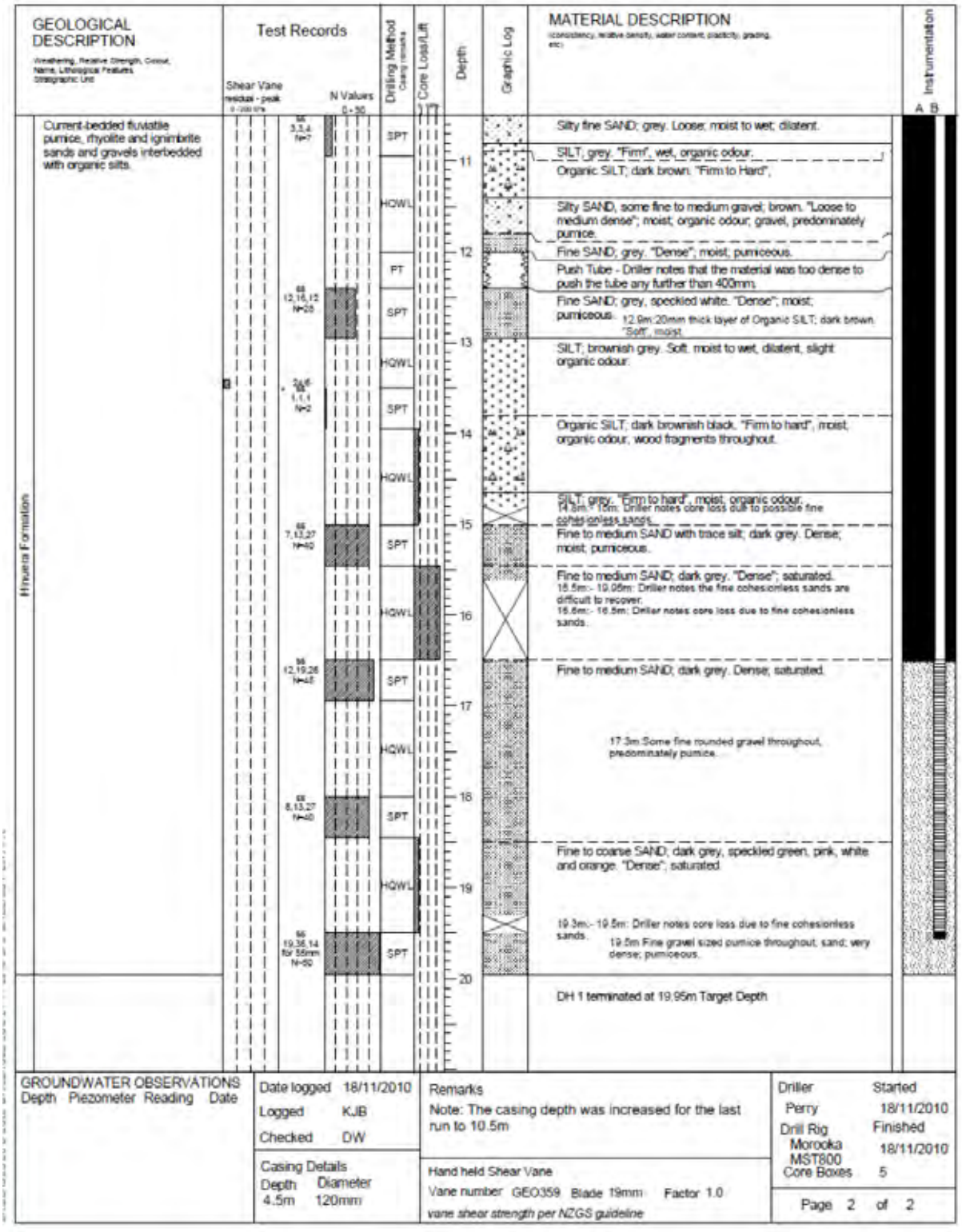
GEOLOGICAL DESCRIPTION
Weathering, Relative Strength, Colour, Name, Lithological Features, Stratigraphic Unit
Test Records
Shear Vane residual - peak
N Values 0 - 30
Drilling Method
Core Loss/Lift
Depth
Graphic Log
MATERIAL DESCRIPTION
(consistency, relative density, water content, plasticity, grading, etc)
Instrumentation
A B
Hinuera Formation
Current-bedded fluviatile pumice, rhyolite and ignimbrite sands and gravels interbedded with organic silts.
Silty fine SAND; grey. Loose; moist to wet; dilatent.
SILT; grey. "Firm", wet, organic odour.
Organic SILT; dark brown. "Firm to Hard",
Silty SAND, some fine to medium gravel; brown. "Loose to medium dense"; moist; organic odour; gravel, predominately pumice.
Fine SAND; grey. "Dense"; moist; pumiceous.
Push Tube - Driller notes that the material was too dense to push the tube any further than 400mm.
Fine SAND; grey, speckled white. "Dense"; moist; pumiceous.
12.9m:20mm thick layer of Organic SILT; dark brown. "Soft", moist.
SILT; brownish grey. Soft; moist to wet, dilatent, slight organic odour.
Organic SILT; dark brownish black. "Firm to hard", moist; organic odour, wood fragments throughout.
SILT; grey. "Firm to hard", moist; organic odour.
14.8m - 15m: Driller notes core loss due to possible fine cohesionless sands.
Fine to medium SAND with trace silt; dark grey. Dense; moist; pumiceous.
Fine to medium SAND; dark grey. "Dense"; saturated.
15.5m:- 16.05m: Driller notes the fine cohesionless sands are difficult to recover.
15.6m:- 16.5m: Driller notes core loss due to fine cohesionless sands.
Fine to medium SAND; dark grey. Dense; saturated.
17.3m Some fine rounded gravel throughout, predominately pumice.
Fine to coarse SAND; dark grey, speckled green, pink, white and orange. "Dense"; saturated
19.3m:- 19.5m: Driller notes core loss due to fine cohesionless sands.
19.5m Fine gravel sized pumice throughout; sand; very dense; pumiceous.
DH 1 terminated at 19.95m Target Depth
SPT
HQWL
PT
11
12
13
14
15
16
17
18
19
20
GROUNDWATER OBSERVATIONS
Depth Piezometer Reading Date
Date logged 18/11/2010
Logged KJB
Checked DW
Casing Details
Depth Diameter
4.5m 120mm
Remarks
Note: The casing depth was increased for the last run to 10.5m
Hand held Shear Vane
Vane number GEO359 Blade 19mm Factor 1.0
vane shear strength per NZGS guideline
Driller Perry
Started 18/11/2010
Drill Rig Morooka MST800
Finished 18/11/2010
Core Boxes 5
Page 2 of 2

B – 4: CPT Soundings

CPT02

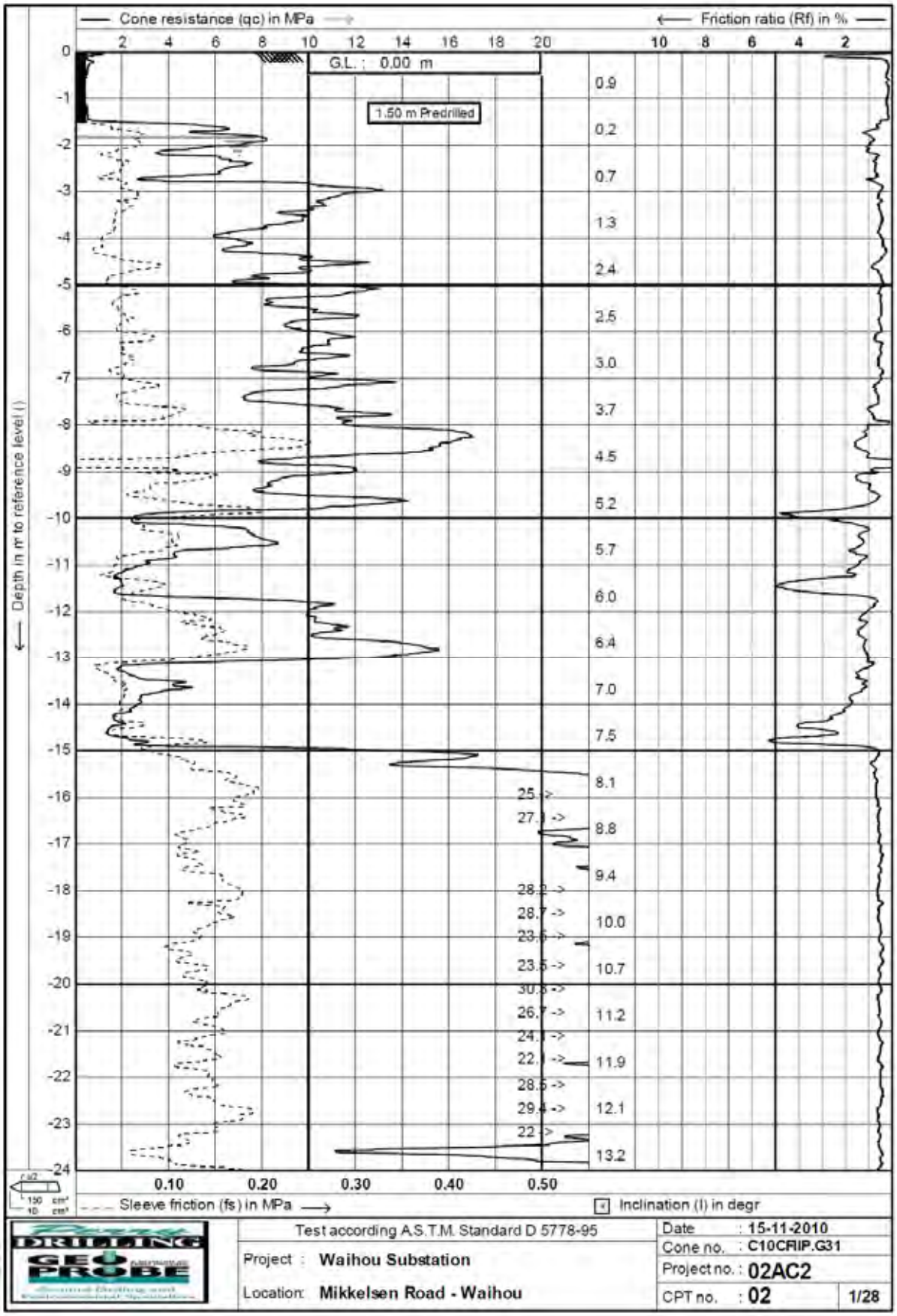

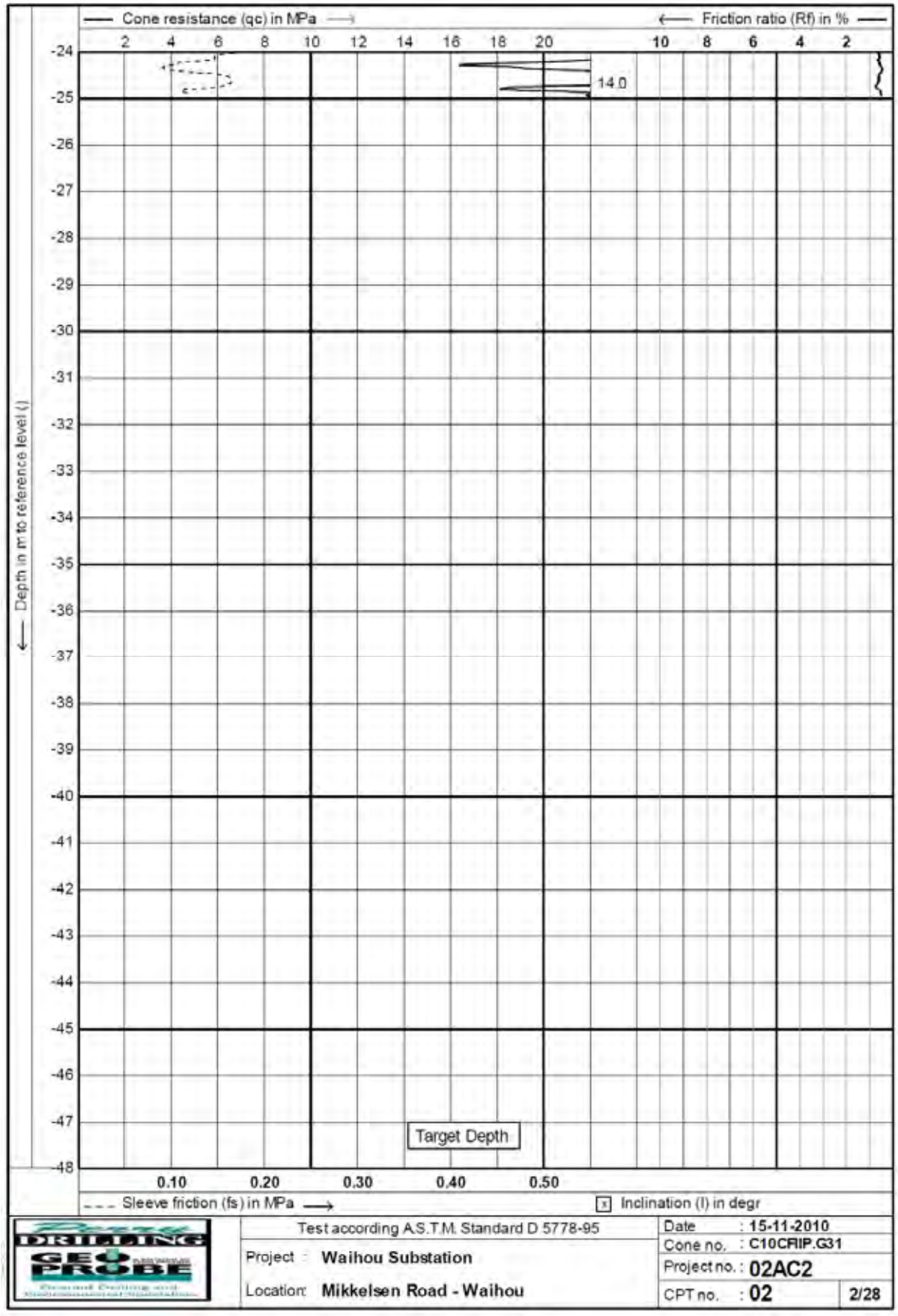
Cone resistance (qc) in MPa
Friction ratio (Rf) in %
2 4 6 8 10 12 14 16 18 20
10 8 6 4 2
14.0
Depth in m to reference level ()
-24 -25 -26 -27 -28 -29 -30 -31 -32 -33 -34 -35 -36 -37 -38 -39 -40 -41 -42 -43 -44 -45 -46 -47 -48
Target Depth
0.10 0.20 0.30 0.40 0.50
Sleeve friction (fs) in MPa
Inclination (I) in degr
DRILLING
GEO PROBE
Test according A.S.T.M. Standard D 5778-95
Project : Waihou Substation
Location: Mikkelsen Road - Waihou
Date : 15-11-2010
Cone no. : C10CRIP.G31
Project no. : 02AC2
CPT no. : 02
2/28

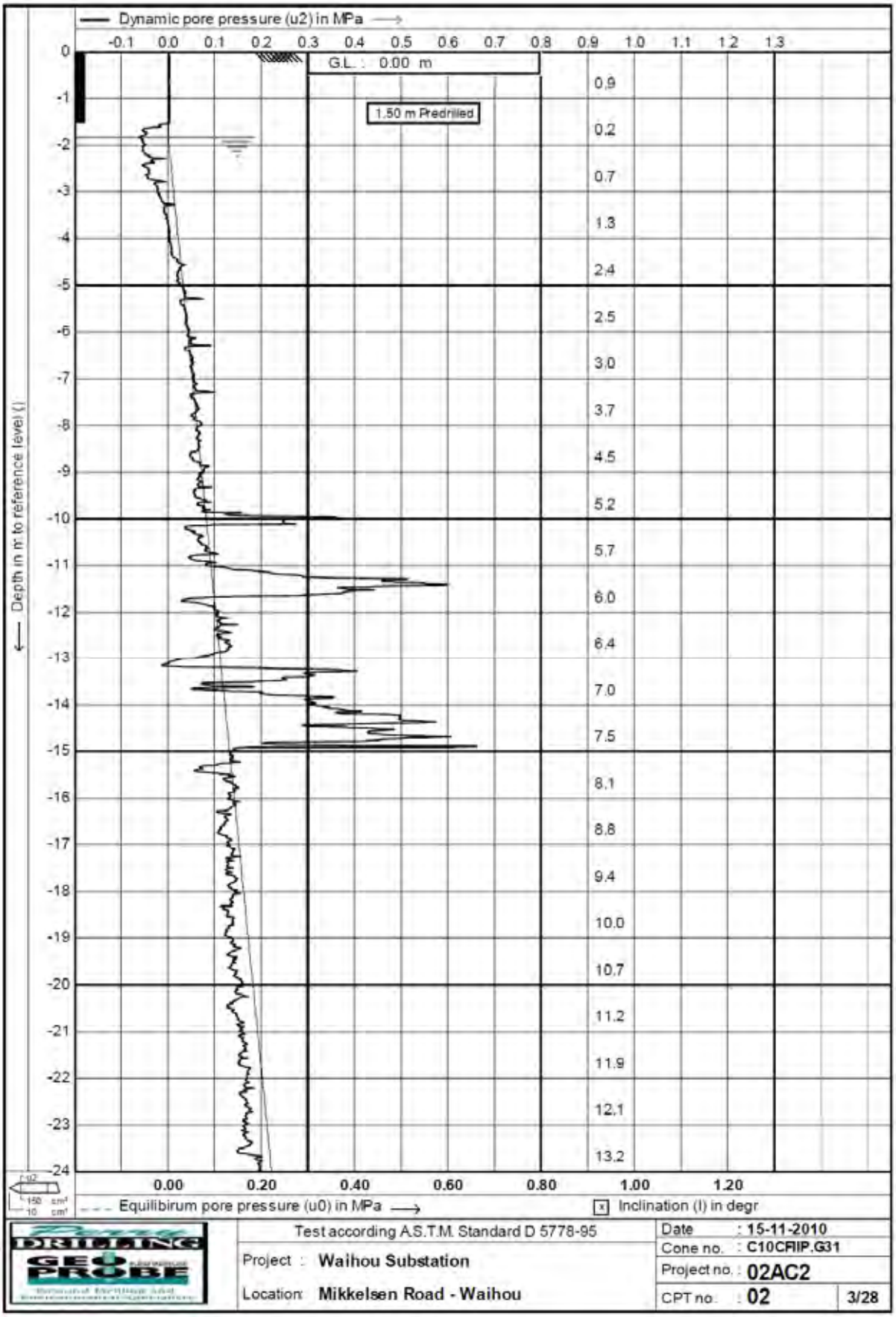
Dynamic pore pressure (u2) in MPa
-0.1 0.0 0.1 0.2 0.3 0.4 0.5 0.6 0.7 0.8 0.9 1.0 1.1 1.2 1.3
G.L. : 0.00 m
1.50 m Predrilled
0.9
0.2
0.7
1.3
2.4
2.5
3.0
3.7
4.5
5.2
5.7
6.0
6.4
7.0
7.5
8.1
8.8
9.4
10.0
10.7
11.2
11.9
12.1
13.2
Depth in m to reference level ()
0.00 0.20 0.40 0.60 0.80 1.00 1.20
Equilibirum pore pressure (u0) in MPa
Inclination (I) in degr
DRILLING
GEOPROBE
Test according A.S.T.M. Standard D 5778-95
Project : Waihou Substation
Location: Mikkelsen Road - Waihou
Date : 15-11-2010
Cone no. : C10CFIIP.G31
Project no. : 02AC2
CPT no. : 02
3/28

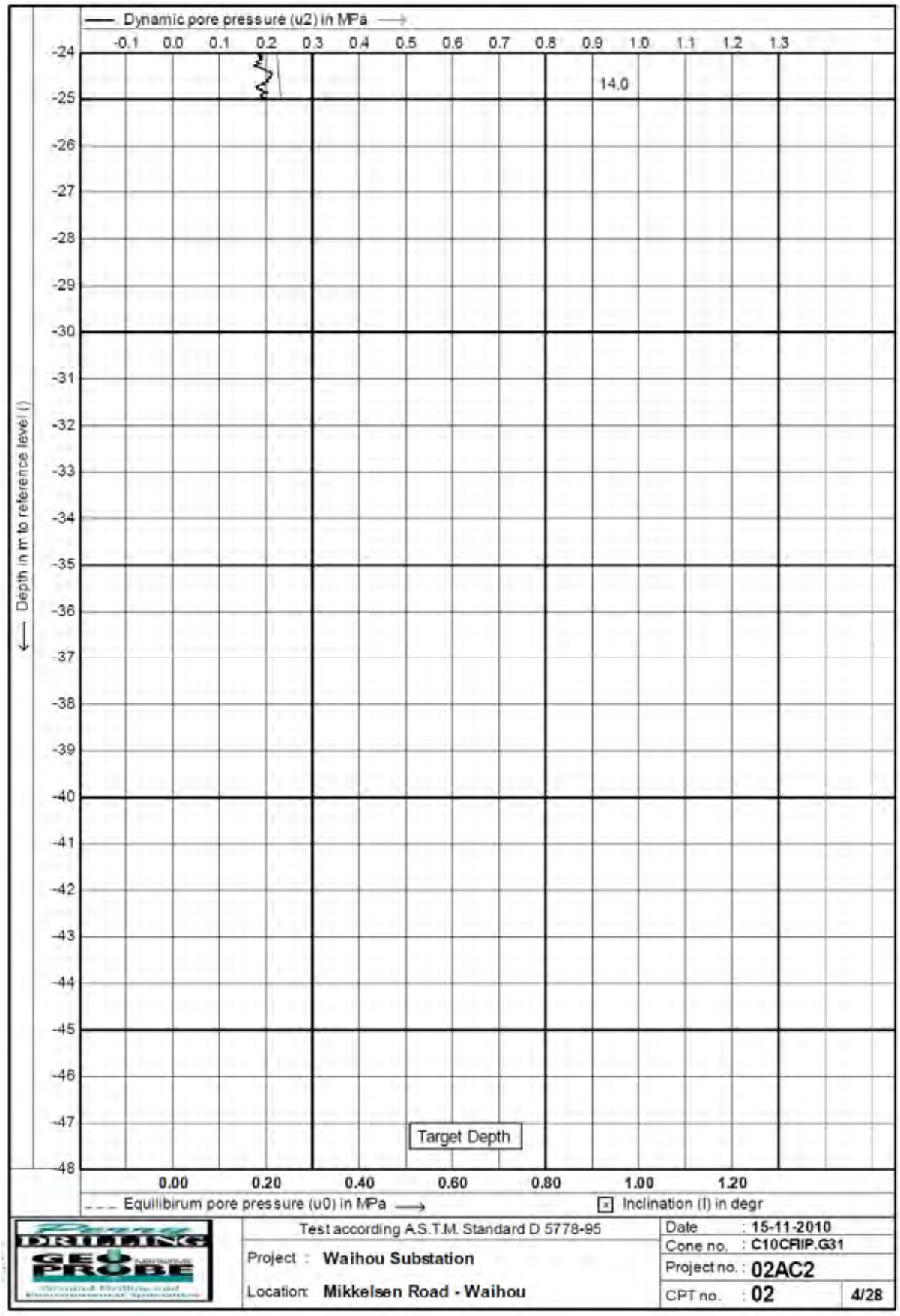
Dynamic pore pressure (u2) in MPa
-0.1 0.0 0.1 0.2 0.3 0.4 0.5 0.6 0.7 0.8 0.9 1.0 1.1 1.2 1.3
14.0
Depth in m to reference level (-)
-24 -25 -26 -27 -28 -29 -30 -31 -32 -33 -34 -35 -36 -37 -38 -39 -40 -41 -42 -43 -44 -45 -46 -47 -48
Target Depth
0.00 0.20 0.40 0.60 0.80 1.00 1.20
Equilibirum pore pressure (u0) in MPa
Inclination (I) in degr
DRILLING
GEO PROBE
Test according A.S.T.M. Standard D 5778-95
Project : Waihou Substation
Location: Mikkelsen Road - Waihou
Date : 15-11-2010
Cone no. : C10CFIIP.G31
Project no. : 02AC2
CPT no. : 02
4/28

CPT01a

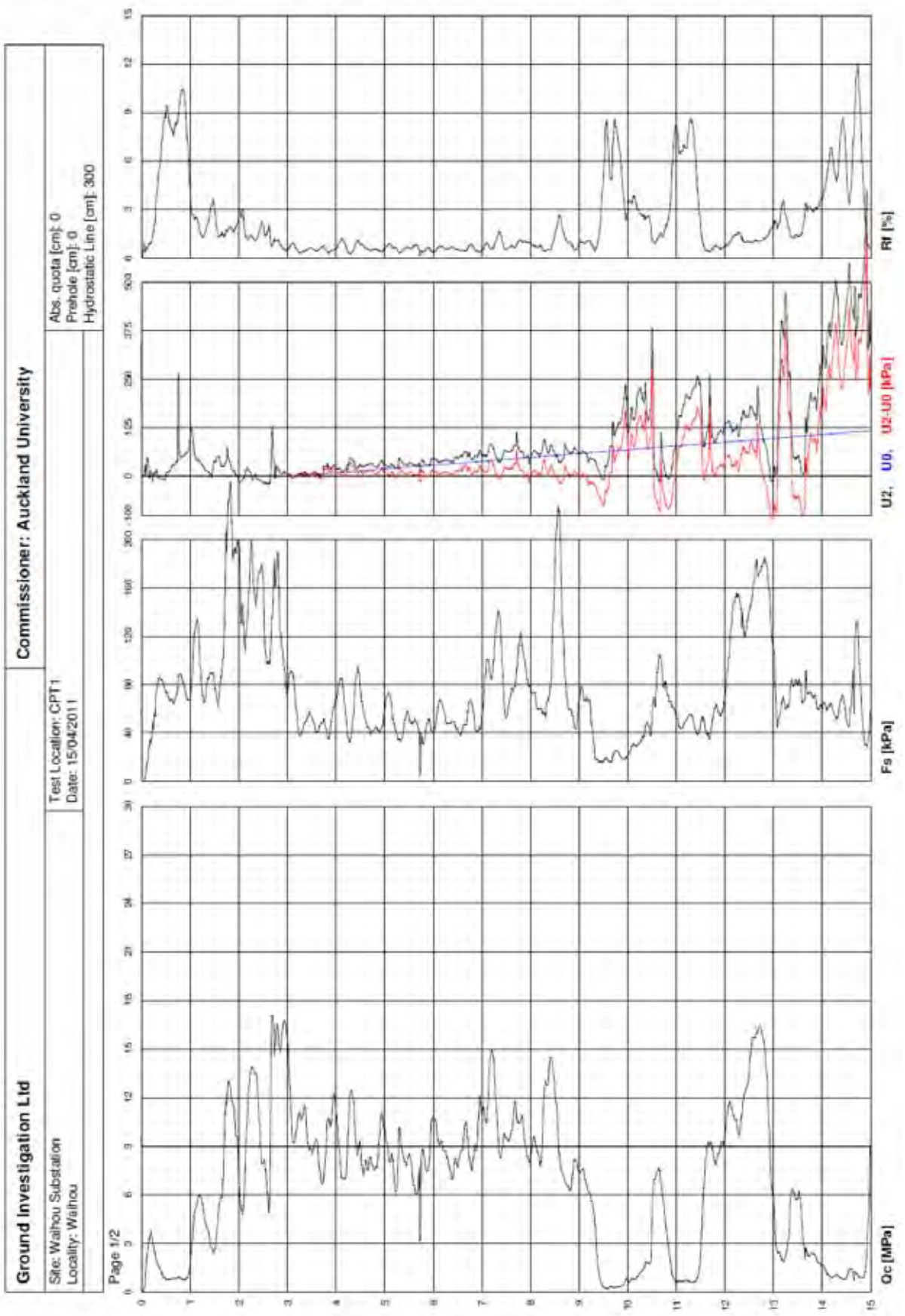
Ground Investigation Ltd
Commissioner: Auckland University
Site: Waihou Substation
Locality: Waihou
Test Location: CPT1
Date: 15/04/2011
Abs. quota [cm]: 0
Prehole [cm]: 0
Hydrostatic Line [cm]: 300
Page 1/2
Rf [%]
U2, U0, U2-U0 [kPa]
Fs [kPa]
Qc [MPa]

Ground Investigation Ltd		Commissioner: Auckland University
Site: Waihou Substation Locality: Waihou	Test Location: CPT1 Date: 15/04/2011	Abs. quota [cm]: 0 Prehole [cm]: 0 Hydrostatic Line [cm]: 300

Page 2/2

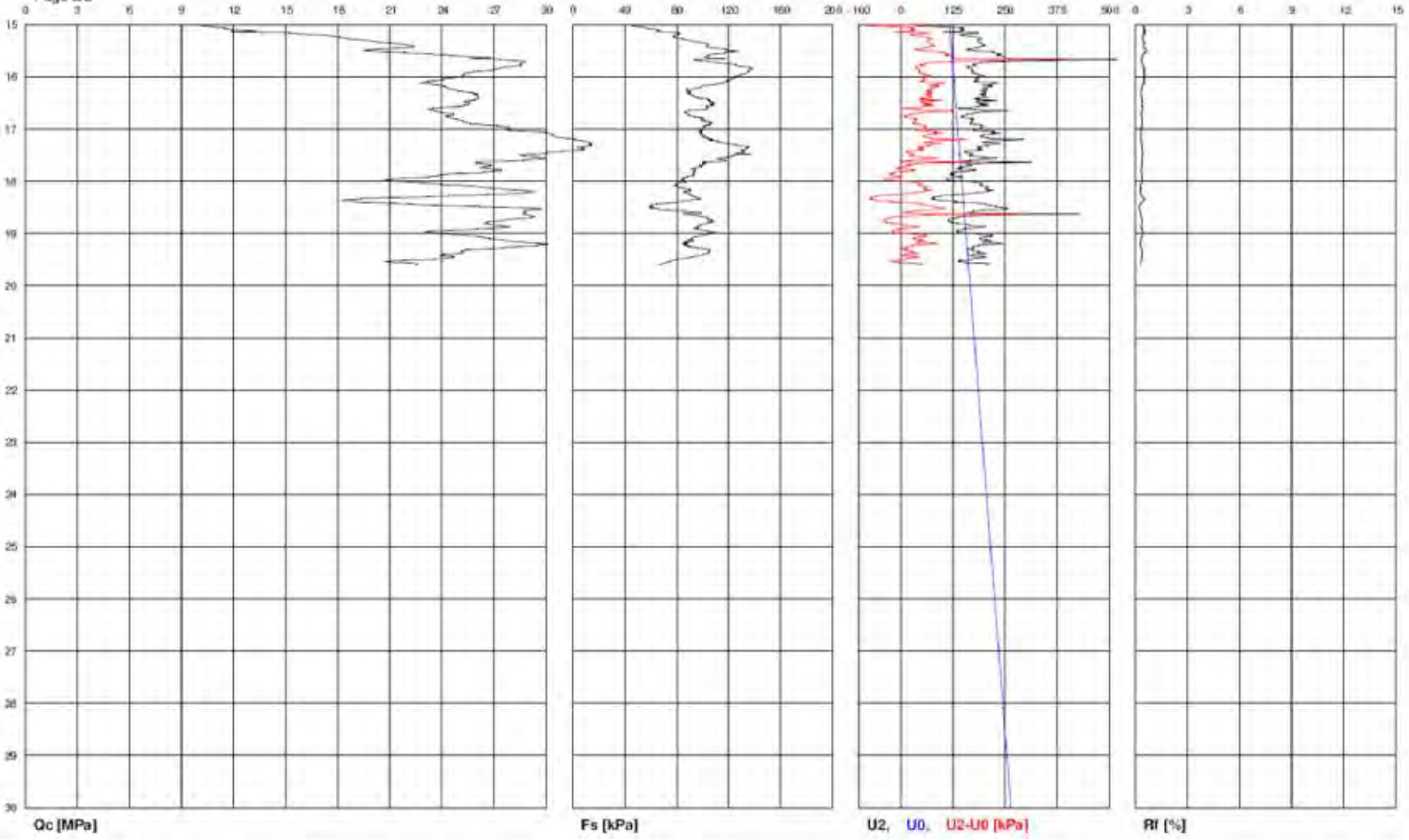

CPT02a

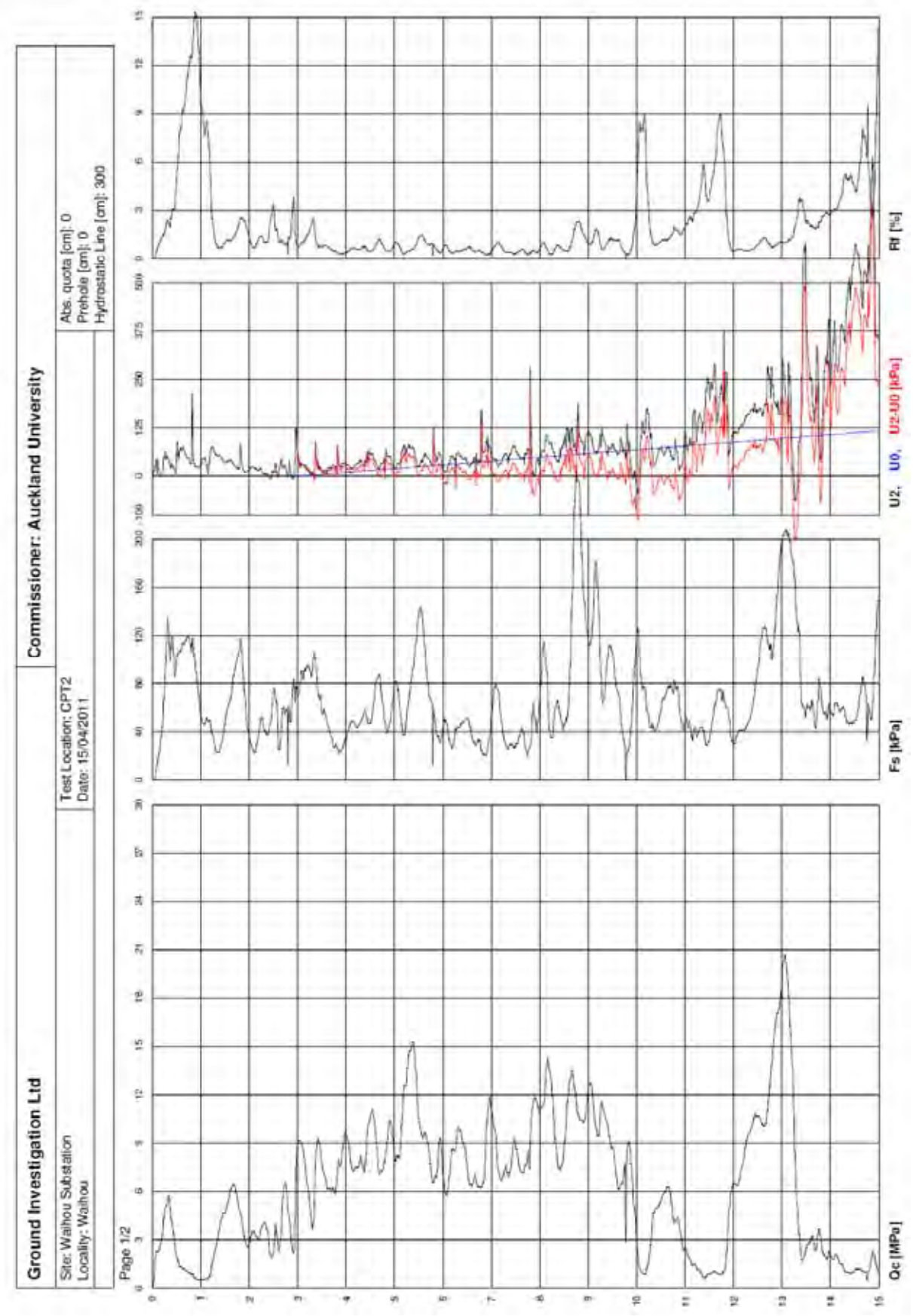
Ground Investigation Ltd
Commissioner: Auckland University
Site: Waihou Substation
Locality: Waihou
Test Location: CPT2
Date: 15/04/2011
Abs. quota [cm]: 0
Prehole [cm]: 0
Hydrostatic Line [cm]: 300
Page 1/2
Rf [%]
U2, U0, U2-U0 [kPa]
Fs [kPa]
Qc [MPa]

Ground Investigation Ltd		Commissioner: Auckland University
Site: Waihou Substation Locality: Waihou	Test Location: CPT2 Date: 15/04/2011	Abs. quota [cm]: 0 Prehole [cm]: 0 Hydrostatic Line [cm]: 300

Page 2/2

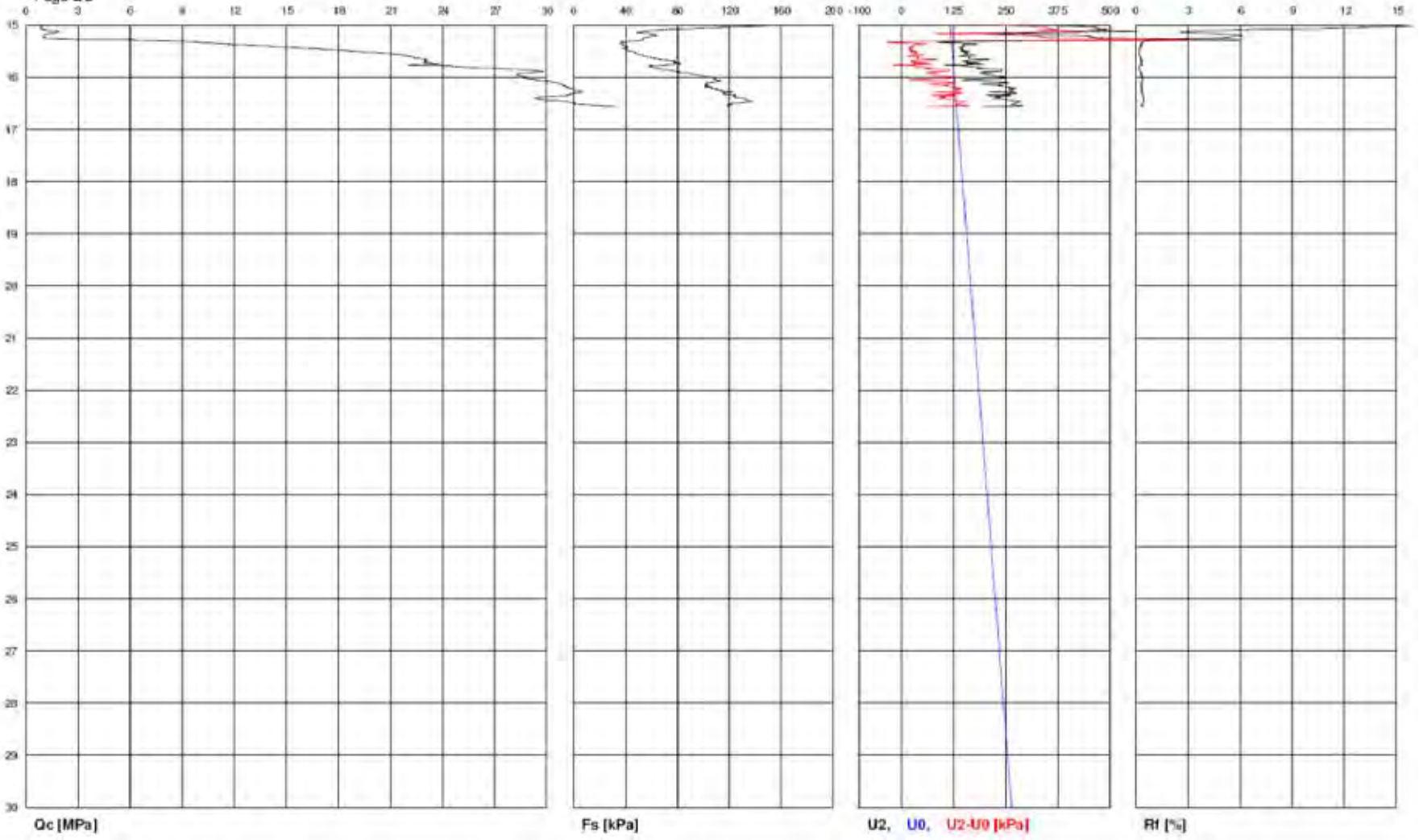

B – 5: SDMT Results

SDMT-01

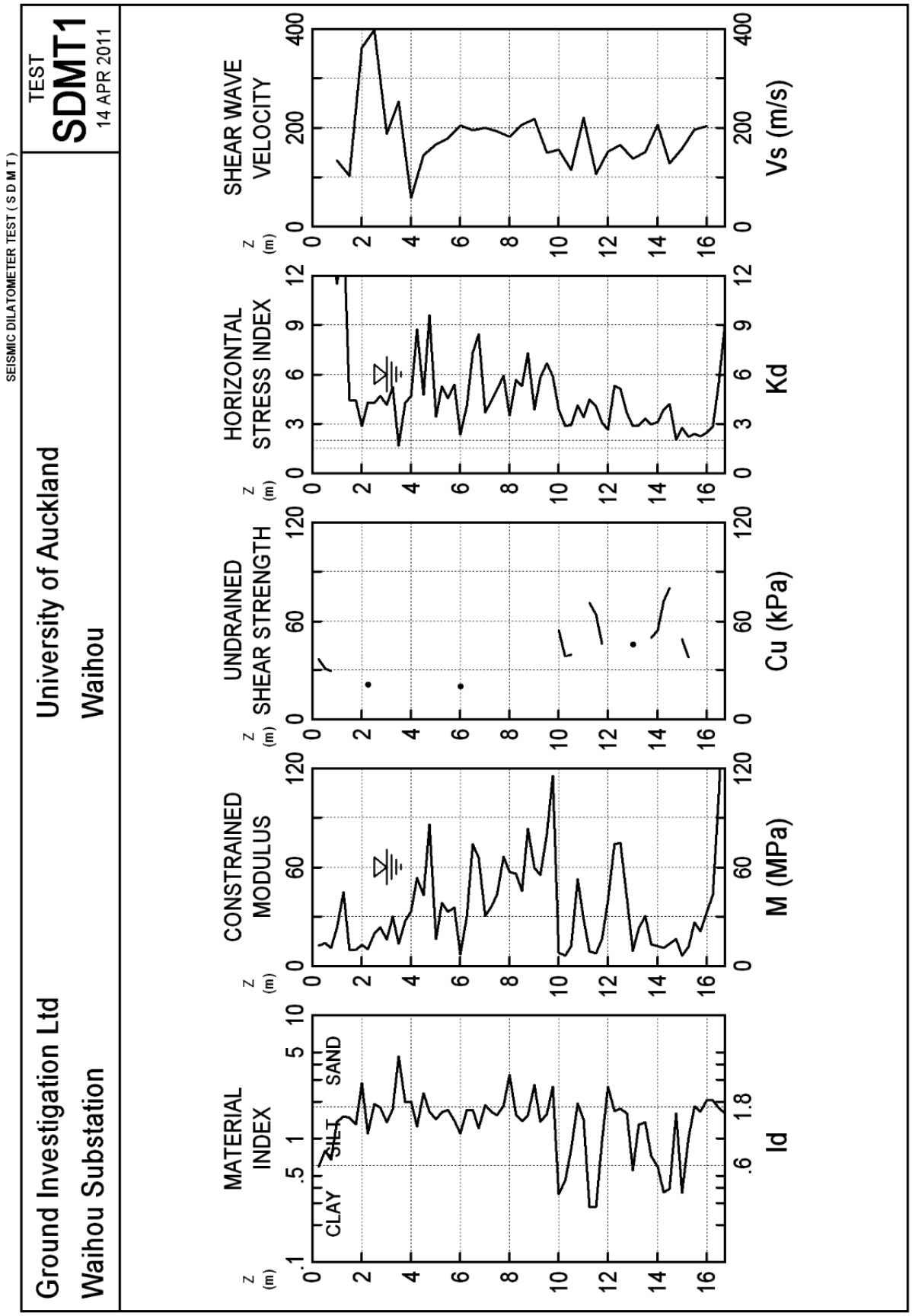

SDMT-02

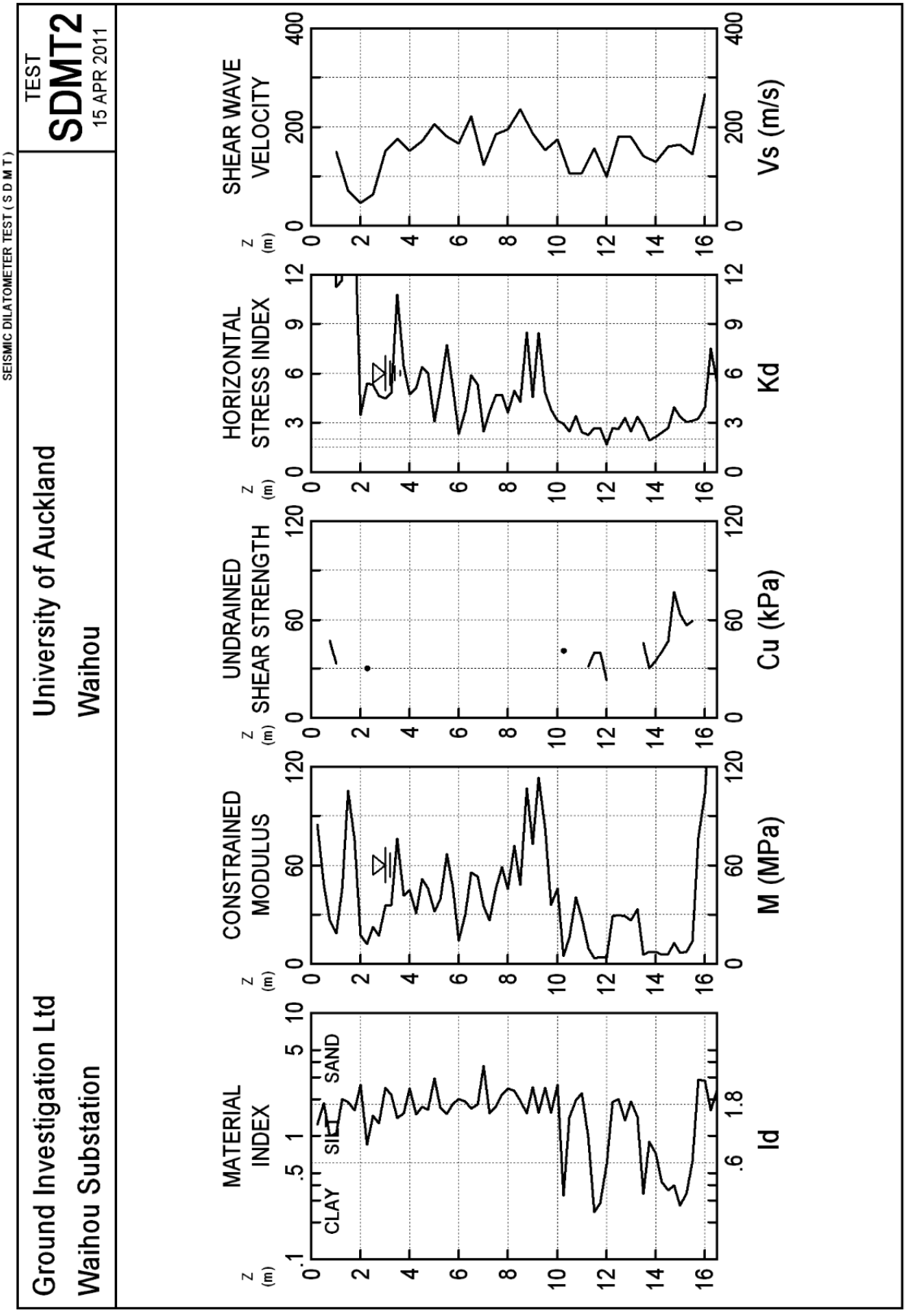
SEISMIC DILATOMETER TEST (S D M T)
Ground Investigation Ltd
Waihou Substation
University of Auckland
Waihou
TEST
SDMT2
15 APR 2011
MATERIAL INDEX
Id
CLAY
SILT
SAND
CONSTRAINED MODULUS
M (MPa)
UNDRAINED SHEAR STRENGTH
Cu (kPa)
HORIZONTAL STRESS INDEX
Kd
SHEAR WAVE VELOCITY
Vs (m/s)
Z (m)

SDMT-03

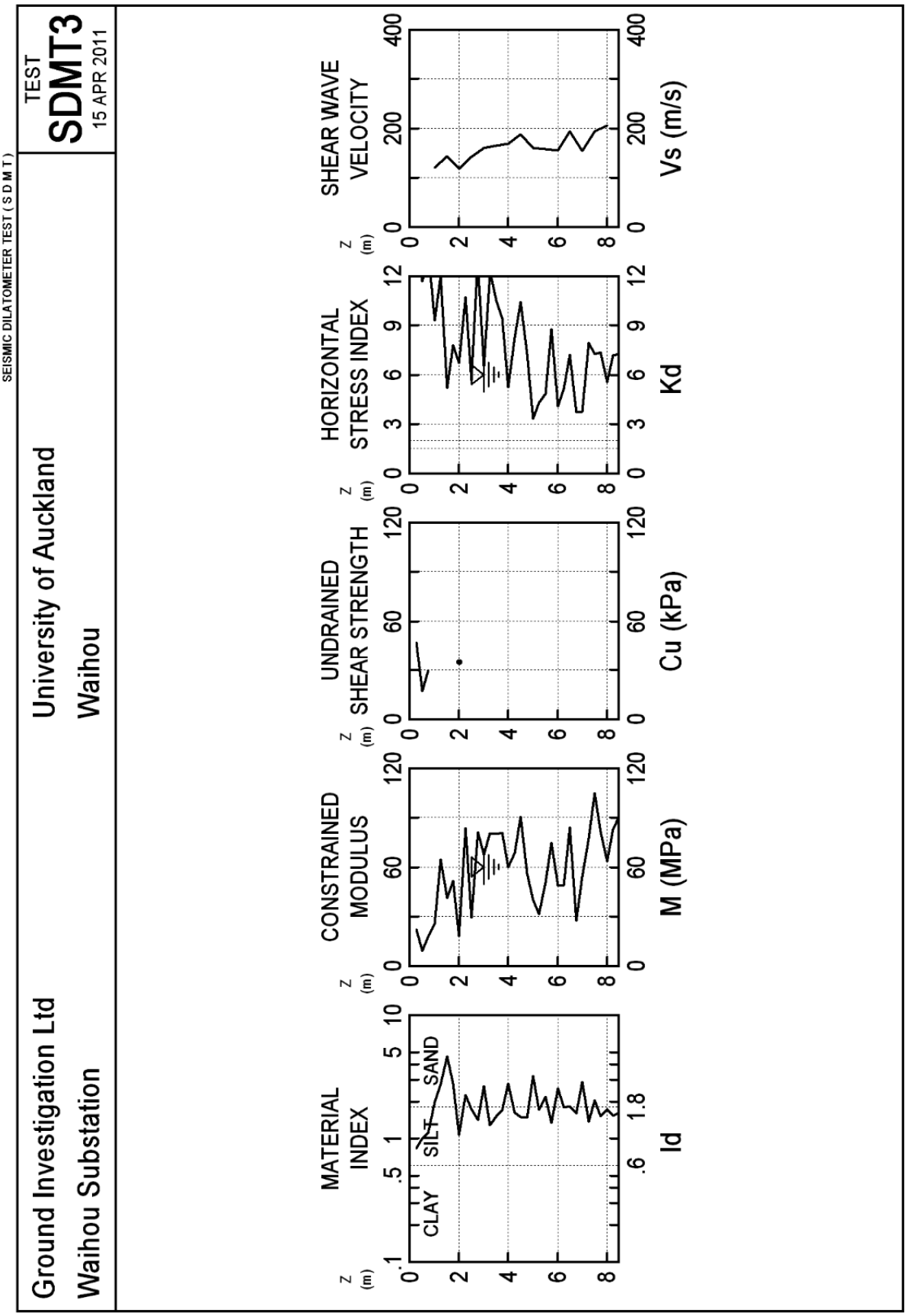
SEISMIC DILATOMETER TEST (S D M T)
Ground Investigation Ltd
Waihou Substation
University of Auckland
Waihou
TEST
SDMT3
15 APR 2011
MATERIAL INDEX
Id
CLAY
SILT
SAND
CONSTRAINED MODULUS
M (MPa)
UNDRAINED SHEAR STRENGTH
Cu (kPa)
HORIZONTAL STRESS INDEX
Kd
SHEAR WAVE VELOCITY
Vs (m/s)
Z (m)

SDMT-03A (Continuation)